Eur. Phys. J. C (2025) 85:1335
https://doi.org/10.1140/epjc/s10052-025-14748-z

THE EUROPEAN PHYSICAL JOURNAL C

Regular Article - Experimental Physics

Search for electroweak production of vector-like leptons in τ-lepton and b-jet final states in pp collisions at $\sqrt{s}$ = 13 TeV with the ATLAS detector

ATLAS Collaboration[*]

CERN, 1211 Geneva 23, Switzerland

Received: 31 March 2025 / Accepted: 10 September 2025

Abstract A search for pair-production of vector-like leptons is presented, considering their decays into a third-generation Standard Model (SM) quark and a vector leptoquark (U_1) as predicted by an ultraviolet-complete extension of the SM, referred to as the '4321' model. Given the assumed decay of U_1 into third-generation SM fermions, the final state can contain multiple τ-leptons and b-quarks. This search is based on a dataset of pp collisions at $\sqrt{s} = 13$ TeV recorded with the ATLAS detector during Run 2 of the Large Hadron Collider, corresponding to an integrated luminosity of up to 140 fb^{-1}. No significant excess above the SM background prediction is observed, and 95% confidence level limits on the cross-section times branching ratio are derived as a function of the vector-like lepton mass. A lower observed (expected) limit of 910 GeV (970 GeV) is set on the vector-like lepton mass. Additionally, the results are interpreted for a supersymmetric model with an R-parity violating coupling to the third-generation quarks and leptons. Lower observed (expected) limits are obtained on the higgsino mass at 880 GeV (940 GeV) and on the wino mass at 1170 GeV (1170 GeV).

1 Introduction

The Standard Model (SM) adequately explains sub-atomic particles and their interactions at the sub-TeV scale. However, a number of phenomena require additional understanding, such as the fine-tuning problem of the Higgs boson mass, the mass hierarchy of the SM particles, the similarities in the lepton and quark flavour generations, the nature of dark matter in the universe, the origin of neutrino oscillations; a selection of them has been discussed in Refs. [1–4]. In the quest to give a coherent explanation of the experimental results which point to deviations from the SM expectation in semileptonic B-meson decays, denoted as 'flavour anomalies' [5–11], a number of beyond-the-SM (BSM) theories are constructed. The minimal requirements for a unified explanation of all anomalies are new physics contributions in neutral currents ($b \to s\mu\mu$ [12]) and charged currents (enhanced decay rates of $b \to c\tau\nu$ [13]), as argued in Ref. [14]. At the same time, the BSM theory also needs to be consistent with the non-observation of related signals in other flavour-changing processes [15], electroweak (EW) precision observables, τ-lepton decays [16,17] and high transverse momentum (p_{T}) searches [18,19].

Typical attempts for the explanation of flavour anomalies often lack consideration of additional observations, like in Refs. [20–30]. Constraints from low-energy precision measurements can be satisfied when considering mainly left-handed semi-leptonic currents and flavour symmetry with dominant couplings to third generation fermions. This can be achieved by supplementing the SM with a single field - a vector leptoquark U_1, where leptoquarks, through their couplings to a quark and a lepton, induce semi-leptonic transitions of B-mesons at tree level. In order to have an ultraviolet (UV) complete theory, massive vectors require either compositeness (e.g. composite vector resonance [31–33]) or a spontaneously broken gauge theory. The second approach [34] of embedding the vector leptoquark U_1 into a spontaneously broken gauge theory is considered in the search presented in this paper.

The gauge structure of the considered model is invariant under the local group $\mathcal{G}_{4321} \equiv SU(4) \times SU(3)' \times SU(2)_L \times U(1)'$ [14], denoted as the '4321' model, which is fully calculable at the UV energy scale. It provides an explanation of the 'flavour anomalies' by allowing sizable (maximal) flavour violation in quark-lepton currents, where the neutral current anomaly can be well accommodated in the model. Consequently, the large leptoquark flavour violating couplings trigger new physics contributions in charged currents. It is also compatible with additional observations, such as the absence of any significant excess in searches for lepto-

[*] e-mail: atlas.publications@cern.ch

quarks [35–40], and the non-observation of flavour anomalies in (first or second generation) purely hadronic and purely leptonic channels [14,34,41,42]. The symmetry breaking leads to the appearance of a TeV-scale vector leptoquark with quantum numbers favoured by the flavour anomalies [4].

The particle content of the model has three heavy gauge bosons: a colour octet (G'), a weak isospin-singlet vector leptoquark (U_1, electric charge 2/3e), and a colour singlet Z' boson. Additionally, there are generations of vector-like fermions: vector-like quarks (VLQ) $U/D, C/S, T/B$ and vector-like leptons (VLL) N_1/E_1, N_2/E_2, N_3/E_3. The VLLs in this model are set to be SU(2) doublets with a charged and a neutral component. Only one generation of VLLs is present in the model, and it is assumed to be fully mass degenerate. The VLLs are hypothetical, non-chiral, colour-singlet, spin-1/2 particles predicted in various BSM scenarios, primarily aimed at addressing the flavour hierarchy in Higgs boson couplings and the fine-tuning problem associated with the Higgs mass. They can be electrically neutral or carry a charge of $\pm 1e$, can decay to the SM leptons via direct mixing or via other BSM portals while conserving their electric charges and lepton numbers, and hence are classified by the SM lepton generation number. This search targets the pair production of VLLs in proton–proton (pp) collisions at $\sqrt{s}$ = 13 TeV using the data collected by the ATLAS detector during Run 2 of the Large Hadron Collider (LHC). A previous search for VLLs in the '4321' model was performed by the CMS Collaboration, where a local 2.8σ excess was reported using the Run-2 data [43] at a representative VLL mass, m_{VLL}, of 600 GeV, while somewhat similar or milder excesses are present for other m_{VLL} values in the range of 500 – 1100 GeV.

The analysis targets the EW production of a pair of VLLs (E^+N, E^+E^- or $N\overline{N}$) via decays of off-shell $W^\pm$ or Z/γ^* bosons in the '4321' model. Each VLL decays through U_1 as $E^+ \to U_1\bar{b}$ and $N \to \overline{U}_1 t$ followed by $U_1 \to t\bar{\nu}_\tau$ or $U_1 \to b\tau^+$, as shown in Fig. 1. The branching ratios (BR) for E and N decays are roughly 50% for all processes (BR($E^+ \to b\bar{b}\tau^+$), BR($E^+ \to t\bar{b}\bar{\nu}_\tau$), BR($N \to \bar{b}t\tau^-$) and BR($N \to \bar{t}t\nu_\tau$)), because U_1 decays with equal probability into $t\bar{\nu}_\tau$ and $b\tau^+$ due to the SU(2) gauge symmetry. The m_{VLL} is the single free parameter of the model, investigated in the range 200–1500 GeV.

The search is performed probing simultaneously the E^+E^-, $E\bar{N}$ and $N\bar{N}$ production, which gives rise to a signature with a large number of jets, of which four contain a b-hadron (b-jets), and up to four hadronically decaying τ-leptons (τ_{had}). The search utilises the full Run-2 pp dataset collected by the ATLAS experiment at a centre-of-mass energy $\sqrt{s}$ = 13 TeV. Events are selected using a combination of triggers satisfying selection requirements for light leptons (ℓ= e, μ), τ_{had}, b-jet, or missing transverse energy ($E_{\text{T}}^{\text{miss}}$). The dataset selected with light leptons, τ_{had}, or $E_{\text{T}}^{\text{miss}}$ triggers corresponds to an integrated luminosity of 140 fb^{-1}, while that selected with b-jet triggers corresponds to 126 fb^{-1}.

An additional interpretation is performed for a supersymmetry (SUSY) model [44–49] with R-parity violation (RPV), which can accommodate 'flavour anomalies' and the $(g-2)_\mu$ anomaly [50]. It is realized using the lepton-number-violating RPV coupling to third generation quarks and leptons ($LQ\bar{D}$, where L, Q and $\bar{D}$ are the lepton doublet, quark doublet and down-type quark superfields, respectively). The corresponding interaction term has a coefficient λ'_{333}, where '333' denotes the assumed couplings to the third generation fermions only. In the minimal SUSY extension of the SM (MSSM) [51,52] the wino, bino and higgsino fields are superpartners of SM gauge boson (W, γ/Z), and Higgs fields, respectively. These states mix to form mass eigenstates at the electroweak scale: the charginos ($\tilde{\chi}^\pm_{1,2}$) and neutralinos ($\tilde{\chi}^0_{1,2,3,4}$), with indices denoting increasing mass order. The interpretation focuses on two dominant particle mixing scenarios: wino-dominated and higgsino-dominated states, which differ in their production cross-sections. The models assume highly decoupled sleptons, light and third generation squarks and gluinos. The simultaneous production of fully degenerate chargino-1 ($\tilde{\chi}^\pm_1$) and/or neutralino-1(2) ($\tilde{\chi}^0_{1,2}$) is considered ($pp \to \tilde{\chi}^\pm_1\tilde{\chi}^0_{1,2}$, $pp \to \tilde{\chi}^\pm_1\tilde{\chi}^\pm_1$, $pp \to \tilde{\chi}^0_1\tilde{\chi}^0_2$), with an assumed 50% branching ratio each for decays of $\tilde{\chi}^0_{1,2} \to \bar{b}t\tau^-(b\bar{b}\nu_\tau)$ and $\tilde{\chi}^\pm_1 \to b\bar{b}\tau^\pm(\bar{b}t\nu_\tau)$, as presented in the Fig. 2. A previous search [53] for a SUSY model with RPV decays of $\tilde{\chi}^\pm_1$ or $\tilde{\chi}^0_{1,2}$ to second- or third-generation of leptons, and third-generation of quarks (λ'_{i33}) was performed by the ATLAS Collaboration, excluding higgsinos (winos) masses between 200–585 (200–670) GeV.

The paper is structured as follows: Sect. 2 provides an overview of the ATLAS detector, followed by a description of the data and simulated samples in Sect. 3. Event reconstruction, object identification, and trigger selections are detailed in Sect. 4. The search strategy, including signal region definitions and the optimisation of signal classification using neural networks, is outlined in Sect. 5. Background estimation and systematic uncertainties are discussed in Sects. 6 and 7, respectively. Finally, Sect. 8 presents the results along with their statistical interpretation, and Sect. 9 concludes the paper.

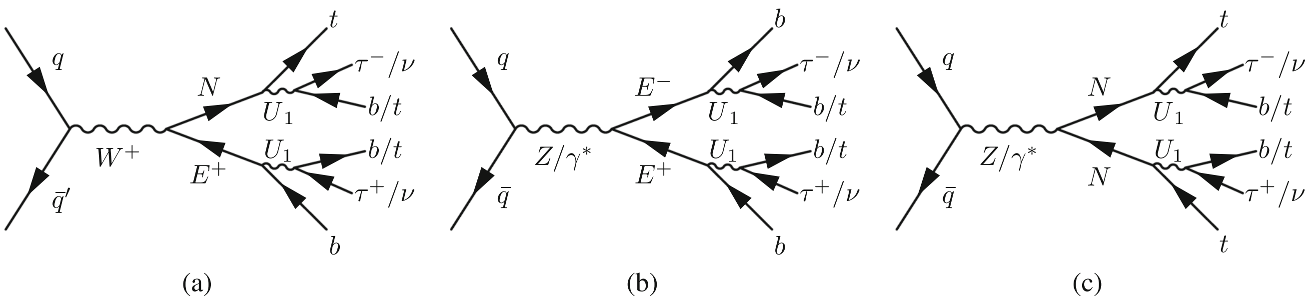

Fig. 1 Vector-like lepton pair production and decays in the '4321' model for **a** $pp \to E^+N$, **b** $pp \to E^+E^-$, **c** $pp \to N\overline{N}$

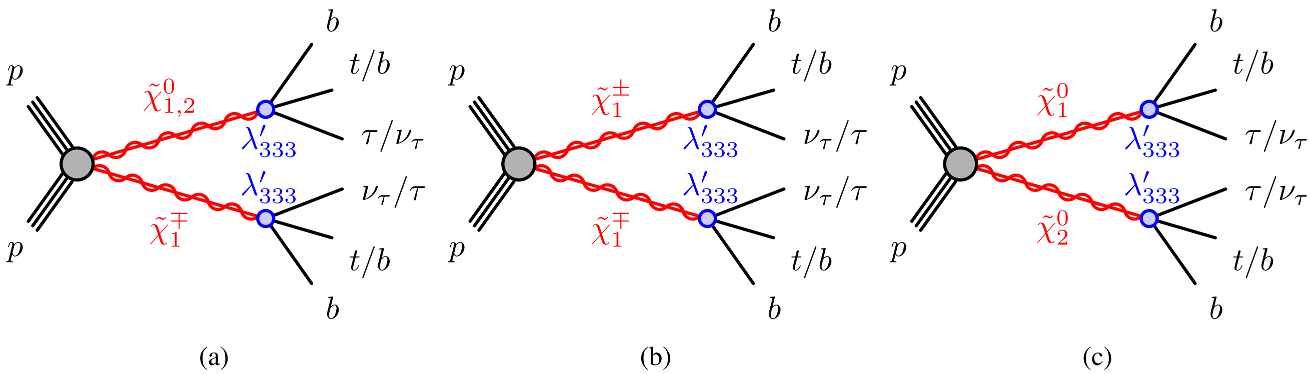

Fig. 2 Diagrams for SUSY R-parity violation model with λ'_{333} coupling for wino or higgsino production of **a** $pp \to \tilde{\chi}^\pm_1 \tilde{\chi}^0_{1,2}$, **b** $pp \to \tilde{\chi}^\pm_1 \tilde{\chi}^\mp_1$, **c** $pp \to \tilde{\chi}^0_1 \tilde{\chi}^0_2$

2 ATLAS detector

The ATLAS detector [54] at the LHC covers nearly the entire solid angle around the collision point.[1] It consists of an inner tracking detector surrounded by a thin superconducting solenoid, electromagnetic and hadron calorimeters, and a muon spectrometer incorporating three large superconducting toroidal magnets.

The inner-detector system is immersed in a 2 T axial magnetic field and provides charged-particle tracking in the range $|\eta| < 2.5$. The high-granularity silicon pixel detector covers the vertex region and typically provides four measurements per track, the first hit normally being in the insertable B-layer installed before Run 2 [55,56]. It is followed by the silicon microstrip tracker, which usually provides eight measurements per track. These silicon detectors are complemented by the transition radiation tracker (TRT), which enables radially extended track reconstruction up to $|\eta| = 2.0$. The TRT also provides electron identification information based on the fraction of hits (typically 30 in total) above a higher energy-deposit threshold corresponding to transition radiation.

The calorimeter system covers the pseudorapidity range $|\eta| < 4.9$. Within the region $|\eta| < 3.2$, electromagnetic calorimetry is provided by barrel and endcap high-granularity lead/liquid-argon (LAr) calorimeters, with an additional thin LAr presampler covering $|\eta| < 1.8$ to correct for energy loss in material upstream of the calorimeters. Hadron calorimetry is provided by the steel/scintillator-tile calorimeter, segmented into three barrel structures within $|\eta| < 1.7$, and two copper/LAr hadron endcap calorimeters. The solid angle coverage is completed with forward copper/LAr and tungsten/LAr calorimeter modules optimised for electromagnetic and hadronic energy measurements respectively.

The muon spectrometer comprises separate trigger and high-precision tracking chambers measuring the deflection of muons in a magnetic field generated by the superconducting toroidal magnets. The field integral of the toroids ranges between 2.0 and 6.0 T m across most of the detector. Three layers of precision chambers, each consisting of layers of monitored drift tubes, cover the region $|\eta| < 2.7$, were complemented by cathode-strip chambers in the forward region, where the background is highest. The muon trigger system covers the range $|\eta| < 2.4$ with resistive-plate chambers in the barrel, and thin-gap chambers in the endcap regions.

[1] ATLAS uses a right-handed coordinate system with its origin at the nominal interaction point (IP) in the centre of the detector and the z-axis along the beam pipe. The x-axis points from the IP to the centre of the LHC ring, and the y-axis points upwards. Cylindrical coordinates (r, ϕ) are used in the transverse plane, ϕ being the azimuthal angle around the z-axis. The pseudorapidity is defined in terms of the polar angle θ as $\eta = -\ln\tan(\theta/2)$ and is equal to the rapidity y in the relativistic limit. Angular distance is measured in units of $\Delta R \equiv \sqrt{(\Delta y)^2 + (\Delta\phi)^2}$.

Interesting events are selected by the first-level trigger system implemented in custom hardware, followed by selections made by algorithms implemented in software in the high-level trigger (HLT) [57]. The first-level trigger accepts events from the 40 MHz bunch crossings at a rate below 100 kHz, which the high-level trigger further reduces in order to record events to disk at about 1 kHz.

A software suite [58] is used in data simulation, in the reconstruction and analysis of real and simulated data, in detector operations, and in the trigger and data acquisition systems of the experiment.

3 Data and simulated event samples

A dataset of pp collisions at a centre-of-mass energy of $\sqrt{s}$ = 13 TeV collected by the ATLAS experiment from 2015 to 2018, and corresponding to integrated luminosity of up to 140 fb^{-1}, is used for this analysis. The number of additional pp interactions per bunch crossing (pile-up) in this dataset ranges from about 8 to 70, with an average of 34. Only events recorded under stable beam conditions and for which all relevant detector subsystems were known to be in a good operating condition are used [59].

Monte Carlo (MC) simulation samples are produced for the different signal and background processes. Pile-up is modelled by overlaying the simulated hard-scattering event with inelastic pp events generated with Pythia 8.186 [61] using the NNPDF2.3$_{\mathrm{LO}}$ set of parton distribution functions (PDF) [77] and the A3 set of tuned parameters [78] (referred to as the 'tune'). The MC samples are produced using either a detailed ATLAS detector simulation [79] based on Geant4 [80] or a faster simulation where the full Geant4 simulation of the calorimeter response is replaced by a parameterisation of the shower shapes [79]. In both cases, the simulated events are processed through the same reconstruction software as the dataset of pp collisions. For all samples of simulated events, except those generated using the Sherpa generator [62–65], the EvtGen program [66] is used to describe the decays of bottom and charm hadrons. The top-quark mass m_t is set to 172.5 GeV and the Higgs boson mass m_H is set to 125 GeV in all relevant samples.

Corrections are applied to the simulated events so that the particle candidates' selection efficiencies, energy scales and energy resolutions match those determined from data control samples. The simulation samples are normalised to their cross-sections, and generated to the highest order available in perturbation theory.

Signal samples for the '4321' model [14,42,81] are generated for VLL masses in the range 200–1500 GeV in intervals of 100GeV. The production via Z' is suppressed by setting the Z' mass to 100 TeV and its couplings to 0. Similarly, G' is not relevant in this search, as this gauge boson couples only to coloured particles. Its mass is therefore set to 5 TeV, in order to suppress processes via its exchange. To suppress the EW production of VLQs, all VLQ masses are set to 3.5 TeV. To accommodate flavour anomalies, the model favours vector leptoquark U_1 and VLL decays to third-generation fermions, as shown in Ref. [42]. Decays to the first two generations are suppressed by fixing the corresponding couplings to 0, while U_1 couplings to third-generation fermions are set to 1. The U_1 width is constrained to 500 GeV by adjusting its couplings to VLLs and VLQs to be between −0.5 and 1. The U_1 couplings to the SM fermions and mass are chosen to also align with flavour anomalies, resulting in two scenarios [42]: one not allowing right-handed currents ($\beta_R^{b\tau} = 0$) and one with maximal right-handed currents ($\beta_R^{b\tau} = -1$). Due to similar kinematics and cross-section for the two scenarios, only the $\beta_R^{b\tau} = 0$ scenario is investigated. The mass and universal coupling of U_1 are set to 3.5 TeV and 3, respectively. This brings to off-shell U_1 decays, allows for consistency with flavour anomalies, and preserves compatibility with the model previously studied by the CMS Collaboration [43]. The VLL widths are in the very narrow range of 10^{-2}–10^{-6} GeV, resulting in 3-body VLL decays. VLL pair production and decay was done using MadGraph5_aMC@NLO 2.2.3 [60,82] at leading order (LO) with the Pythia 8.186 [61] interface for the parton shower (PS), hadronisation and underlying event modelling, utilising the A14 tune [69]. The matrix element (ME) is calculated at tree level, with emission of up to two additional partons. The PDF set used is NNPDF3.0$_{\mathrm{LO}}$ [68], and the ME-PS matching uses the CKKW-L prescription [83,84]. The VLL pair production cross-section is calculated using MadGraph at next-to-leading order (NLO) accuracy in Quantum Chromodynamics (QCD). The RPV SUSY signal samples are generated using MadGraph5_aMC@NLO 2.9.9 at LO, with up to two initial state radiation jets at LO in QCD, and the Pythia 8.307 [85] interface for the PS, hadronisation and underlying event modelling, utilising the A14 tune [69]. The matching scale is set to 1/4 of the produced SUSY particle mass. The cross-section is calculated at NLO in QCD, with added resummation of soft gluon emission at next-to-leading-logarithmic accuracy (NLL) using Resummino [86]. The nominal cross-section and uncertainty are calculated from an envelope of calculations using different PDF sets and factorisation and renormalisation scales following the prescription described in Ref. [87].

Samples for $t\bar{t}$ production, single top production, vector boson (V) production in association with the Higgs boson (VH), and the associated production of a top-quark pair and a Higgs boson ($t\bar{t}H$) are generated using the NLO generator Powheg- Box [70,76,88–90] with the NNPDF3.0nlo PDF set; interfaced with Pythia 8.2 with the A14 tune. The h_{damp} parameter, which controls the p_{T} of the first additional emission beyond the Born configuration and therefore regulates the high-p_T radiation, is set to $3(2m_t + m_H)/4$ in the $t\bar{t}H$ sample and to $1.5m_t$ in the $t\bar{t}$ + jets and single top samples.

The $Z(\to l^+l^-)$ + jets and $W(\to l\nu)$ + jets events are simulated using the SHERPA 2.2.1 generator [73] with NLO-accurate MEs for up to two partons and LO-accurate MEs for up to four partons. The MC yields are normalised to the next-to-NLO (NNLO) cross-sections, computed using FEWZ [91] with the MSTW2008NNLO [92] PDF set.

The sample used to model the $t\bar{t}W$ ($t\bar{t}Z/\gamma^*$) background process is generated using SHERPA 2.2.10 (SHERPA 2.2.11), where the ME is calculated for up to one (zero) additional parton at NLO in QCD and up to two partons at LO in QCD using COMIX [63] and OPENLOOPS [62] and merged with the SHERPA PS [64] using the MEPS@NLO prescription [65]. A CKKW merging scale of 30 GeV is used for the $t\bar{t}W$ sample. These samples are generated using the NNPDF3.0NNLO PDF set. Both the factorisation and renormalisation scales are set to $\mu_R = \mu_F = H_T/2$ in the $t\bar{t}W$ sample, where H_T is defined as the scalar sum of the transverse masses $\sqrt{p_T^2 + m^2}$ of all final state particles. The $t\bar{t}W$ LO EW contributions are obtained from a dedicated sample simulated with SHERPA 2.2.10 and are added together with the NLO QCD sample described above.

Diboson (WZ, ZZ and WW including off-shell productions) background processes are simulated with SHERPA 2.2.2. The ME is calculated using COMIX and OPENLOOPS at NLO accuracy in QCD for up to one additional parton and at LO accuracy for up to three additional partons, and merged with the SHERPA PS model using the MEPS@NLO prescription. The NNPDF3.0NNLO set of PDFs is used, along with the dedicated set of tuned PS parameters developed by the SHERPA authors.

Table 1 shows the configurations for all MC samples used in this analysis, with the samples in parentheses indicating those used to estimate the systematic uncertainties.

4 Event reconstruction and object identification

Events are selected using requirements involving the reconstructed primary interaction vertex, triggers, and reconstructed jets, b-jets and τ_{had} candidates. Additionally, events with light leptons are used to estimate the background from $t\bar{t}$ and Z + jets processes. The primary interaction vertices of the pp collision events are reconstructed based on at least two tracks that are consistent with originating from the beam collision region and have p_T higher than 500 MeV. Of all primary vertex candidates, the one associated with the highest sum of squared p_T for its associated tracks is taken as the hard-scatter primary vertex [93]. Events are required to satisfy data quality criteria to remove significant noise in the calorimeters or data corruption [59]. Additional quality cuts are applied to discard jet candidates originating from non-collision sources or detector noise, as well as to remove muon candidates with significantly worse momentum resolution.

Electron candidates are reconstructed from energy clusters in the electromagnetic calorimeter that are associated with charged particle tracks reconstructed in the inner detector [94–96]. These candidates are required to satisfy $p_T > 10$ GeV and $|\eta_{cluster}| < 2.47$, and they must not be in the transition region between different electromagnetic calorimeter components, $1.37 < |\eta_{cluster}| < 1.52$. A multivariate likelihood discriminant combining shower shape and track information is used to distinguish real electrons from hadronic showers [94,96]. A loose electron discriminant working point, denoted as 'LooseLH', is employed for the preselection, which is further tightened to 'TightLH' working point in certain analysis regions.

Muon candidates are reconstructed by combining inner-detector tracks with track segments or full tracks in the muon spectrometer [97,98]. Candidates are preselected with the Loose identification working point, and they are required to satisfy $p_T > 10$ GeV and $|\eta| < 2.5$.

The electron (muon) candidate track is associated with the primary vertex by restricting the significance of its transverse impact parameter, d_0, to be such that $|d_0/\sigma(d_0)| < 5(3)$, where $\sigma(d_0)$ denotes the measured uncertainty in d_0. Furthermore, the longitudinal impact parameter z_0 must satisfy $|z_0 \sin\theta| < 0.5$ mm, where θ is the polar angle of the track. The electron or muon candidates are also required to be isolated in the tracker and in the calorimeter. A track-based lepton isolation criterion is defined by calculating the quantity $I_R = \sum p_T^{trk}$, where the scalar sum includes all tracks (excluding the lepton candidate itself) within a cone defined by $\Delta R < R_{cut}$ around the direction of the lepton. The value of R_{cut} is the smaller of r_{min} and $10\ \text{GeV}/p_T^{\ell}$, where r_{min} is set to 0.2 (0.3) for electron (muon) candidates and where p_T^{ℓ} is the lepton p_T. All lepton candidates must satisfy $I_R/p_T^{\ell} < 0.15$. Additionally, electrons (muons) are required to satisfy a calorimeter-based isolation criterion: the sum of the transverse energy within a cone of size $\Delta R = 0.2$ around the lepton, after subtracting the contributions from pile-up and the energy deposit of the lepton itself, is required to be less than 20% (30%) of p_T^{ℓ}.

The τ_{had} candidates are reconstructed from energy clusters in the calorimeters and associated inner-detector tracks [99]. They are required to have either one or three associated tracks (referred to as 1-prong and 3-prong τ_{had} candidates, respectively), with a total charge of $\pm 1e$. The candidates are required to satisfy $p_T > 20$GeV and $|\eta| < 2.5$, excluding the electromagnetic calorimeter's transition region. A recurrent neural network discriminant using calorimeter- and tracking-based variables is used to identify real τ_{had} candidates and suppress mis-reconstructed jet backgrounds [100]. Three identification working points of 1-prong and 3-prong

Table 1 The configurations used for event generation of signal and background processes. The samples used to estimate the systematic uncertainties are indicated in grey between parentheses. V refers to the production of an EW boson (W or Z/γ^*), and l refers to a lepton (e, μ or τ). The column labelled 'Parton shower' refers to the generator used for the parton shower (PS), hadronisation and underlying events. The parton distribution function (PDF) used for the matrix element (ME) is shown. Tune refers to the underlying-event tune of the PS generator. MG5_AMC refers to MADGRAPH5_AMC@NLO 2.2 or 2.3 [60]; PYTHIA 8 refers to version 8.2 or 8.3 [61]; MEPS@NLO refers to the method used in SHERPA [62–65] to match the ME to the PS. Samples using PYTHIA 8 have heavy flavour hadron decays modelled by EVTGEN 1.2.0 [66]. All samples include leading-logarithm photon emission, either modelled by the PS generator or by PHOTOS [67]

Process	Generator	ME order	Parton shower	PDF	Tune
VLL signal	MG5_AMC [60]	LO	PYTHIA 8 [61]	NNPDF3.0 NLO [68]	A14 [69]
RPV SUSY signal	MG5_AMC	LO	PYTHIA 8	NNPDF3.0 NLO	A14
$t\bar{t}$ + jets	POWHEGBOX [70]	NLO	PYTHIA 8	NNPDF3.0 NLO	A14
	(POWHEGBOX)	(NLO)	(PYTHIA 8, $p_{\mathrm{T}}^{\mathrm{hard}} = 1$)	(NNPDF3.0 NLO)	(A14)
	(POWHEGBOX)	(NLO)	(HERWIG7.1.3 [71])	(NNPDF3.0 NLO)	(H7.1 default)
($t\bar{t}b\bar{b}$)	(POWHEGBOXRES [72])	(NLO)	(PYTHIA8)	(NNPDF3.0 NLO)	(A14)
$Z(\to l^+l^-)$ + jets	SHERPA 2.2.1 [73]	NLO	SHERPA	NNPDF3.0 NLO	SHERPA default
$W(\to l\nu)$ + jets	SHERPA 2.2.1	NLO	SHERPA	NNPDF3.0 NLO	SHERPA default
$t\bar{t}t\bar{t}$	MG5_AMC	NLO	PYTHIA 8	NNPDF3.1 NLO	A14
	(SHERPA 2.2.11)	(NLO)	(SHERPA)	(NNPDF3.0 NNLO)	(SHERPA default)
$t\bar{t}W$	SHERPA 2.2.10	NLO	SHERPA	NNPDF3.0 NNLO	SHERPA default
	(MG5_AMC)	(NLO)	(PYTHIA 8)	(NNPDF3.0 NLO)	(A14)
$t\bar{t}H$	POWHEGBOX	NLO	PYTHIA 8	NNPDF3.0 NLO	A14
	(POWHEGBOX)	(NLO)	(HERWIG7.0.4 [74])	(NNPDF3.0 NLO)	(H7 default)
	(MG5_AMC)	(NLO)	(PYTHIA 8)	(NNPDF3.0 NLO)	(A14)
$t\bar{t}(Z/\gamma^* \to l^+l^-)$	SHERPA 2.2.11	NLO	SHERPA	NNPDF3.0 NNLO	SHERPA default
	(MG5_AMC)	(NLO)	(PYTHIA 8)	(NNPDF3.0 NLO)	(A14)
Single top: tW, s-, t-channel	POWHEGBOX [75,76]	NLO	PYTHIA 8	NNPDF3.0 NLO	A14
VH	POWHEGBOX	NLO	PYTHIA 8	NNPDF3.0 NLO	A14
VV, $qqVV$, VVV	SHERPA 2.2.2	NLO	SHERPA	NNPDF3.0 NNLO	SHERPA default
$t(Z/\gamma^*)$	MG5_AMC	NLO	PYTHIA 8	NNPDF2.3 LO	A14
$tHjb$	MG5_AMC	NLO	PYTHIA 8	NNPDF2.3 LO	A14
$tW(Z/\gamma^*)$	MG5_AMC	NLO	PYTHIA 8	NNPDF2.3 LO	A14
tWH	MG5_AMC	NLO	PYTHIA 8	NNPDF2.3 LO	A14
$t\bar{t}W^+W^-$	MG5_AMC	LO	PYTHIA 8	NNPDF2.3 LO	A14
$t\bar{t}t$	MG5_AMC	LO	PYTHIA 8	NNPDF2.3 LO	A14
$t\bar{t}ZZ$	MADGRAPH [60]	LO	PYTHIA 8	NNPDF2.3 LO	A14
$t\bar{t}HH$	MADGRAPH	LO	PYTHIA 8	NNPDF2.3 LO	A14
$t\bar{t}WH$	MADGRAPH	LO	PYTHIA 8	NNPDF2.3 LO	A14

τ_{had} candidates are used for different levels of efficiencies and background rejections. The selected τ_{had} candidates are referred to as 'Loose', 'Medium', and 'Tight', respectively [100]. The loose working point has a target efficiency of 85% (75%) for 1-prong (3-prong) τ_{had} candidates, with an expected rejection factor against light-jets of 21 (90). The corresponding efficiencies and rejections for the medium working point are 75% (60%) and 35 (240) for 1-prong (3-prong) τ_{had} candidates, respectively. The tight working point has average efficiency of 60% (45%) for 1-prong (3-prong) τ_{had} candidates, respectively. Electrons that are reconstructed as 1-prong τ_{had} candidates are removed using a boosted decision tree algorithm [100]. The τ_{had} reconstruction and identification efficiencies and the τ_{had} energy scale in the simulation are calibrated to those measured in a data control sample of $Z \to \tau^+\tau^-$ events [101], and the associated uncertainties are considered in the analysis.

The constituents for jet reconstruction are identified by combining measurements from both the inner-detector and the calorimeter using a particle flow (PFlow) algorithm [102,103]. Jet candidates are reconstructed from these PFlow objects using the anti-k_t algorithm [104,105] with a radius parameter of $R = 0.4$. They are calibrated using simulation with corrections obtained from *in situ* techniques in data [103]. Only jet candidates with a $p_{\mathrm{T}} > 25$ GeV and within $|\eta| < 2.5$ are selected. In order to reduce the effect from pile-up, each jet with $p_{\mathrm{T}} < 60$ GeV and $|\eta| < 2.4$ is required to satisfy the tight working point of the jet vertex tagger (JVT) [106] criteria used to identify the jets as originating from the selected primary vertex.

Jets containing b-hadrons are identified (b-tagged) via the `DL1r` multivariate discriminant combining information from the impact parameters of displaced tracks with topological properties of secondary and tertiary decay vertices reconstructed within the jet [107,108]. Each jet can be sorted into a pseudo-continuous binned distribution of the DL1r discriminant score, where each bin corresponds to a certain range of b-tagging efficiencies defined by the working points corresponding to an average efficiency of 60, 70, 77 and 85% for b-jets with $p_{\mathrm{T}} > 20$ GeV and $|\eta| < 2.5$ in $t\bar{t}$ events. The 85% working point is used in the event selection of channels used for background estimation in this analysis ($\geq 1\ell$ channels). The 77% working point is applied in channels of both signal and control regions (0ℓ channels). Operating at the 77% working point, the tagging algorithm achieves a rejection factor of about 170 against light-jets (jets that do not contain b- or c-hadrons) and of approximately 5 against c-jets. The pseudo-continuous b-tagging information is used as an input variable in the signal region optimisation.

The $E_{\mathrm{T}}^{\mathrm{miss}}$ is defined as the magnitude of the negative vector sum of the transverse momenta of all objects in the event. It also includes a term for the transverse momentum coming from all soft particles that are not associated with any of the objects in the event [109], which is calculated from inner detector tracks that can be matched to the primary vertex.

In order to resolve ambiguities in object reconstruction, an algorithm is used to avoid double counting of two different close-by objects that pass the selection requirements and overlap with each other. The overlapping objects are removed according to the following procedure. Electrons and muons that pass the loose selections are considered for overlap removal, together with calorimeter jets which pass the JVT requirement and τ_{had} candidates identified using the Loose criteria. If the electron and muon share a track, the electron is removed if the muon is associated with a signature in the muon spectrometer, otherwise the muon is removed. For a surviving electron which overlaps with a jet within $\Delta R < 0.2$, the jet is removed. If an electron and a jet overlap within $\Delta R < 0.4$, the electron is removed. If a muon and a jet overlap with $\Delta R < 0.2$, the jet is removed, unless the number of tracks in the jet is more than 2. If a muon and a jet overlap with $\Delta R < 0.4$, the muon is removed. If a surviving electron overlaps with a loose τ_{had} within $\Delta R < 0.2$, the electron is kept and the τ_{had} object is removed. If a surviving muon overlaps with a loose τ_{had} within $\Delta R < 0.2$, the muon is kept and the τ_{had} object is removed. If a surviving jet overlaps with a loose τ_{had} within $\Delta R < 0.2$, the jet is removed.

4.1 Trigger selection

The analysis employs different trigger strategies for the 0ℓ events, which contain at least one τ_{had} and no isolated light leptons. The $\geq 1\ell$ channels, which include at least one isolated light lepton and are used only for the background estimations, are selected using single-light-lepton (SLT) or double-light-lepton (DLT) triggers.

The various types of triggers considered in the analysis are described in the following. At the HLT, the $E_{\mathrm{T}}^{\mathrm{miss}}$ triggers (MET) [110] have minimum thresholds ranging from 90 GeV to 110 GeV depending on the data-taking period. The single-τ_{had} triggers (STT) [111] select a τ_{had} candidate satisfying HLT quality criteria and with a p_{T} threshold ranging from 80 GeV to 160 GeV, where the 160 GeV threshold is used for the majority of the data-taking period. The di-τ_{had} (DTT) triggers have kinematic thresholds on two τ_{had} candidates, as well as on the leading[2] and sub-leading jet p_{T} in certain triggers depending on the data-taking period, as described in Ref. [112]. The p_{T} threshold of the leading (sub-leading) τ_{had} is 35(25) GeV across all data-taking periods. For the years 2017–2018, a subset of triggers introduces an additional requirement on the angular separation $\Delta R(\tau_{\mathrm{had}}, \tau_{\mathrm{had}})$ between two τ_{had} candidates. This subset also includes a single jet requirement. These requirements were designed to reduce trigger rates by suppressing back-to-back τ_{had} pairs. There are b-jet triggers (BJET) [113] employed during the data taking period from 2016–2018, which require at least one jet with p_{T} above 100 GeV or 110 GeV depending on the data-taking period and two b-tagged jets identified with the HLT algorithm based on multivariate analysis techniques. The b-tagged jets have p_{T} above the 35–55 GeV range depending on the data-taking year. Furthermore, the data are selected using a combination of SLT or DLT triggers, with requirements on the identification, isolation, and p_{T} of the light leptons to maintain a high efficiency across the full momentum range while controlling the trigger rates [114,115]. The electron (muon) SLT has the lowest p_{T} thresholds of 24–26 (20–26) GeV, while the electron (muon) DLT has the lowest p_{T} threshold requirements of 12–24 (14–22) GeV for the leading lepton, depending on the data-taking period and trigger combination.

In the 0ℓ channels, events are selected using a combination of triggers in order to enhance the signal acceptance. These triggers are used with a set of requirements on the kinematic thresholds of the τ_{had}, light-jet, or b-jet candidates, or the $E_{\mathrm{T}}^{\mathrm{miss}}$. Events are classified into orthogonal categories based

[2] In this paper, the offline physics objects are ordered in p_{T}, with the leading object referring to the one with the highest p_{T}.

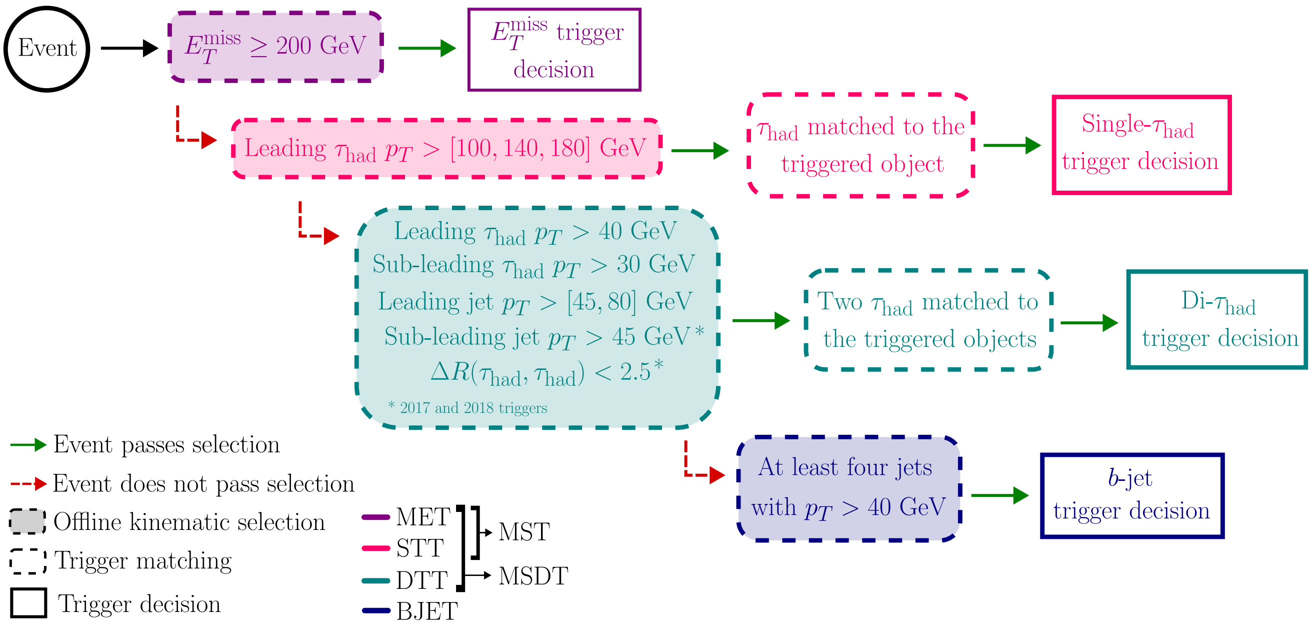

Fig. 3 Trigger selection strategy for 0ℓ channels using multiple triggers to maximise signal acceptance, where the kinematic selections in the analysis are chosen in the plateau region of the trigger efficiency, followed by corresponding trigger matching and trigger decisions. The E_T^{miss} (MET) trigger category targets events with $E_T^{miss} \geq 200$ GeV, the single-τ_{had} (STT) triggers select events with single τ_{had} of p_T above the thresholds indicated in the diagram, the di-τ_{had} (DTT) triggers recover events with two τ_{had} with relatively lower thresholds, and the b-jet (BJET) triggers recover events that have low τ_{had} p_T but a large multiplicity of b-jets. The MST category refers to events that pass either the STT or the MET trigger chain. Similarly, events that belong to the STT, the DTT, or the MET trigger chains are collectively labelled as MSDT. Variations in the offline thresholds are due to changes in trigger thresholds across different data-taking periods

on the kinematic selections which are chosen in the plateau region of trigger efficiency. This methodology was previously used in Refs. [112,116]. Furthermore, in the offline analysis, the reconstructed τ_{had} are geometrically matched to the HLT τ_{had} that triggered the event. A diagram laying out the trigger strategy in the 0ℓ channels can be found in Fig. 3.

There are four different trigger chains based on the type of the trigger used in the 0ℓ event selection. The selection starts with MET triggers, which are fully efficient for events with $E_T^{miss} > 200$ GeV. No efficiency corrections are applied to simulated events selected with MET triggers. For events with $E_T^{miss} < 200$ GeV, the STT triggers are used, where the reconstructed τ_{had} candidate satisfy p_T thresholds, as illustrated in Fig. 3, with efficiencies at plateau. The selection threshold is up to 20 GeV above the trigger threshold. Signal events with one τ_{had} or two or more τ_{had} that pass the orthogonal offline selections have an STT trigger efficiency ranging from 88 to 92%, depending on the τ_{had} multiplicity and signal mass. The events that do not meet the criteria for MET and STT triggers are recovered with the use of the DTT triggers that have requirements on the p_T of two τ_{had} candidates and the leading jet. The reconstructed τ_{had} candidate p_T must be 5 GeV above the trigger threshold applied to the τ_{had} at HLT, as highlighted in Fig. 3, while the leading reconstructed jet must have $p_T > 80$ GeV. For the events selected with DTT triggers that required two or more jets, a lower threshold of 45 GeV is used for the leading jet. The DTT trigger efficiency for signal events with two τ_{had} passing the offline selection ranges from 82–90%, depending on the signal mass. The STT and DTT trigger efficiencies are corrected in the simulated events. Other remaining events that fail to satisfy the above triggers are selected with BJET triggers if the events contain at least four jets with $p_T > 40$ GeV. The BJET trigger efficiency ranges from 56 to 90%, depending on the signal mass. Events from the BJET trigger category have efficiency corrections related to b-tagging. These corrections are evaluated using a technique previously applied in Ref. [116].

SLT and DLT triggers are used to select events with two or more light leptons that have $E_T^{miss} < 200$ GeV. The reconstructed leptons in the event are required to be matched to the triggered objects at the HLT from the SLT or DLT, with reconstructed lepton p_T 1 GeV higher than the threshold set on the HLT trigger object. To allow full trigger efficiency, the events having an E_T^{miss} of at least 200 GeV are selected with the MET trigger. These events are used in the determination of kinematic dependent corrections for the $t\bar{t}$ and $Z+$jets processes, and for the estimations of the scale factors for the misidentified τ_{had}, as will be discussed in Sect. 6.

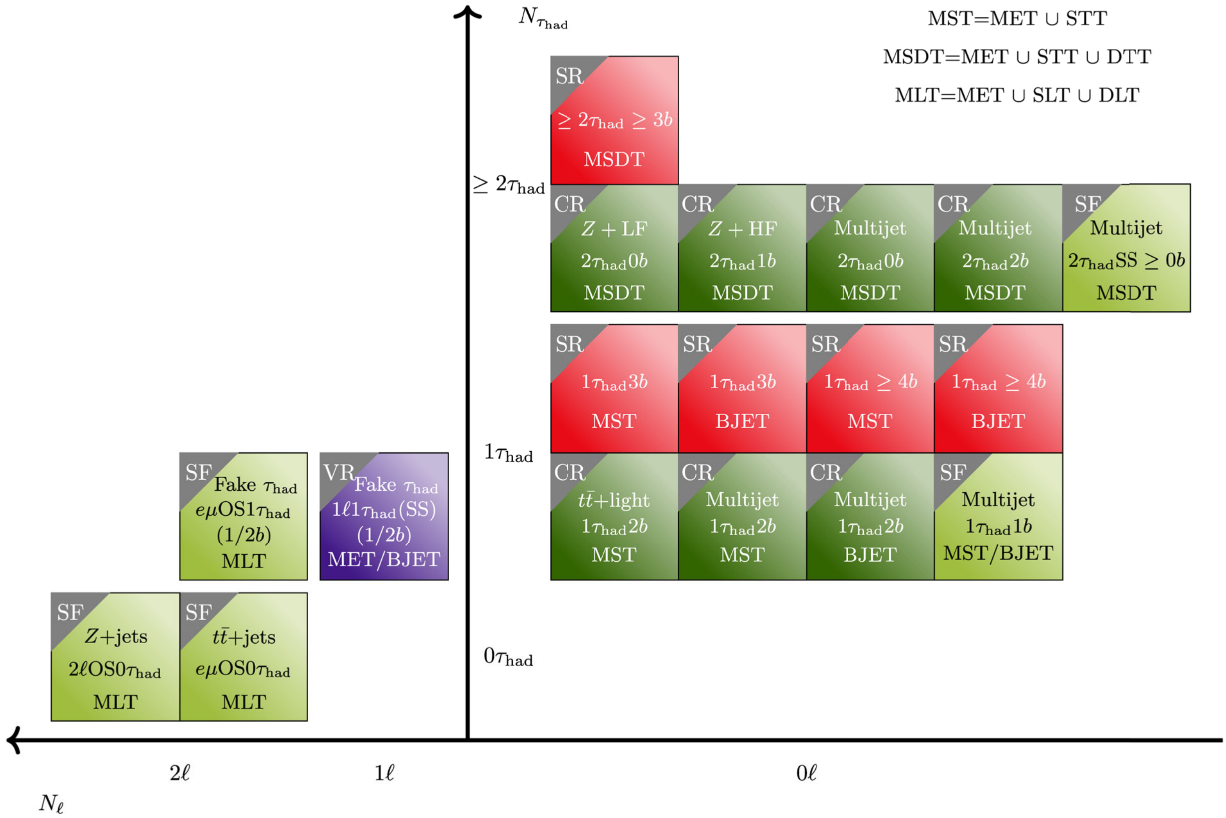

Fig. 4 A sketch of the analysis regions considered in this '4321' VLL search. The regions labelled with 'SR' ('CR') refer to the signal (control) regions, as summarised in Tables 2 and 5. They are used in the simultaneous profile likelihood fit, as discussed in Sect. 8. The regions labelled with 'SF' are used for the derivation of correction factors which depend on event kinematics for the $t\bar{t}$ + jets, Z + jets, fake τ_{had} and multijet background. The validation region 'VR' is used to verify the modelling of the fake τ_{had} background mainly originating from $t\bar{t}$ + jets and W/Z + jets processes. The selections for 'SF' and 'VR' regions are summarised in Table 4. The Z + LF (Z + HF) region is enriched in Z boson events without (with) additional b-tagged jets. A few analysis regions with different trigger selections are labelled with abbreviated notations: MST for the combined MET and STT trigger categories, MSDT for the combined MET, STT and DTT trigger categories, and MLT for the combination of MET triggers with SLT or DLT triggers

5 Search strategy

Based on the considered model, the analysis targets VLL pair production in the final state with one or more τ_{had} candidates and three or more b-jets. A set of orthogonal analysis regions are defined to constrain the background and to maximise the signal sensitivity. Given the different thresholds and topologies of the triggers considered, the analysis regions are categorised with a combination of trigger selections to capture events with a single high-p_T τ_{had} candidate, multiple τ_{had} candidates with softer p_T, large multiplicity of b-jets, or high E_T^{miss}. Furthermore, the signal events are split depending on the number of τ_{had} and the number of b-jets, leading to five signal regions (SRs) in total, as highlighted in the schematic diagram of Fig. 4 and described in Sect. 5.1. These regions are devoid of any isolated light leptons satisfying loose identification with a minimum p_T of 10 GeV. Each of these categories shows a different composition of background, with main contributions from $t\bar{t}$ + jets (with real τ_{had} or with jets misidentified as τ_{had}, also called fake τ_{had}), Z + jets and multijet productions. Multivariate analysis techniques are used to search for a VLL pair in all signal regions, and the distribution of a neural network (NN) discriminant score is used in the final likelihood fit discussed in Sect. 8 to extract the signal yield.

The data-driven estimation of $t\bar{t}$ + jets and Z + jets backgrounds is carried out in two main steps. First, kinematic-dependent corrections are derived to address MC mismodelling using dedicated scale-factor (SF) regions and are then applied to the respective background events in all relevant analysis regions. Dedicated regions enriched in either $t\bar{t}$+jets or Z + jets featuring two light leptons, as shown in Fig. 4, are used only for deriving these corrections. In a second stage, the normalisation of individual processes, categorised into light- and heavy-flavour additional jets, is determined from the likelihood fit. The associated production of $t\bar{t}$ with additional b-jets or c-jets from QCD emissions is known to be poorly modelled in the MC simulations [117,118]. Three individual

Table 2 Summary of the selections in each of the five signal regions. The 'OS' refers to an opposite-charge τ_{had} pair. A few combinations of trigger selections used in the analysis regions are labelled with abbreviated notations: MST for the combined MET and STT trigger categories, and MSDT for the combined MET, STT and DTT trigger categories. The last row refers to the neural network (NN) score distributions in the specified event categories considered for the optimisation of the signal classification, as described in Sect. 5.2

Signal Region	$1\tau_{had}3b$ MST	$1\tau_{had} \geq 4b$ MST	$1\tau_{had}3b$ BJET	$1\tau_{had} \geq 4b$ BJET	$\geq 2\tau_{had} \geq 3b$ MSDT		
Triggers	MET $\cup$ STT		BJET		MET	STT	DTT
Number of τ_{had}	1				≥ 2	2 (OS) or ≥ 3	
τ_{had} identification	Tight				≥ 1 Loose	≥ 1 Medium	≥ 2 Medium
Number of b-tags @77%	3	≥ 4	3	≥ 4	≥ 3		
Number of jets	≥ 4				≥ 3		
NN score distribution	NN ($1\tau_{had}$ MST)		NN ($1\tau_{had}$ BJET)		NN ($\geq 2\tau_{had}$ MSDT)		

categories are hence considered for the $t\bar{t}$ + jets process, and the corresponding normalisations are determined from the fit to data, as discussed in Sect. 6.1.

Dedicated control regions, as shown in Fig. 4, are defined to estimate the multijet background separately in events with $1\tau_{had}$ and $\geq 2\tau_{had}$ using data-driven techniques as described in Sect. 6.

5.1 Signal region definitions

The signal events selected with at least one τ_{had} satisfying loose identification with p_T above 20 GeV and three or more b-jets with $p_T > 25$ GeV are required to pass either of the four trigger categories: STT, DTT, MET and BJET. The τ_{had} identification criteria are further tightened depending on the τ_{had} multiplicity and the trigger selections, as summarised in Table 2 for the five signal regions. Events consisting of a single τ_{had} candidate passing the high p_T threshold STT or MET trigger are dominated by backgrounds from $t\bar{t}$ + jets with real or fake τ_{had}, while those passing the BJET trigger category have substantial contributions from multijet events. Due to these differences in the background composition, the single τ_{had} events are categorised into MST and BJET triggers, which are further split into two regions: one selecting exactly three b-tagged jets ($3b$), and the other at least four b-tagged jets ($\geq 4b$) thus allowing an improved estimation of the background with higher heavy-flavour jet content. The MST refers to the combined MET and STT trigger category. No further splitting is done in the region with two or more τ_{had}, because of limited statistics. This region is referred to as $\geq 2\tau \geq 3b$ MSDT, where the acronym MSDT refers to the combined MET, STT and DTT trigger categories. The events selected by the BJET triggers are not considered in this region given their negligible additional contribution to the signal acceptance. The main background source in this region is $t\bar{t}$ + jets with substantial contributions from processes with fake τ_{had} candidates. The signal acceptance times efficiency is presented in Fig. 5 for the three categories of selections: $1\tau_{had} \geq 3b$ MST, $1\tau_{had} \geq 3b$ BJET, and $\geq 2\tau_{had} \geq 3b$ MSDT, illustrating complementary contributions to the signal acceptance from various trigger combinations. The $1\tau_{had} \geq 3b$ MST region is the combination of the $1\tau_{had}3b$ MST and $1\tau_{had} \geq 4b$ MST signal regions, whereas the region $1\tau_{had} \geq 3b$ BJET is the combination of the $1\tau_{had}3b$ BJET and $1\tau_{had} \geq 4b$ BJET signal regions.

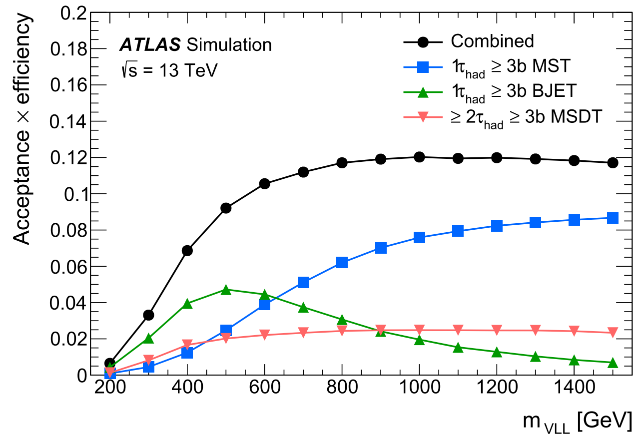

Fig. 5 The expected acceptance times efficiency (including object identification and reconstruction, trigger selection, and event selection) for VLL signal as a function of m_{VLL} for the combined signal regions as well as for three signal region categories: $1\tau_{had} \geq 3b$ MST, $1\tau_{had} \geq 3b$ BJET and $\geq 2\tau_{had} \geq 3b$ MSDT. The region $1\tau_{had} \geq 3b$ MST refers to the combination of the $1\tau_{had}3b$ MST and $1\tau_{had} \geq 4b$ MST signal regions, while the region $1\tau_{had} \geq 3b$ BJET refers to the combination of the $1\tau_{had}3b$ BJET and $1\tau_{had} \geq 4b$ BJET signal regions

5.2 Optimisation of signal classification with neural networks

Three NNs are optimised based on the type and composition of backgrounds in specific signal regions, while the statistical interpretation is performed using the score distribution in the five SRs as the final discriminant variables to extract the signal. The NNs are parameterised in terms of the VLL mass to obtain optimal signal sensitivity and smooth interpolations across the mass range [119]. This approach is equivalent to training the signal against the background for each signal mass hypothesis separately. Each NN is conditioned on a

Table 3 Summary of variables used as input to the parameterised neural network trained for three different event categories

Variable	Event category		
	$1\tau_{\text{had}} \geq 3b$ MST	$1\tau_{\text{had}} \geq 3b$ BJET	$\geq 2\tau_{\text{had}} \geq 3b$ MSDT
n^{trig}	✓		✓
$p_{\text{T},\tau_{\text{had}},0}$	✓	✓	✓
$p_{\text{T},\tau_{\text{had}},1}$			✓
$p_{\text{T},\tau_{\text{had}},2}$			✓
N_{jets}	✓	✓	✓
$N_{\tau_{\text{had}}}$			✓
$H_{\text{T,jets}}$	✓	✓	✓
$E_{\text{T}}^{\text{miss}}$	✓	✓	✓
$m(\tau_{\text{had},0}, \tau_{\text{had},1})$			✓
$m(\tau_{\text{had},0}, b_0)$	✓	✓	✓
$m(b_0 b_1, \tau_{\text{had},0})$	✓	✓	✓
$m(b_0 b_1, E_{\text{T}}^{\text{miss}})$	✓	✓	✓
Σb^{PCB}	✓		✓
$n^{\tau_{\text{had}}\text{ID}}$			✓
$\min(\Delta\phi(E_{\text{T}}^{\text{miss}}, \text{jets}))$	✓	✓	✓
$\min(\Delta\phi(E_{\text{T}}^{\text{miss}}, \tau_{\text{had}}))$	✓	✓	✓
$N_{\text{trk}}^{\tau_{\text{had}}}$	✓	✓	✓
$Q_{\tau_{\text{had},0}}$	✓	✓	✓
$\Sigma Q_{\tau_{\text{had}}}$			✓

signal mass parameter which scans the range of VLL masses under investigation. For each VLL mass point considered, a distinct NN score distribution for the signal, the SM background, and data is evaluated. Hence, the statistical analysis is performed separately for each assumed mass value of the VLL signal model, as the data and background distributions of the NN score change with the mass value. The NN consists of two hidden dense layers with 35 nodes each and an output layer with two nodes, implemented in Keras [120] with the Tensorflow [121] backend.

Three event categories are used to train separate NNs, as listed in Table 3. The NNs are trained using input variables based on jet and τ_{had} multiplicities, b-jets and τ_{had} identification qualities, the trigger categories, and kinematics and angular quantities. The input variables are defined below:

- n^{trig} is a trigger category index referring to which trigger has selected the event inside the category, i.e. 1 for MET, 2 for STT, and 3 for DTT. This variable is used as an input to an NN only when the multiple event categories are merged.
- $p_{\text{T},\tau_{\text{had}},0}$ is the p_{T} of the leading τ_{had} in the event.
- $p_{\text{T},\tau_{\text{had}},1}$ is the p_{T} of the sub-leading τ_{had} in the event.
- $p_{\text{T},\tau_{\text{had}},2}$ is the p_{T} of the third-leading τ_{had} in the event.
- N_{jets} is the number of reconstructed jets.
- $N_{\tau_{\text{had}}}$ is the number of τ_{had} candidates.
- $H_{\text{T,jets}}$ is the scalar sum of p_{T} of all jets in the event.
- $E_{\text{T}}^{\text{miss}}$ is the missing transverse energy.
- $m(\tau_{\text{had},0}, \tau_{\text{had},1})$ is the invariant mass of the two leading τ_{had} candidates.
- $m(\tau_{\text{had},0}, b_0)$ is the invariant mass of the leading τ_{had} and the leading b-jet.
- $m(b_0 b_1, \tau_{\text{had},0})$ is the invariant mass of the system of the leading b-jets pair and the leading τ_{had}.
- $m(b_0 b_1, E_{\text{T}}^{\text{miss}})$ is the invariant mass of the system of the two leading b-jets and the $E_{\text{T}}^{\text{miss}}$.
- Σb^{PCB} is the sum of the pseudo-continuous b-tagging efficiency score for all jets in the event. Each jet score ranges from 1 to 5, corresponding to a certain range of b-tagging efficiencies defined by the working points: 100–85%, 85–77%, 77–70%, 70–60%, and $< 60\%$.
- $n^{\tau_{\text{had}}\text{ID}}$ is an integer variable (0–8) that encodes the τ_{had}-identification working points of up to two leading τ_{had} candidates in an event. The exclusive identification working points considered are Loose-not-Medium, Medium-not-Tight, and Tight. The event score is determined by the combination of working points assigned to the leading and sub-leading τ_{had}.
- $\min(\Delta\phi(E_{\text{T}}^{\text{miss}}, \text{jets}))$ is the minimum angle in the transverse plane between the $E_{\text{T}}^{\text{miss}}$ and any jets.

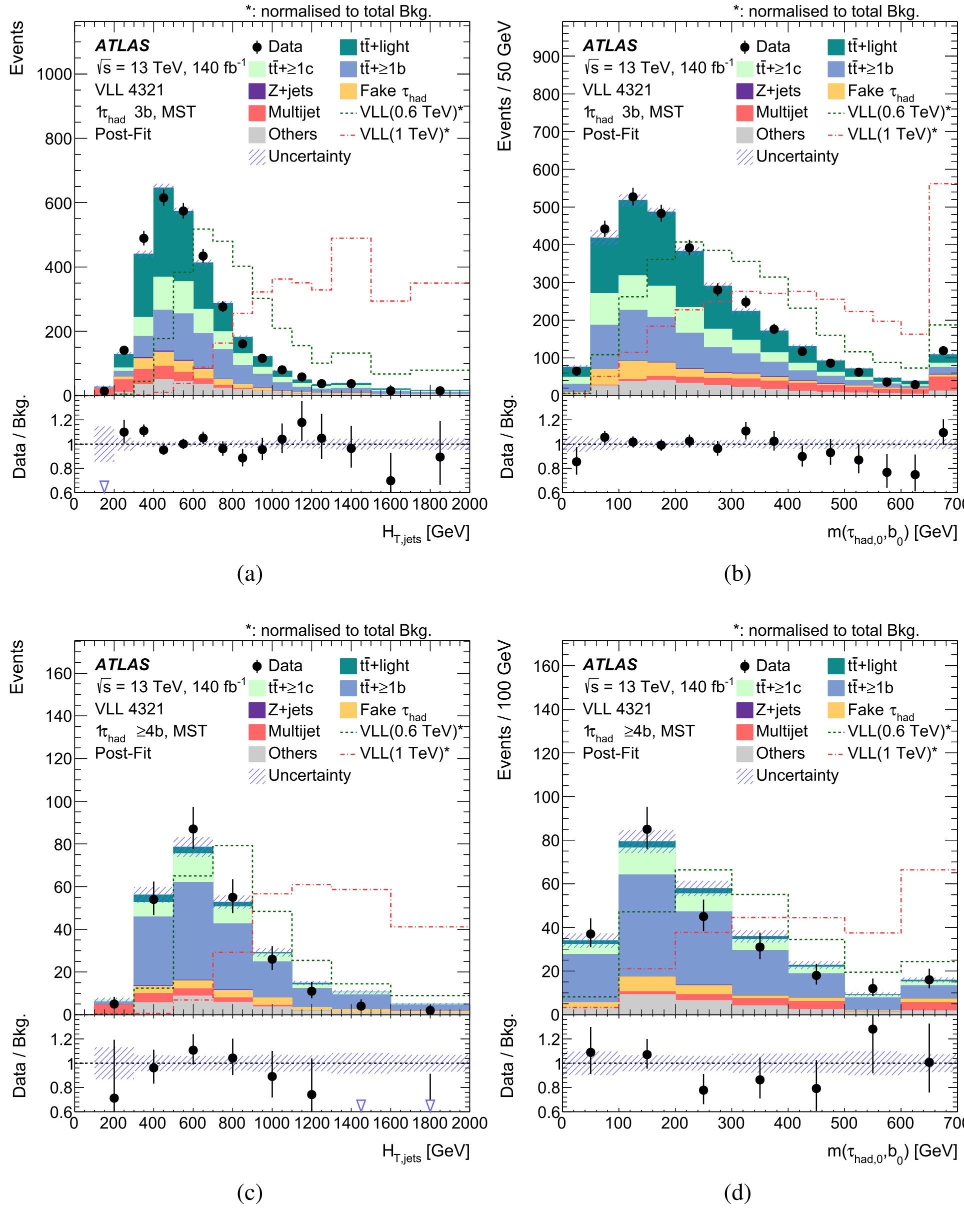

Fig. 6 Post-fit background (filled histograms) and data (dots with statistical error bars) distributions of representative NN input variables in the $1\tau_{\mathrm{had}} \geq 3b$ MST signal regions; **a** $H_{\mathrm{T,jets}}$ and **b** $m(\tau_{\mathrm{had},0}, b_0)$ in the $1\tau_{\mathrm{had}}3b$ MST region, **c** $H_{\mathrm{T,jets}}$ and **d** $m(\tau_{\mathrm{had},0}, b_0)$ in the $1\tau_{\mathrm{had}} \geq 4b$ MST region. The normalisation and shape of the backgrounds are determined from the background-only likelihood fit to data and the ratios of the data to the sum of the predicted backgrounds are shown in the lower panels. The hatched band indicates the combined statistical and systematic uncertainty in the total background prediction. The expected distributions for 0.6 TeV and 1.0 TeV VLL signals, normalised to the background yields, are overlaid (dashed lines). The last bin includes the overflow

- $\min(\Delta\phi(E_{\mathrm{T}}^{\mathrm{miss}}, \tau_{\mathrm{had}}))$ is the minimum angle in the transverse plane between the $E_{\mathrm{T}}^{\mathrm{miss}}$ and any τ_{had}.
- $N_{\mathrm{trk}}^{\tau_{\mathrm{had}}}$ is the number of reconstructed tracks associated with the leading τ_{had}.
- $Q_{\tau_{\mathrm{had},0}}$ is the charge of the leading τ_{had}.
- $\Sigma Q_{\tau_{\mathrm{had}}}$ denotes the sum of charges of up to four τ_{had} candidates ordered in p_{T}. This variable is considered in events with two or more τ_{had} candidates.

A selection of representative input distributions, after the background corrections described in Sect. 6 and the final fit outlined in Sect. 8, are presented in Figs. 6, 7, and 8 for the $1\tau_{\mathrm{had}} \geq 3b$ MST, the $1\tau_{\mathrm{had}} \geq 3b$ BJET, and the $\geq 2\tau_{\mathrm{had}} \geq 3b$ MSDT signal regions, respectively. The $1\tau_{\mathrm{had}} \geq 3b$ MST region is dominated by contributions from $t\bar{t}$+jets processes, the $1\tau_{\mathrm{had}} \geq 3b$ BJET region has substantial contributions from the multijet production, while the $\geq 2\tau_{\mathrm{had}} \geq 3b$ MSDT region suffers from large contributions from the $t\bar{t}$ + jets processes with real or misidentified τ_{had}. The input variables in these regions are consistent between the data and the SM background predictions within two standard deviations.

The NNs are trained against the main $t\bar{t}$ + jets, Z + jets, and multijet backgrounds taking into account both the true and misidentified τ_{had} components with the latter corrected as described in Sect. 6. The jet multiplicity and additional jets flavour components are corrected in the $t\bar{t}$ + jets sample, as described in Sect. 6, before employing them for training. For the signals, the generated mass m_{VLL} is used as a parameterisation input in addition to the input variables described above, while in the case of the backgrounds a pseudo-mass is assigned based on the generated m_{VLL} value such that the training is dependent on the m_{VLL} mass. Sample weights are

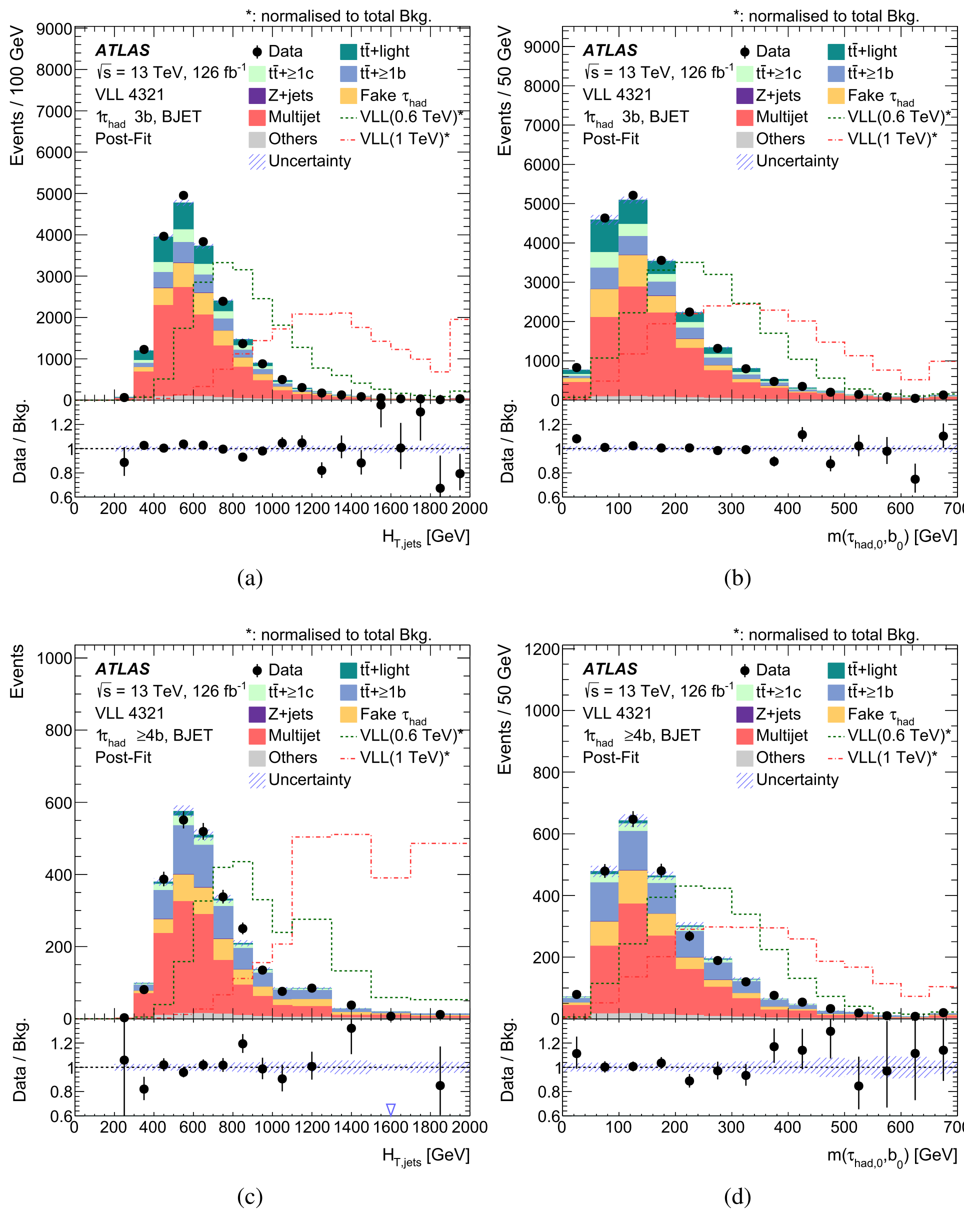

Fig. 7 Post-fit background (filled histograms) and data (dots with statistical error bars) distributions of representative NN input variables in $1\tau_{\text{had}} \geq 3b$ BJET signal regions; **a** $H_{\text{T,jets}}$ and **b** $m(\tau_{\text{had},0}, b_0)$ in the $1\tau_{\text{had}}3b$ BJET region, **c** $H_{\text{T,jets}}$ and **d** $m(\tau_{\text{had},0}, b_0)$ in the $1\tau_{\text{had}} \geq 4b$ BJET region. The normalisation and shape of the backgrounds are determined from the background-only likelihood fit to data and the ratios of the data to the sum of the predicted backgrounds are shown in the lower panels. The hatched band indicates the combined statistical and systematic uncertainty in the total background prediction. The expected distributions for 0.6 TeV and 1.0 TeV VLL signals, normalised to the background yields, are overlaid (dashed lines). The last bin includes the overflow

calculated such that the signal-to-background ratio is balanced across all mass points. Comparing the output between the training dataset and an independent testing dataset shows no sign of overtraining. The resulting NN score distributions, which peak at higher values for VLL signals than for the background processes, are used as the analysis discriminants. The NN score distributions are binned to maximise the signal significance against the background in each SR while ensuring sufficient statistics in each bin.

6 Background estimation

The composition of the SM processes varies in different signal regions, with major contributions arising from $t\bar{t}$ + jets events with real or fake τ_{had} components and from multijet production. The Z + jets process enhanced in heavy-

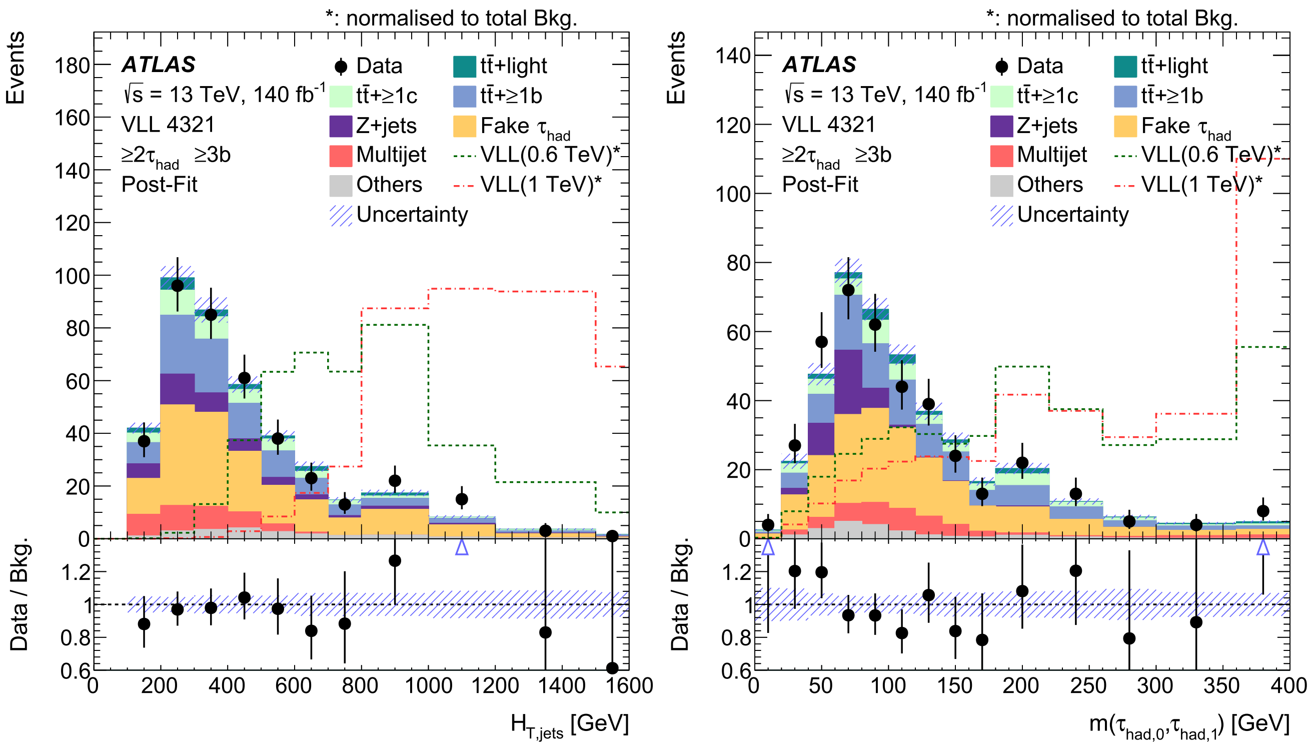

(a) (b)

Fig. 8 Post-fit background (filled histograms) and data (dots with statistical error bars) distributions of representative NN input variables in the $2\tau_{\mathrm{had}} \geq 3b$ MSDT signal region: **a** $H_{\mathrm{T,jets}}$ and **b** $m(\tau_{\mathrm{had},0}, \tau_{\mathrm{had},1})$. The normalisation and shape of the backgrounds are determined from the background-only likelihood fit to data and the ratios of the data to the sum of the predicted backgrounds are shown in the lower panels. The hatched band indicates the combined statistical and systematic uncertainty in the total background prediction. The expected distributions for 0.6 TeV and 1.0 TeV VLL signals, normalised to the background yields, are overlaid (dashed lines). The last bin includes the overflow

flavour component, labelled $Z+\mathrm{HF}$ hereafter, contributes as a small background. As the processes with a large heavy-flavour content contributing to the analysis regions are poorly modelled, the contributions from these aforementioned processes are estimated using data-driven techniques in dedicated control regions, where the signal contamination is negligible. Other rare processes contributing as irreducible background are estimated using MC simulations. The modelling of background processes is validated in the five SRs with $1\tau_{\mathrm{had}}$ and $\geq 2\tau_{\mathrm{had}}$ event selections using the lower bins of NN score variable distributions. The data-driven estimation of the $t\bar{t}+\mathrm{jets}$, $Z+\mathrm{jets}$ and multijet background processes are described in the following sections.

6.1 $t\bar{t}+\mathrm{jets}$ background

The $t\bar{t}+\mathrm{jets}$ processes are an important background in this search, in particular the processes with at least one additional heavy-flavour jet. The jets mis-tagged as b-jets further enhance the background rate. The state-of-the-art predictions of $t\bar{t}+\mathrm{jets}$ processes at NLO in QCD suffer from large uncertainties in the phase space with multiple jets. The kinematics of the top quark as predicted in the NNLO+NNLL QCD and NLO EW calculation [122] better describe the measurements as compared with the predictions at NLO. However, these calculations are inclusive in additional jet flavour, and may not describe the data well at high jet multiplicities. It is therefore crucial and common to constrain the modelling of $t\bar{t}+\mathrm{jets}$ process using data. The $t\bar{t}$ process with both top quarks decaying semileptonically (into e or μ) provides a much cleaner final state compared to that with hadronic decays (into hadrons or τ_{had}). A scale factor region selected with an electron, a muon and two or more jets is used to first derive $t\bar{t}$ modelling corrections for the reconstructed jet multiplicity spectrum and for the composition of additional flavoured jets in the $t\bar{t}+\mathrm{jets}$ sample. The final normalisation of $t\bar{t}+\mathrm{jets}$ with heavy-flavour components in the signal regions is determined from the simultaneous fit to data in the signal and control regions selected with at least one τ_{had} and no light leptons. The multiple steps involved in deriving the corrections are described in the following.

First, the MC simulated $t\bar{t}$ events are reweighted using an iterative recursive procedure to correct the parton level distributions of the top quark p_{T}, invariant mass of the $t\bar{t}$

Table 4 Summary of the selections which define the regions used to determine the reducible background shape correction to the $t\bar{t}+$jets, $Z+$jets and fake τ_{had} processes, and to validate the fake τ_{had} modelling. The 'SF' ('VR') stands for the scale factor determination (validation) region. The 'OS′ refers to an opposite-charge light-lepton pair, $m_{\ell\ell}$ denotes the invariant mass of two light leptons, and m_Z is the Z boson mass. The two columns under the fake τ_{had} SF category refer to the regions enriched in $t\bar{t}+$jets and $Z+$jets, in respective order. The 'SS′ refers to the same-charge τ_{had} pair

Selections	$t\bar{t}+$jets SF	$Z+$jets SF	Fake τ_{had} SF		Fake τ_{had} VR	Multijet SF	
Triggers	SLT ∪ DLT ∪ MET				MET || BJET	STT || BJET	STT || DTT
Number of b-tags	—		1 or 2 @85%		1 or 2 @77%	1@77%	0,1,2, ≥3@77%
Number of jets	≥2					≥1	≥3
Number of τ_{had}	0		1			1	2(SS)
Number of e/μ	$e\mu$OS	eeOS or $\mu\mu$OS	$e\mu$OS	eeOS or $\mu\mu$OS	1 (same charge as τ_{had})	0	
Lepton p_{T} [GeV]	(20, 20)					—	
Lepton identification	Electron: TightLH					—	
	Muon: Medium					—	
$m_{\ell\ell}$ [GeV]	—	> 15			—	—	
$\|m_{\ell\ell} - m_Z\| < 10$ [GeV]	—	yes	—	yes	—	—	

system, and the p_{T} of the $t\bar{t}$ system to those predicted by the NNLO+NNLL QCD and NLO EW corrections [122]. Second, the corrections for the jet multiplicity are determined for the reweighted $t\bar{t}$ sample using a scale factor region as described in the second column of Table 4. The background contamination from other processes is less than 11% in this region. The corrections are defined as the ratio of data events after subtracting all non-$t\bar{t}$ background to the predicted $t\bar{t}$ events in each jet multiplicity bin. They range from 5% for events with two jets to about 30% for 10 or more jets.

In the next step, the MC events in the above mentioned scale factor region are further categorised (following the definitions described in Ref. [123,124]) depending on the truth flavour of additional QCD jets produced with $t\bar{t}$. If there is at least one additional b-jet, the event is classified as $t\bar{t}+\geq 1b$; if there is no additional b-jet, but an additional c-jet is present, it is classified as $t\bar{t}+\geq 1c$, or else, as $t\bar{t}+$ light. Templates are created for the three components of $t\bar{t}$ in terms of a discriminating variable defined as the sum of b-tagging score (Σb^{PCB}), where each jet score refers to a range of average b-tagging efficiencies. A likelihood fit is performed to data in the scale factor determination region for the estimation of the normalisation factors of the three $t\bar{t}+$jets categories. These estimated normalisation factors are used as initial corrections to the $t\bar{t}$ MC events in all analysis regions.

Finally, the normalisation of $t\bar{t}+\geq 1b$, $t\bar{t}+\geq 1c$ and $t\bar{t}+$light processes is determined in the simultaneous likelihood fit to data in the signal and control regions consisting of one or more τ_{had} but depleted in light leptons. The fit setup is outlined in Sect. 8. The control region, as summarised in Table 5, is characterised by events with one τ_{had}, at least four jets, of which two are b-tagged at the 77% efficiency working point [108], and $E_{\text{T}}^{\text{miss}}$ above 100 GeV. Events are required to satisfy the MET or STT triggers. The normalisation of $t\bar{t}+\geq 1b$, $t\bar{t}+\geq 1c$ and $t\bar{t}+$ light categories in the alternative $t\bar{t}+$jets samples used to estimate systematic uncertainties are scaled to the estimation of $t\bar{t}+\geq 1b$, $t\bar{t}+\geq 1c$ and $t\bar{t}+$ light yields in the nominal $t\bar{t}$ sample, such that only the shape uncertainties are taken into account in the final fit. The measured normalisation factors (including the initial normalisation corrections estimated from scale factor regions selected with light leptons) are 0.93 ± 0.10, 1.27 ± 0.53, and 1.41 ± 0.32 for $t\bar{t}+$light, $t\bar{t}+\geq 1c$ and $t\bar{t}+\geq 1b$ components, respectively, where the quoted error includes all uncertainties. The correlation factor between the $t\bar{t}+$light ($t\bar{t}+\geq 1c$) and $t\bar{t}+\geq 1b$ normalisation estimators is about 50% (60%), whereas the normalisation factors of $t\bar{t}+$light and $t\bar{t}+\geq 1c$ have an anti-correlation factor of 60%. The measured values refer to the case where the NN score is evaluated for data and the SM background corresponding to a VLL mass of 1 TeV, they do not change significantly for the other mass values.

6.2 $Z+$jets background

The corrections to the MC simulated $Z+$jets events are derived in terms of the reconstructed jet multiplicity using the region consisting of two opposite-charge same-flavour light leptons, each with p_{T} above 20 GeV and with an invariant mass within 10 GeV of the Z boson mass. The number of jets exhibits good consistency between the data and MC at low multiplicity of up to five jets. However, it requires a correction at the level of 25% when it increases to 10 jets.

After the scale factors are applied to the $Z+$jets MC events correcting for the reconstructed jet multiplicity, the normalisation of $Z+$jets is determined using events containing at least two τ_{had} and no light leptons. The $Z+$jets MC events are split in two orthogonal components, denoted as as $Z+$LF and $Z+$HF, depending on the truth flavour of the jets produced in association with the Z boson. The $Z+$HF component

Table 5 Summary of the selection requirements for each of the seven control regions. Each control region is labelled depending on the combination of triggers, the multiplicity of τ_{had} candidates, number of b-jets, and other kinematic requirements. The $E_{\text{T,lo}}^{\text{miss}}$ ($E_{\text{T,hi}}^{\text{miss}}$) refers to the low (high) $E_{\text{T}}^{\text{miss}}$ regions. The $m_{\tau\tau,\text{lo}}^{\text{coll}}$ ($m_{\tau\tau,\text{hi}}^{\text{coll}}$) refers to regions with low (high) range of the invariant mass variable $m_{\tau\tau}^{\text{coll}}$ as described in Sect. 6.2. The 'OS' refers to opposite charge τ_{had} pair. The $Z+$LF ($Z+$HF) refers to the region enriched in Z boson events without (with) additional b-tagged jets

Control region	$t\bar{t}+$light $1\tau_{\text{had}}2b$ $E_{\text{T,hi}}^{\text{miss}}$ MST	Multijet $1\tau_{\text{had}}2b$ $E_{\text{T,low}}^{\text{miss}}$ MST	 $1\tau_{\text{had}}2b$ $E_{\text{T,low}}^{\text{miss}}$ BJET	 $2\tau_{\text{had}}0b$ $m_{\tau\tau,\text{hi}}^{\text{coll}}$	$Z+$LF $2\tau_{\text{had}}0b$ $m_{\tau\tau,\text{low}}^{\text{coll}}$	$Z+$HF $2\tau_{\text{had}}1b$ $m_{\tau\tau,\text{low}}^{\text{coll}}$	Multijet $2\tau_{\text{had}}2b$
Triggers	MET ∪ STT		BJET	MET ∪ STT ∪ DTT			
Number of τ_{had}	1			2 (OS) or ≥ 3 (STT, DTT), or ≥ 2 (MET)			
Number of e/μ	0						
Number of jets	≥ 4			≥ 3			
Number of b-tags	2@77%			0@77%		1@77%	2@77%
$m_{\tau\tau}^{\text{coll}}$	-			> 120 GeV	< 120 GeV		-
E_T^{miss}	> 100 GeV	< 100 GeV		-			
Fit variable	Event yield						$n^{\tau_{\text{had}}\text{ID}}$

consists of events with at least one reconstructed jet matched to a truth b-jet or c-jet, and all remaining events are classified as $Z+$LF. Two orthogonal control regions selected with events containing two τ_{had} candidates and at least three jets are summarised in Table 5. One region is dominated with $Z+$LF events with the presence of no b-tagged jet and the other, having one b-tagged jet, is enriched in $Z+$HF events. A mass variable $m_{\tau\tau}^{\text{coll}}$ is constructed under the approximation [125] that the neutrino is collinear with the visible decay products of τ_{had} and is the only source of $E_{\text{T}}^{\text{miss}}$ in the event. It is defined as $m_{\tau_{\text{had}}\tau_{\text{had}}}/\sqrt{x_{\tau_{\text{had},0}}x_{\tau_{\text{had},1}}}$, where $m_{\tau_{\text{had}}\tau_{\text{had}}}$ is the invariant mass of the τ_{had} pair and $x_{\tau_{\text{had},0}}$ ($x_{\tau_{\text{had},1}}$) is the fraction of the original p_{T} of the leading (sub-leading) reconstructed τ_{had} that is carried by its visible decay products. The original p_{T} refers to the total estimated p_{T} of τ_{had}, obtained by combining the visible decay products with a component of the $E_{\text{T}}^{\text{miss}}$ associated with neutrinos from tau decay. The variable $x_{\tau_{\text{had},0/1}}$ expressed in terms of the kinematic variables of τ_{had} and $E_{\text{T}}^{\text{miss}}$ is given by

$$x_{\tau_{\text{had},0/1}} = \frac{p_{\text{T},\tau_{\text{had},0/1}}}{p_{\text{T},\tau_{\text{had},0/1}} + \frac{E_T^{\text{miss}}(\sin(\phi_{E_T^{\text{miss}}})-\sin(\phi_{\tau_{\text{had},1/0}}))}{\sin(\phi_{\tau_{\text{had},0/1}})-\sin(\phi_{\tau_{\text{had},1/0}})}},$$

where $\phi_{E_T^{\text{miss}}}$ is the azimuth coordinate of the missing transverse momentum, and $\phi_{\tau_{\text{had},0}}$ ($\phi_{\tau_{\text{had},1}}$) is the azimuth coordinate of the leading (sub-leading) τ_{had}. The $Z+$jets enriched region is selected with the requirement of $m_{\tau\tau}^{\text{coll}}$ below 120 GeV. The measured values of normalisation factors for $Z+$LF and $Z+$HF determined from the fit to data in the signal and control regions considering the background-only hypothesis and an m_{VLL} of 1 TeV for the NN score distribution are 1.23 ± 0.11 and 1.13 ± 0.10, respectively, where the quoted error includes all uncertainties. The fitted values of the $Z+$LF and $Z+$HF normalisation factors have a correlation factor of about 50%.

6.3 Fake τ_{had} background in non-multijet production

The $t\bar{t}+$jets process also contributes as a non-negligible background when at least one of the jets is misidentified as a τ_{had}. This is one of the important contributions in the $\geq 2\tau_{\text{had}} \geq 3b$ MSDT signal region. The background is estimated using a semi-data-driven approach, where the predictions from the MC simulations are taken as baseline, and corrections are applied to the MC simulated events containing one or more fake τ_{had} depending on each fake τ_{had} p_{T} and number of associated tracks. The corrections are derived using a dedicated region enriched in $t\bar{t}+$jets events consisting of one τ_{had} with a minimum p_{T} of 20 GeV, as summarised in Table 4. As discussed in Sect. 6.1, the $t\bar{t}+$jets MC events are first corrected for the mis-modelling in the top quark kinematics at the truth level, the reconstructed jet multiplicity mis-modelling, and for the relative contributions of $t\bar{t}+\geq 1b$, $t\bar{t}+\geq 1c$ and $t\bar{t}+$light processes. The scale factors are defined as the ratio of observed yields in the control region after subtracting the non-fake-τ_{had} background to the simulated fake τ_{had} predictions in bins of the p_{T} and associated track multiplicity (1-prong or 3-prong) of the fake τ_{had}. They are also separated in terms of exclusive efficiencies of τ_{had} identification. The fake τ_{had} with $p_{\text{T}} \leq 100$ GeV have scale factors ranging from about 0.7 to 1.2 (0.8 to 1.2) for 1-prong (3-prong) fake τ_{had}, depending on the p_{T} and the identification working point. The relative statistical uncertainties in these corrections range from 10 to 30%. The scale factors for fake τ_{had} with $p_{\text{T}} > 100$ GeV range between 0.5 and 0.9 (0.9 and 1.2) for 1-prong (3-prong) fake τ_{had}, with statistical uncertainties of up to 30% ($20 - -60\%$). The fake τ_{had} rate depends on whether τ_{had} originates from a quark jet or a gluon jet. Any mis-modelling depending on the fake τ_{had} origin from quark- or gluon-jets is accounted for as systematic uncertainties in the scale factors. As the composition of quark and gluon jets is different between the $t\bar{t}$+jets and Z+jets processes, the scale factors are similarly derived using an alternative determination region dominated by Z + jets events, as listed in the right sub-column of the fake τ_{had} SF column in Table 4. These alternative SFs are consistent with the nominal within 10%. They are used as systematic variations to cover for potential differences in the fake τ_{had} origin across the control regions and the signal regions.

The estimated scale factors are validated in an independent validation region selected with one light lepton and one τ_{had} with the same charge, as summarised in Table 4. Events selected with the MET or BJET trigger category, at least two jets (of which one or two are b-tagged) and exactly one light lepton include fake τ_{had} contributions arising from various processes, such as $t\bar{t}$ + jets, W + jets and Z + jets. These processes lead to different jet flavor composition faking τ_{had}. The data show consistency with the modelling of the fake τ_{had} backgrounds. The validation of fake τ_{had} scale factors is further demonstrated in the distributions of $H_{\text{T,jets}}$ and $m(\tau_{\text{had},0}, \tau_{\text{had},1})$, as shown in Fig. 8, in the $2\tau_{\text{had}} \geq 3b$ region where the fake τ_{had} background is the dominant contribution.

6.4 Multijet production background

The multijet background originating from QCD processes is estimated using two data-driven methods: for channels with a single τ_{had} the fake factor method [126] is used, while for two or more τ_{had} channels the charge symmetry in the multijet production is exploited. Details on the selection regions used for the calculation of the scale factors can be found in Table 4.

The multijet QCD background estimate in the single τ_{had} selection uses the fake factor method and relies on Loose, Loose-not-Tight and Tight τ_{had} identification working points, where Loose-not-Tight refers to the τ_{had} identification passing the Loose but failing the Tight definition. Two independent control regions are used to estimate this background: 1) a region with Loose-not-Tight τ_{had}, but otherwise the same event selection as the $1\tau_{\text{had}}$ SRs described in Table 2; 2) a region with Loose τ_{had} and with one b-tagged jet, as described in the second-to-last column of Table 4. A transfer factor parameterised in $p_{\text{T}}^{\tau_{\text{had}}}$, defined as $\varepsilon_{\text{QCD}}(p_{\text{T}}^{\tau_{\text{had}}}) = \tilde{N}_{\text{QCD}}^{\text{T}}(p_{\text{T}}^{\tau_{\text{had}}})/\tilde{N}_{\text{QCD}}^{\text{L}}(p_{\text{T}}^{\tau_{\text{had}}})$, is derived using the region 2), where $\tilde{N}_{\text{QCD}}^{\text{T}}(p_{\text{T}}^{\tau_{\text{had}}})$ and $\tilde{N}_{\text{QCD}}^{\text{L}}(p_{\text{T}}^{\tau_{\text{had}}})$ represent the number of Tight and Loose data events, after subtracting the non-QCD background. The $\varepsilon_{\text{QCD}}(p_{\text{T}}^{\tau_{\text{had}}})$ is used to evaluate the number of QCD data events, $N_{\text{QCD}}^{\text{T}}(p_{\text{T}}^{\tau_{\text{had}}})$, in the $1\tau_{\text{had}} \geq 3b$ SRs with Tight selection:

$$N_{QCD}^{\text{T}}(p_{\text{T}}^{\tau_{\text{had}}}) = \frac{\varepsilon_{\text{QCD}}(p_{\text{T}}^{\tau_{\text{had}}})}{1-\varepsilon_{\text{QCD}}(p_{\text{T}}^{\tau_{\text{had}}})} \left[N_{\text{data}}^{\text{T-L}}(p_{\text{T}}^{\tau_{\text{had}}}) - N_{\text{nonQCD}}^{\text{T-L}}(p_{\text{T}}^{\tau_{\text{had}}})\right]$$

where $N_{\text{data}}^{\text{T-L}}(p_{\text{T}}^{\tau_{\text{had}}})$ refers to the observed event count passing Loose-not-Tight τ_{had} in region 1) and $N_{\text{nonQCD}}^{\text{T-L}}(p_{\text{T}}^{\tau_{\text{had}}})$ is the non-QCD event yield from the simulation in the same selection. This method uses the fact that the number of data events in the Loose region equals the sum of events in the Loose-not-Tight and Tight regions. The parameterised ε_{QCD} estimate is done in binned $p_{\text{T}}^{\tau_{\text{had}}}$ distributions separately for 1- and 3-prong τ_{had} in each of the STT and BJET selections. A shifted inverse power-law (linear) fit function is used for the 1-prong (3-prong) τ_{had}.

The estimated multijet background, derived from the parameterised fit functions is validated using events containing single Tight-τ_{had}, one b-jet, and at least four jets in the MST and BJET trigger categories. The data show good agreement with the predicted τ_{had} p_{T} and jet multiplicity distributions, both before and after the fit. Furthermore, Fig. 7 shows that the multijet background in the $\geq 3b$ region is well-modelled across key kinematic variables used in NN training.

Channels containing two oppositely charged τ_{had} candidates use the charge symmetry method to obtain the multijet background. In this method, the multijet yields in regions with two opposite-charge τ_{had} and two same-charge τ_{had} are assumed to be equal, $N_{\text{QCD}}^{2\tau_{\text{had}}\text{OS}} = N_{\text{QCD}}^{2\tau_{\text{had}}\text{SS}}$. The number of events in the $2\tau_{\text{had}}$SS selection is obtained from the data subtracted by the non-QCD MC events, for which corrections are applied as highlighted in Sects. 6.1 to 6.3.

The final normalisations of multijet background in the signal regions are determined in the simultaneous fit to data in the signal and control regions, as summarised in Tables 2 and 5, respectively. The measured values of the three normalisation factors in the $1\tau_{\text{had}} \geq 3b$ MST, $1\tau_{\text{had}} \geq 3b$ BJET, and $2\tau_{\text{had}} \geq 3b$ MSDT regions are 0.97 ± 0.20, 0.89 ± 0.04, 1.02 ± 0.04, respectively, with correlations of less than 20% among the corresponding fitted parameters. These values refer to the scenario where the NN score distributions in a signal region are evaluated considering the signal generated mass of 1 TeV. The multijet background estimate is validated using regions selected with $0b$, $1b$, $2b$ and $\geq 3b$ and two opposite-charge τ_{had} for the STT and DTT trigger categories, with an additional requirement of at least three jets in the region, and good agreement is found in all regions.

7 Systematic uncertainties

Various sources of systematic uncertainties are considered in the analysis. These include the uncertainties from the reconstructed objects and from the theory modelling of various physics processes that can impact the estimated signal and background rates and the shape of the fitted distributions in multiple event categories. The uncertainty on the integrated luminosity is 0.83% [127].

The uncertainties in the scale factors applied to correct for the efficiency differences between the data and MC simulations in τ_{had} [111], b-jet and $E_{\text{T}}^{\text{miss}}$ triggers, τ_{had} reconstruction and identification [100,101,128], jet reconstruction and vertex tagging [129,130], b-tagged jet identification [107], and for the pile-up modelling [131] in the simulated events as discussed in Sect. 4, are accounted for and they have a minor impact on the results. Furthermore, uncertainties are considered for the energy scale and resolution of the jets [103], τ_{had} [100] and $E_{\text{T}}^{\text{miss}}$ [109], and are found to be negligible. All of these experimental uncertainties are treated as correlated among the signal and background processes.

In order to estimate the effect of higher-order corrections in the calculations, the impact of variations in the QCD renormalisation (μ_R) and factorisation (μ_F) scales, with respect to the nominal scales, as well as the uncertainties in the PDFs are evaluated on the VLL signal acceptance in the signal regions.

Modelling uncertainties associated with the $t\bar{t}+$jets processes are evaluated by comparing the fit distributions from the nominal MC $t\bar{t}$ samples with those from the alternative MC generator predictions, as listed in Table 1. For these uncertainties, the nuisance parameters (NPs) representing the $t\bar{t}+\geq 1c$ and $t\bar{t}+$ light processes, as well as those representing various $t\bar{t}+\geq 1b$ processes ($t\bar{t}+1b$ with the additional b-jet containing one b-hadron, $t\bar{t}+1B$ with the additional b-jet containing more than one b-hadrons, $t\bar{t}+2b$, and $t\bar{t}+\geq 3b$) are treated independently in the fit. Furthermore, the overall acceptance and shape effects are estimated separately. The impact of producing the additional b-jets by an NLO QCD calculation is evaluated using the $t\bar{t}b\bar{b}$ four-flavour scheme sample as listed in Table 1. Additional uncertainties are evaluated from variations of the renormalisation and factorisation scales in the matrix element calculations by a factor of 0.5 and 2 and from the upward and downward variations of QCD scales for the initial- and final-state radiations as implemented in the parton shower model. As the $t\bar{t}+$jets events are reweighted according to NNLO+NNLL QCD and NLO EW theory predictions in terms of top quark p_{T} and the $t\bar{t}$ system p_{T} and mass, the corresponding uncertainties are applied in the analysis. As mentioned in Sect. 6.1, the normalisations of $t\bar{t}+\geq 1b$, $t\bar{t}+\geq 1c$ and $t\bar{t}+$light processes in each alternative $t\bar{t}$ MC sample are scaled, before employing the corresponding distributions in the fit, to the respective estimated yields in the nominal $t\bar{t}$ MC sample.

For the $Z+$jets process, which has a very small contribution in the signal regions, only the uncertainties in the $Z+$LF and $Z+$HF normalisation parameters are taken into account. The $W+$jets process gives a negligible contribution, so only a 5% theory uncertainty in the production cross-section is taken into account [132]. The multijet background has corresponding uncertainties assigned depending on the estimation method used for $1\tau_{\text{had}}$ and $\geq 2\tau_{\text{had}}$ regions. The statistical and systematics uncertainties in the fake τ_{had} scale factors, as discussed in Sect. 6.3, are taken into account depending on the τ_{had} p_{T} and prongness. The diboson processes have negligible contributions in the signal and control regions. The uncertainties due to the modelling of these processes are evaluated by varying the QCD renormalisation and factorisation scales by a factor of 0.5 and 2, relative to the nominal scales. A 4% uncertainty is taken in the inclusive production cross-section, and an additional uncertainty of 30% is considered for the process with heavy-flavour jets [133].

Theory uncertainties due to the modelling of $t\bar{t}W$, $t\bar{t}Z$, and $t\bar{t}H$ processes are included in the analysis. The uncertainties are evaluated by comparing the fit distributions from nominal MC samples to those from the alternative MC generator predictions of each process, as listed in Table 1. Further uncertainties are evaluated from the QCD renormalisation and factorisation scale variations by a factor of 0.5 and 2, relative to the nominal scales used in each MC sample. Uncertainties of 50% [133], 15%, [134,135] and 11% [136] are assigned on the theory cross-sections for the $t\bar{t}W$, $t\bar{t}Z$, and $t\bar{t}H$ processes, respectively.

Uncertainties in the modelling of other rare processes (such as $t(Z/\gamma^*)$, $tW(Z/\gamma^*)$, $t\bar{t}t$, $t\bar{t}W^+W^-$, VH, triboson) are taken into account by assigning uncertainties up to 50% in the production cross-sections. These are conservative uncertainties to account for limited information on the correct modelling of these background processes. The choice of the size of these uncertainties has a negligible impact on the results. The $t\bar{t}t\bar{t}$ cross-section is scaled to the measured value [137] and a 29% uncertainty is assigned as normalisation uncertainty on this background.

The impact of various categories of uncertainties on the observed signal-strength parameter μ is quantified. The parameter μ is defined as a multiplicative factor applied to the predicted yield for the pair-produced VLL signal. Table 6 summarises the impact on μ for the 0.4 TeV and 1 TeV VLL signal hypotheses. The impact of each NP on the μ is evaluated by comparing the nominal best-fit value of μ with the result of the fit when fixing the considered NP to its best-fit value shifted by its post-fit uncertainty.

8 Results

A maximum-likelihood fit is performed for each signal hypothesis on all bins of the seven CRs and five SRs defined in Sect. 5 to determine the VLL signal cross-section and the normalisation factors of the $t\bar{t}+\geq 1b$, $t\bar{t}+\geq 1c$,

Table 6 Contribution of different uncertainties to the combined likelihood fit for the observed signal strength μ, assuming a VLL mass of either 0.4 TeV or 1 TeV. The impact of each nuisance parameter (NP) is computed by comparing the nominal best-fit value of μ with the result of the fit when fixing the considered NP to its best-fit value shifted by its post-fit uncertainty. The impact of a group of NPs is obtained by summing in quadrature the impacts of all nuisance parameters in this category. The fractional contribution of an uncertainty source refers to the ratio of the uncertainty in μ resulting from the fit when fixing the corresponding NP to the uncertainty in the best-fit value of μ. The 'Other background' category refer to the uncertainties from the fake τ_{had} and the rare SM background contributions such as $t\bar{t}W$ and $t\bar{t}t\bar{t}$, the relative contribution of these backgrounds vary with the signal mass

Uncertainty component	Fractional contribution [%] $m_{\text{VLL}} = 0.4$ TeV	Fractional contribution [%] $m_{\text{VLL}} = 1$ TeV
Experimental		
Jet energy scale	5.2	3.5
Jet energy resolution	4.6	1.9
τ_{had} energy scale	9.7	1.1
τ_{had} identification	6.3	2.5
Flavour tagging	6.0	4.3
BJET trigger scale factors	6.2	2.1
STT trigger scale factors	0.2	0.3
DTT trigger scale factors	0.8	1.6
$E_{\text{T}}^{\text{miss}}$ scale and resolution	1.7	0.8
Others (JVT, pileup reweighting, luminosity)	4.3	1.1
Signal and background modelling		
Background normalisations	34	16
$t\bar{t}$ + jets modelling	47	11
QCD modelling	14	8
Other background	10	11
Signal modelling	0.1	0.1
MC statistics	34	39
Total systematics	74	46
Data statistics	67	88

$t\bar{t}$ + light, Z + LF, Z + HF, Multijet $1\tau_{\text{had}} \geq 3b$ MST, Multijet $1\tau_{\text{had}} \geq 3b$ BJET and Multijet $2\tau_{\text{had}} \geq 3b$ MSDT processes. The Multijet $2\tau_{\text{had}}2b$ control region is binned in the $n^{\tau_{\text{had}}\text{ID}}$ distribution, whereas the total event yield (i.e. a single bin) is used in the remaining control regions.

The likelihood function $\mathcal{L}(\mu, \vec{\lambda}, \vec{\theta})$ is constructed as a product of Poisson probability terms over all bins considered in the search. It depends on μ, $\vec{\lambda}$, the normalisation factors for several backgrounds (see Sect. 6), and $\vec{\theta}$, a set of NPs encoding systematic uncertainties in the signal and background expectations [138]. The predicted signal yield depends on the assumed mass m_{VLL}. Systematic uncertainties, summarised in Sect. 7, can impact the estimated signal and background rates, the migration of events between categories, and the shape of the fitted distributions. Both μ and $\vec{\lambda}$ are treated as free parameters in the likelihood fit. The NPs $\vec{\theta}$ allow variations of the expectations for signal and background according to the systematic uncertainties, subject to Gaussian constraints in the likelihood fit. Their fitted values represent the deviations from the nominal expectations that globally provide the best fit to the data. Statistical uncertainties in each bin due to the limited size of the simulated samples are taken into account by dedicated parameters using the Beeston–Barlow 'lite' technique [139].

The test statistic q_μ is defined as the profile likelihood ratio: $q_\mu = -2\ln(\mathcal{L}(\mu, \hat{\hat{\vec{\lambda}}}_\mu, \hat{\hat{\vec{\theta}}}_\mu)/\mathcal{L}(\hat{\mu}, \hat{\hat{\vec{\lambda}}}_{\hat{\mu}}, \hat{\hat{\vec{\theta}}}_{\hat{\mu}}))$, where $\hat{\mu}$, $\hat{\hat{\vec{\lambda}}}_{\hat{\mu}}$, and $\hat{\hat{\vec{\theta}}}_{\hat{\mu}}$ are the values of the parameters that maximise the likelihood function, and $\hat{\hat{\vec{\lambda}}}_\mu$ and $\hat{\hat{\vec{\theta}}}_\mu$ are the values of the parameters that maximise the likelihood function for a given value of μ. The test statistic q_μ is evaluated with the RooFit package [140]. A related statistic is used to determine the probability that the observed data are compatible with the background-only hypothesis (i.e. the discovery test) by setting $\mu = 0$ in the profile likelihood ratio (q_0). The p-value (referred to as p_0) representing the probability of the data being compatible with the background-only hypothesis is approximated using the asymptotic formulae given in Ref. [141], above the observed value of q_0.

A comparison of the distributions of observed and expected events in the five SRs is presented in Figs. 9 and 10 after the combined likelihood fit under the background-only hypothe-

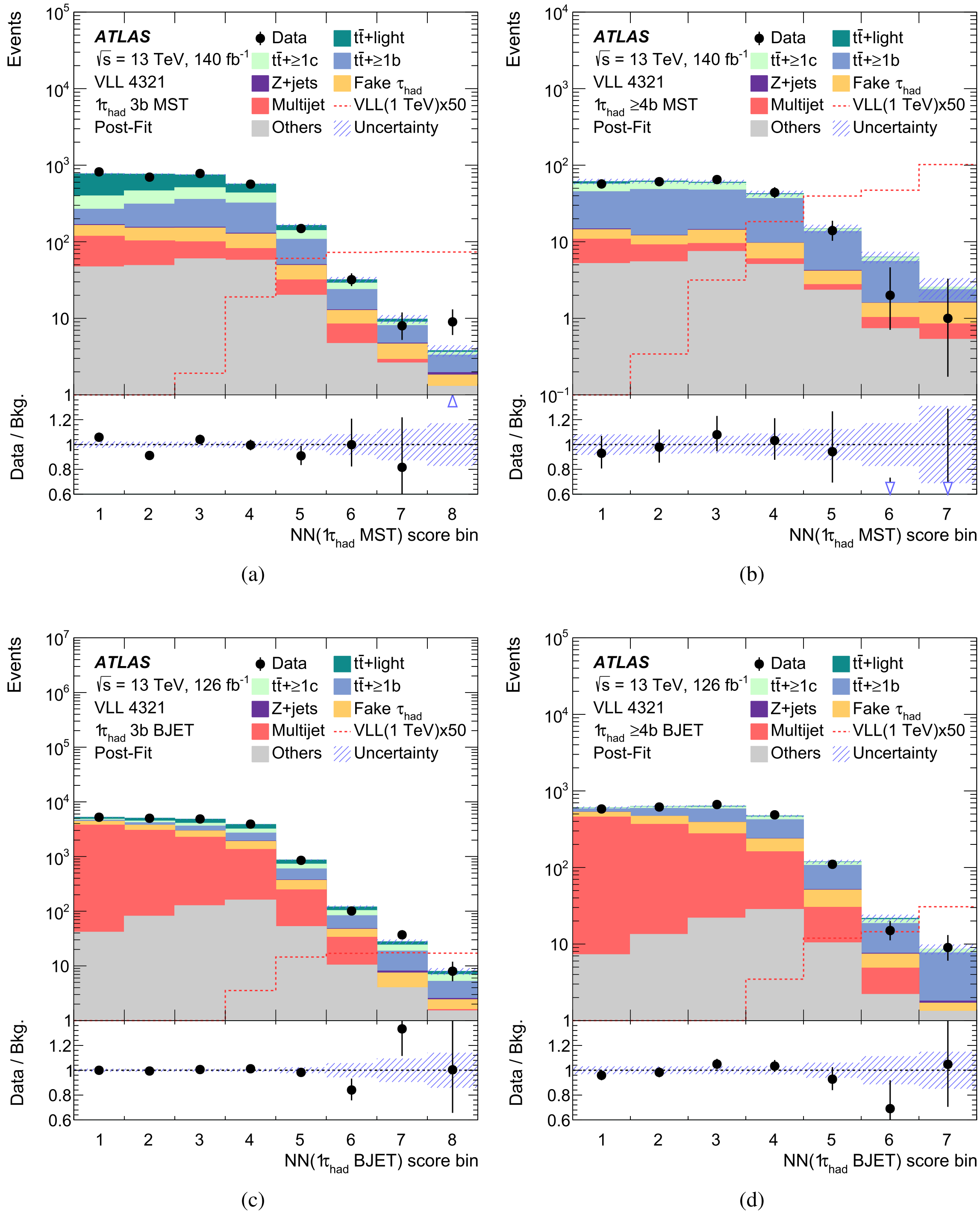

Fig. 9 Comparison between data and the background prediction for the event yields in all four $1\tau_{\text{had}}$ signal region categories: **a** $1\tau_{\text{had}}3b$ MST, **b** $1\tau_{\text{had}} \geq 4b$ MST, **c** $1\tau_{\text{had}}3b$ BJET, and **d** $1\tau_{\text{had}} \geq 4b$ BJET, with the NN distributions corresponding to m_{VLL} =1 TeV. The background contributions after the likelihood fit to data ('Post-Fit') under the background-only hypothesis are shown as filled histograms. The ratio of the data to the background ('Bkg.') prediction is shown in the lower panel. The size of the combined statistical and systematic uncertainty in the background prediction is indicated by the blue hatched band. The blue triangles indicate points that are outside the vertical range of the figure

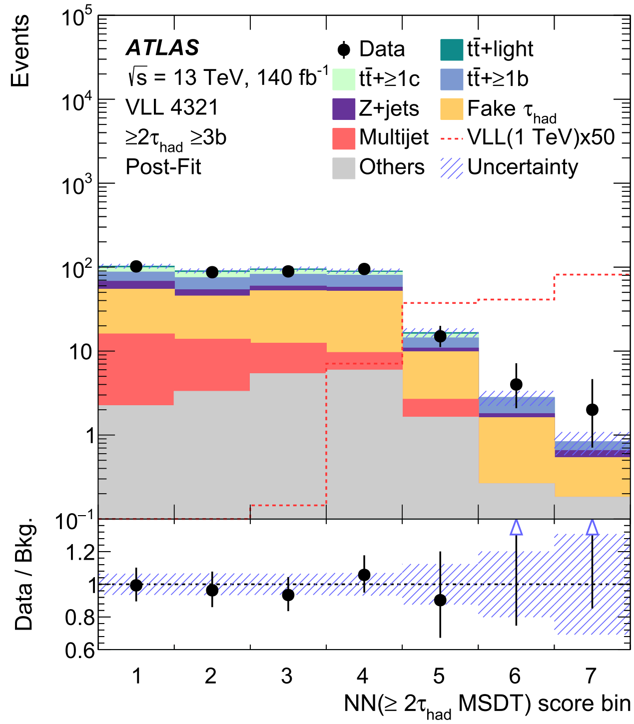

Fig. 10 Comparison between data and the background prediction for the event yields in the $2\tau_{\text{had}} \geq 3b$ MSDT signal region category with the NN distribution corresponding to m_{VLL} =1 TeV. The background contributions after the likelihood fit to data ('Post-Fit') under the background-only hypothesis are shown as filled histograms. The ratio of the data to the background ('Bkg.') prediction is shown in the lower panel. The size of the combined statistical and systematic uncertainty in the background prediction is indicated by the blue hatched band. The blue triangles indicate points that are outside the vertical range of the figure

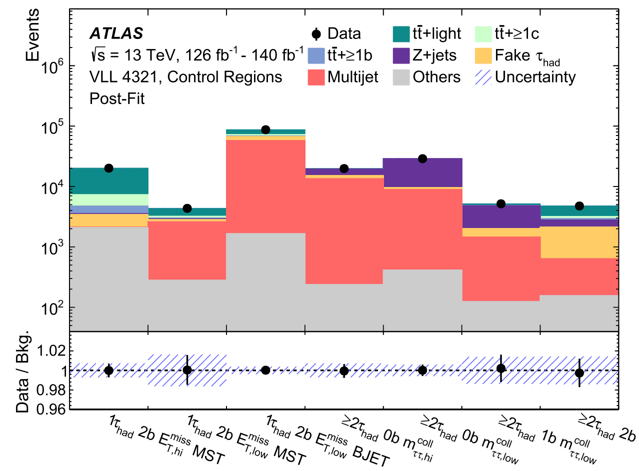

Fig. 11 Comparison between data and the background prediction for the event yields in the seven control region categories. The ratio of the data to the background ('Bkg.') prediction is shown in the lower panel. The size of the combined statistical and systematic uncertainty in the background prediction is indicated by the blue hatched band

sis, considering a mass of 1 TeV in the evaluation of NN score distribution. Overall, there is good agreement between the data and the predicted background yields across all event categories, with the lowest p-value for data-background compatibility of 0.043 observed in the $1\tau_{\text{had}}$ $3b$ MST region. After the fit, no NPs show significant deviations or constraints from their nominal values, indicating that all the systematic uncertainties considered in the analysis are well-behaved. There are also no strong correlation factors among the fitted values of the normalisation parameters of $t\bar{t}$+jets, Z+jets and multijet background. The main uncertainty in this analysis comes

Table 7 Summary of observed and predicted yields in the five signal region categories, corresponding to their respective data luminosities. The background prediction is shown after the combined likelihood fit to data under the background-only hypothesis across all control region and signal region categories, while the NN score is evaluated for a 1 TeV mass in the signal region. The expected signal yields that are obtained by using their theory cross-sections are also shown with their pre-fit uncertainties, assuming μ=1 for an m_{VLL} mass of 1 TeV. The uncertainties correspond to the combined statistical and systematic uncertainties in the predicted yields. Total background yield uncertainties are smaller than the quadratic sum of individual backgrounds due to correlations in uncertainty components and normalisation factors. The 'Others' contribution is dominated by $t\bar{t}t\bar{t}$ and $t\bar{t}W$

	$1\tau_{\text{had}} 3b$ MST (140 fb^{-1})	$1\tau_{\text{had}} \geq 4b$ MST (140 fb^{-1})	$1\tau_{\text{had}} 3b$ BJET (126 fb^{-1})	$1\tau_{\text{had}} \geq 4b$ BJET (126 fb^{-1})	$\geq 2\tau_{\text{had}} \geq 3b$ MSDT (140 fb^{-1})
Data	3062	244	20020	2482	394
Total background	3070 ± 50	250 ± 13	20010 ± 140	2490 ± 50	398 ± 18
$t\bar{t}+ \geq 1b$	720 ± 140	141 ± 22	2300 ± 500	620 ± 90	90 ± 18
$t\bar{t}+ \geq 1c$	590 ± 230	41 ± 17	1600 ± 600	130 ± 50	41 ± 17
$t\bar{t}$ + light	1080 ± 120	10.3 ± 2.9	2650 ± 340	45 ± 11	15.5 ± 3.3
Z + jets	16.6 ± 1.7	1.08 ± 0.16	79 ± 14	8.4 ± 1.8	36.0 ± 3.1
Multijets	200 ± 40	13 ± 5	10200 ± 500	1210 ± 70	36 ± 9
Others	240 ± 50	27 ± 4	480 ± 110	85 ± 12	18.9 ± 3.1
Fake τ_{had}	214 ± 23	18 ± 4	2730 ± 270	390 ± 40	160 ± 18
m_{VLL} 1.0 TeV	6.07 ± 0.23	4.37 ± 0.24	1.32 ± 0.13	1.10 ± 0.14	3.41 ± 0.19

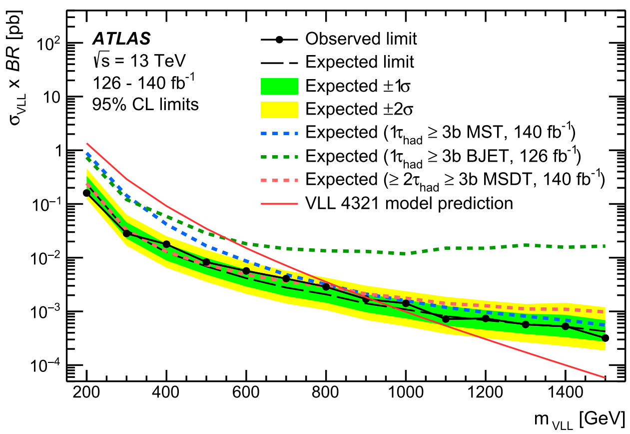

Fig. 12 Observed (solid line with markers) and expected (dashed line) 95% CL upper limits on the VLL pair production cross-section (σ_{VLL}) times branching ratio (BR) to third generation quarks and leptons as a function of m_{VLL}. The limits presented in black lines are obtained after combining all five signal regions. The inner green (outer yellow) band corresponds to the $\pm 1\sigma$ ($\pm 2\sigma$) uncertainty around the combined expected limit. The 95% CL expected upper limits in the three individual channels ($1\tau_{\text{had}} \geq 3b$ MST, $1\tau_{\text{had}} \geq 3b$ BJET and $\geq 2\tau_{\text{had}} \geq 3b$ MSDT) are shown for comparison. The solid red line represents the theory prediction of the VLL pair production cross-section at NLO in QCD

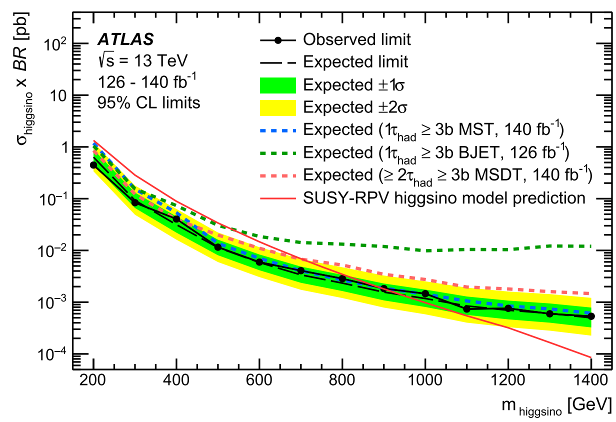

Fig. 13 Observed (solid line with markers) and expected (dashed line) 95% CL upper limits on the higgsino pair production cross-section (σ_{higgsino}) times branching ratio (BR) to third generation quarks and leptons as a function of m_{higgsino}. The limits presented in black lines are obtained after combining all five signal regions. The inner green (outer yellow) band corresponds to the $\pm 1\sigma$ ($\pm 2\sigma$) uncertainty around the combined expected limit. The 95% CL expected upper limits in the three individual channels ($1\tau_{\text{had}} \geq 3b$ MST, $1\tau_{\text{had}} \geq 3b$ BJET and $\geq 2\tau_{\text{had}} \geq 3b$ MSDT) are shown for comparison. The solid red line represents the theory prediction of the higgsino pair production cross-section at NLO in QCD

from the limited data statistics. The corresponding post-fit yields for the five SRs can be found in Table 7. The data and expected yields in the seven CRs after the combined likelihood fit under the background-only hypothesis are shown in Fig. 11. As summarised in Table 6, the systematic uncertainty with the largest impact on the signal strength originates from the background MC statistical uncertainty as well as from the $t\bar{t}+$jets background modelling. In general, good agreement between the data and predicted background yields is found across all event categories. The observed p_0 is checked for each explored signal scenario, and the smallest value is found to be 0.13, corresponding to a local significance of 1.1σ, for the 400 GeV signal point.

In the absence of any significant excess, upper limits on the signal production cross-section for each of the signal scenarios considered are derived by using q_μ in the CL_s method [142,143]. For a given signal scenario, values of the production cross-section (parameterised by μ) yielding $\text{CL}_\text{s} < 0.05$, where CL_s is computed using the asymptotic approximation [141], are excluded at $\geq 95\%$ confidence level (CL).

Figure 12 shows the 95% CL upper limits on the VLL pair production cross-section times branching ratio as a function of m_{VLL}. The observed and expected 95% CL lower limits on m_{VLL} are 910 GeV and 970 GeV, respectively. When accounting for systematic uncertainties, the cross-section limits degrade by only 8% for VLL masses around 1 TeV, and they degrade by 25–70% for VLL masses below 0.6 TeV. The upper limits on the VLL production cross-section, calculated using pseudo-experiments for the CL_s method, are consistent with the presented results within 5% in the most sensitive regions. However, for m_{VLL} below 600 GeV or above 1100 GeV, the limits derived from pseudo-experiments are up to 20% higher due to low background yields in the most sensitive bins.

This analysis, the first search from the ATLAS Collaboration for VLLs decaying through U_1 to third generation SM fermions, excludes the 600 GeV VLL mass, which is a representative point within the mass range where the CMS Collaboration reports an excess, including a 2.8σ excess at this specific mass [43]. The observed p_0 in the analysis presented here for the same representative signal mass point is 0.18, corresponding to a local significance of 0.9σ. The 95% CL observed (expected) upper limit on the signal cross-section for the VLL mass of 600 GeV is 5.8 fb (4.1 fb). In the CMS Collaboration analysis [43], the corresponding expected upper limit is about 10 fb, with the most sensitive channel selected with: a trigger requiring three b-tagged jets and event selections with at least four jets (p_{T} thresholds of 80, 65, 50, and 50 GeV), three or more of which are b-tagged jets, along with two or more τ_{had} ($p_{\text{T}} > 20$ GeV), $H_{\text{T,jets}} > 400$ GeV and $E_{\text{T}}^{\text{miss}} > 40$ GeV. The ATLAS search sensitivity is driven by the $\geq 2\tau_{\text{had}} \geq 3b$ MSDT channel in the investigated mass range (200 GeV–1500 GeV). At high mass ($m_{\text{VLL}} > 700$ GeV), the $1\tau_{\text{had}} \geq 3b$ MST channels reinforce the sensitivity further as illustrated in Fig. 12.

The NN optimised for the VLL signal is also applied to the RPV SUSY signal, with the corresponding distributions from the signal and control regions included in the simulta-

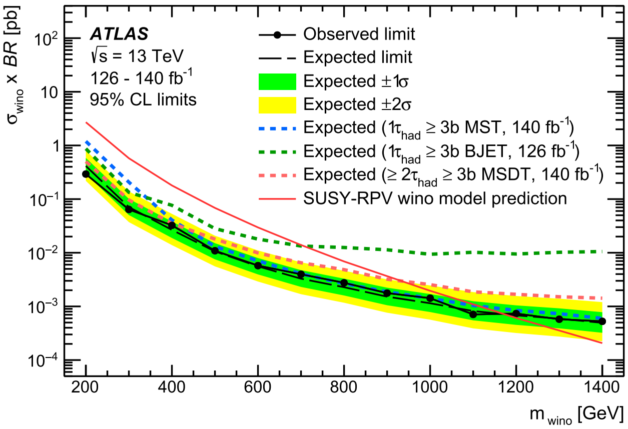

Fig. 14 Observed (solid line with markers) and expected (dashed line) 95% CL upper limits on the wino pair production cross-section (σ_{wino}) times branching ratio (BR) to third generation quarks and leptons as a function of m_{wino}. The limits presented in black lines are obtained after combining all five signal regions. The surrounding inner green (outer yellow) band corresponds to the $\pm 1\sigma$ ($\pm 2\sigma$) uncertainty around the combined expected limit. The 95% CL expected upper limits in the three individual channels ($1\tau_{\text{had}} \geq 3b$ MST, $1\tau_{\text{had}} \geq 3b$ BJET and $\geq 2\tau_{\text{had}} \geq 3b$ MSDT) are shown for comparison. The solid red line represents the theory prediction of the wino pair production cross-section at NLO in QCD

neous fit. The resulting cross-section times branching ratio limits are derived for electroweakino pair production under the higgsino or wino mixing assumptions in the RPV SUSY models, as shown in Figs. 13 and 14. The kinematic distributions of the final states from these SUSY models, where the chargino/neutralino decays into third generation fermions, are close to those obtained from the VLL pair processes. The signal cross-sections in these models show only minimal differences compared to the background size, and the background normalisation factors obtained from the fit remain unchanged. The 95% CL lower limits were set on the higgsino mass m_{higgsino} of 880 GeV (940 GeV) and on the wino mass m_{wino} of 1170 GeV (1170 GeV) for the observed (expected) values.

9 Conclusion

A search for electroweak production of vector-like leptons as predicted in the ‘4321’ model is performed using the $\sqrt{s} = 13$ TeV dataset collected with the ATLAS detector at the LHC, corresponding to an integrated luminosity of 126 fb^{-1} to 140 fb^{-1}. The signal regions characterised by the presence of b-jets and hadronically decaying τ-leptons are optimised using neural networks parameterised in the generated mass of the vector-like lepton signal. The likelihood fits to data using the discriminant score distributions across the signal and control regions show good consistency of data with the SM background predictions. Upper limits at 95% CL on the production cross-section times branching ratio into third generation SM fermions are derived as a function of vector-like lepton mass, setting a lower observed (expected) limit on the vector-like lepton mass at 910 GeV (970 GeV). The results are also interpreted in context of RPV SUSY models leading to similar final states, for which the observed (expected) lower limits on the higgsino mass in the higgsino mixing model is 880 GeV (940 GeV) and on the wino mass in the wino mixing model is 1170 GeV (1170 GeV).

Acknowledgements We thank CERN for the very successful operation of the LHC and its injectors, as well as the support staff at CERN and at our institutions worldwide without whom ATLAS could not be operated efficiently. The crucial computing support from all WLCG partners is acknowledged gratefully, in particular from CERN, the ATLAS Tier-1 facilities at TRIUMF/SFU (Canada), NDGF (Denmark, Norway, Sweden), CC-IN2P3 (France), KIT/GridKA (Germany), INFN-CNAF (Italy), NL-T1 (Netherlands), PIC (Spain), RAL (UK) and BNL (USA), the Tier-2 facilities worldwide and large non-WLCG resource providers. Major contributors of computing resources are listed in Ref. [144]. We gratefully acknowledge the support of ANPCyT, Argentina; YerPhI, Armenia; ARC, Australia; BMWFW and FWF, Austria; ANAS, Azerbaijan; CNPq and FAPESP, Brazil; NSERC, NRC and CFI, Canada; CERN; ANID, Chile; CAS, MOST and NSFC, China; Minciencias, Colombia; MEYS CR, Czech Republic; DNRF and DNSRC, Denmark; IN2P3-CNRS and CEA-DRF/IRFU, France; SRNSFG, Georgia; BMFTR, HGF and MPG, Germany; GSRI, Greece; RGC and Hong Kong SAR, China; ICHEP and Academy of Sciences and Humanities, Israel; INFN, Italy; MEXT and JSPS, Japan; CNRST, Morocco; NWO, Netherlands; RCN, Norway; MNiSW, Poland; FCT, Portugal; MNE/IFA, Romania; MSTDI, Serbia; MSSR, Slovakia; ARIS and MVZI, Slovenia; DSI/NRF, South Africa; MICIU/AEI, Spain; SRC and Wallenberg Foundation, Sweden; SERI, SNSF and Cantons of Bern and Geneva, Switzerland; NSTC, Taipei; TENMAK, Türkiye; STFC/UKRI, United Kingdom; DOE and NSF, United States of America. Individual groups and members have received support from BCKDF, CANARIE, CRC and DRAC, Canada; CERN-CZ, FORTE and PRIMUS, Czech Republic; COST, ERC, ERDF, Horizon 2020, ICSC-NextGenerationEU and Marie Skłodowska-Curie Actions, European Union; Investissements d’Avenir Labex, Investissements d’Avenir Idex and ANR, France; DFG and AvH Foundation, Germany; Herakleitos, Thales and Aristeia programmes co-financed by EU-ESF and the Greek NSRF, Greece; BSF-NSF and MINERVA, Israel; NCN and NAWA, Poland; La Caixa Banking Foundation, CERCA Programme Generalitat de Catalunya and PROMETEO and GenT Programmes Generalitat Valenciana, Spain; Göran Gustafssons Stiftelse, Sweden; The Royal Society and Leverhulme Trust, United Kingdom. In addition, individual members wish to acknowledge support from Armenia: Yerevan Physics Institute (FAPERJ); CERN: European Organization for Nuclear Research (CERN DOCT); Chile: Agencia Nacional de Investigación y Desarrollo (FONDECYT 1230812, FONDECYT 1240864); China: Chinese Ministry of Science and Technology (MOST-2023YFA1605700, MOST-2023YFA1609300), National Natural Science Foundation of China (NSFC - 12175119, NSFC 12275265); Czech Republic: Czech Science Foundation (GACR - 24-11373S), Ministry of Education Youth and Sports (ERC-CZ-LL2327, FORTE CZ.02.01.01/00/22_008/0004632), PRIMUS Research Programme (PRIMUS/21/SCI/017); EU: H2020 European Research Council (ERC - 101002463); European Union: European Research Council (BARD No. 101116429, ERC - 948254, ERC 101089007), European Regional Development Fund (SMASH COFUND 101081355, SLO ERDF), Horizon 2020 Framework Programme (MUCCA - CHIST-ERA-19-XAI-00), European Union, Future Artificial Intelligence Research (FAIR-NextGenerationEU PE00000 013), Horizon 2020 (EuroHPC - EHPC-DEV-2024D11-051), Italian Center for High Performance Computing, Big Data and Quantum Computing (ICSC, NextGenerationEU); France: Agence Nationale de la Recherche (ANR-21-CE31-0022, ANR-22-EDIR-0002); Germany: Baden-Württemberg Stiftung (BW Stiftung-Postdoc Eliteprogramme), Deutsche Forschungsgemeinschaft (DFG - 469666862, DFG - CR 312/5-2); China: Research Grants Council (GRF); Italy: Istituto Nazionale di Fisica Nucleare (ICSC, NextGenerationEU), Ministero dell'Università e della Ricerca (NextGenEU 153D23001490006 M4C2.1.1, NextGenEU I53D23000820006 M4C2.1.1, NextGenEU I53D23001490006 M4C2.1.1); Japan: Japan Society for the Promotion of Science (JSPS KAKENHI JP22H01227, JSPS KAKENHI JP22H04944, JSPS KAKENHI JP22KK0227, JSPS KAKENHI JP23KK0245, JSPS KAKENHI JP24K23939); Norway: Research Council of Norway (RCN-314472); Poland: Ministry of Science and Higher Education (IDUB AGH, POB8, D4 no 9722), Polish National Science Centre (NCN 2021/42/E/ST2/00350, NCN OPUS 2023/51/B/ST2/02507, NCN OPUS nr 2022/47/B/ST2/03059, NCN UMO-2019/34/E/ST2/00393, UMO-2022/47/O/ST2/00148, UMO-2023/49/B/ST2/04085, UMO-2023/51/B/ST2/00920, UMO-2024/53/N/ST2/00869); Portugal: Foundation for Science and Technology (FCT); Spain: Generalitat Valenciana (Artemisa, FEDER, IDIFEDER/2018/048), Ministry of Science and Innovation (MCIN & NextGenEU PCI2022-135018-2, MICIN & FEDER PID2021-125273NB, RYC2019-028510-I, RYC2020-030254-I, RYC2021-031273-I, RYC2022-038164-I); Sweden: Carl Trygger Foundation (Carl Trygger Foundation CTS 22:2312), Swedish Research Council (Swedish Research Council 2023-04654, VR 2021-03651, VR 2022-03845, VR 2022-04683, VR 2023-03403, VR 2024-05451), Knut and Alice Wallenberg Foundation (KAW 2018.0458, KAW 2022.0358, KAW 2023.0366); Switzerland: Swiss National Science Foundation (SNSF - PCEFP2_194658); United Kingdom: Leverhulme Trust (Leverhulme Trust RPG-2020-004), Royal Society (NIF-R1-231091); United States of America: U.S. Department of Energy (ECA DE-AC02-76SF00515), Neubauer Family Foundation.

Data Availability Statement This manuscript has no associated data. [Authors' comment: The public release of data supporting the findings of this article will follow the CERN Open Data Policy https://cds.cern.ch/record/2745133. The values of relevant plots and tables associated with this article are stored in HEPData.]

Code Availability Statement Thsi manuscript has no associated code/software. [Authors' comment: The ATLAS Collaboration's Athena software, including the configuration of the event generators, is open source (http://gitlab.cern.ch/atlas/athena).]

References

1. L. Susskind, Dynamics of spontaneous symmetry breaking in the Weinberg–Salam theory. Phys. Rev. D **20**, 2619 (1979). https://doi.org/10.1103/PhysRevD.20.2619
2. S. Dimopoulos, H. Georgi, Softly broken supersymmetry and SU(5). Nucl. Phys. B **193**, 150 (1981). https://doi.org/10.1016/0550-3213(81)90522-8
3. M.W. Goodman, E. Witten, Detectability of certain dark-matter candidates. Phys. Rev. D **31**, 3059 (1985). https://doi.org/10.1103/PhysRevD.31.3059
4. Particle Data Group Collaboration, Review of particle physics. Phys. Rev. D **110**, 030001 (2024). https://doi.org/10.1103/PhysRevD.110.030001
5. B.B. Collaboration, Evidence for an excess of $\bar{B} \to D^{(*)}\tau^-\bar{\nu}_\tau$ decays. Phys. Rev. Lett. **109**, 101802 (2012). https://doi.org/10.1103/PhysRevLett.109.101802. arXiv:1205.5442 [hep-ex]
6. B.B. Collaboration, Measurement of an excess of $\bar{B} \to D^{(*)}\tau^-\bar{\nu}_\tau$ decays and implications for charged Higgs bosons. Phys. Rev. D **88**, 072012 (2013). https://doi.org/10.1103/PhysRevD.88.072012. arXiv:1303.0571 [hep-ex]
7. B. Collaboration, Measurement of $\mathcal{R}(D)$ and $\mathcal{R}(D^*)$ with a semileptonic tagging method. Phys. Rev. Lett. **124**, 161803 (2020). https://doi.org/10.1103/PhysRevLett.124.161803. arXiv:1910.05864 [hep-ex]
8. LHCb Collaboration, Angular analysis of the $B^+ \to K^{*+}\mu^+\mu^-$ decay. Phys. Rev. Lett. **126**, 161802 (2021). https://doi.org/10.1103/PhysRevLett.126.161802. arXiv:2012.13241 [hep-ex]
9. LHCb Collaboration, Measurement of CP-averaged observables in the $B^0 \to K^{*0}\mu^+\mu^-$ decay. Phys. Rev. Lett. **125**, 011802 (2020). https://doi.org/10.1103/PhysRevLett.125.011802. arXiv:2003.04831 [hep-ex]
10. LHCb Collaboration, Measurement of the ratio of the $B^0 \to D^{*-}\tau^+\nu_\tau$ and $B^0 \to D^{*-}\mu^+\nu_\mu$ branching fractions using three-prong τ-lepton decays. Phys. Rev. Lett. **120**, 171802 (2018). https://doi.org/10.1103/PhysRevLett.120.171802. arXiv:1708.08856 [hep-ex]
11. LHCb Collaboration, Measurement of the ratios of branching fractions $\mathcal{R}(D^*)$ and $\mathcal{R}(D^0)$. Phys. Rev. Lett. **131**, 111802 (2023). https://doi.org/10.1103/PhysRevLett.131.111802. arXiv:2302.02886 [hep-ex]
12. LHCb Collaboration, Test of lepton universality in $B \to S\ell^+\ell^-$ decays. Phys. Rev. Lett. **131**, 051803 (2023). https://doi.org/10.1103/PhysRevLett.131.051803. arXiv:2212.09152 [hep-ex]
13. Z.-R. Huang, Y. Li, C.-D. Lu, M.A. Paracha, C. Wang, Footprints of new physics in $B \to C\tau\nu$ transitions. Phys. Rev. D **98**, 095018 (2018). https://doi.org/10.1103/PhysRevD.98.095018. arXiv:1808.03565 [hep-ph]
14. L. Luzio, J. Fuentes-Martin, A. Greljo, M. Nardecchia, S. Renner, Maximal flavour violation: a Cabibbo mechanism for leptoquarks. JHEP **11**, 081 (2018). https://doi.org/10.1007/JHEP11(2018)081. arXiv:1808.00942 [hep-ph]
15. R. Alonso, B. Grinstein, J. Martin Camalich, Lifetime of B_c^- constrains explanations for anomalies in $B \to D^{(*)}\tau\nu$. Phys. Rev. Lett. **118**, 081802 (2017). https://doi.org/10.1103/PhysRevLett.118.081802. arXiv:1611.06676 [hep-ph]
16. F. Feruglio, P. Paradisi, A. Pattori, Revisiting lepton flavor universality in B decays. Phys. Rev. Lett. **118**, 011801 (2017). https://doi.org/10.1103/PhysRevLett.118.011801. arXiv:1606.00524 [hep-ph]
17. F. Feruglio, P. Paradisi, A. Pattori, On the importance of electroweak corrections for B anomalies. JHEP **09**, 061 (2017). https://doi.org/10.1007/JHEP09(2017)061. arXiv:1705.00929 [hep-ph]
18. D.A. Faroughy, A. Greljo, J.F. Kamenik, Confronting lepton flavor universality violation in B decays with high-p_T tau lepton

searches at LHC. Phys. Lett. B **764**, 126 (2017). https://doi.org/10.1016/j.physletb.2016.11.011. arXiv:1609.07138 [hep-ph]
19. A. Greljo, D. Marzocca, High-p_T dilepton tails and flavor physics. Eur. Phys. J. C **77**, 548 (2017). https://doi.org/10.1140/epjc/s10052-017-5119-8. arXiv:1704.09015 [hep-ph]
20. B. Bhattacharya, A. Datta, D. London, S. Shivashankara, Simultaneous explanation of the R_K and $R(D^{(*)})$ puzzles. Phys. Lett. B **742**, 370 (2015). https://doi.org/10.1016/j.physletb.2015.02.011. arXiv:1412.7164 [hep-ph]
21. R. Alonso, B. Grinstein, J.M. Camalich, Lepton universality violation with lepton flavor conservation in B-meson decays. JHEP **10**, 184 (2015). https://doi.org/10.1007/JHEP10(2015)184. arXiv:1505.05164 [hep-ph]
22. A. Greljo, G. Isidori, D. Marzocca, On the breaking of lepton flavor universality in B decays. JHEP **07**, 142 (2015). https://doi.org/10.1007/JHEP07(2015)142. arXiv:1506.01705 [hep-ph]
23. L. Calibbi, A. Crivellin, T. Ota, Effective field theory approach to $B \to S\ell\ell^{(\prime)}$, $B \to K^{(*)}\nu\bar{\nu}$ and $B \to D^{(*)}\tau\nu$ with third generation couplings. Phys. Rev. Lett. **115**, 181801 (2015). https://doi.org/10.1103/PhysRevLett.115.181801. arXiv:1506.02661 [hep-ph]
24. M. Bauer, M. Neubert, Minimal leptoquark explanation for the $R_{D^{(*)}}$, R_K, and $(g-2)_\mu$ anomalies. Phys. Rev. Lett. **116**, 141802 (2016). https://doi.org/10.1103/PhysRevLett.116.141802. arXiv:1511.01900 [hep-ph]
25. S. Fajfer, N. Košnik, Vector leptoquark resolution of R_K and $R_{D^{(*)}}$ puzzles. Phys. Lett. B **755**, 270 (2016). https://doi.org/10.1016/j.physletb.2016.02.018. arXiv:1511.06024 [hep-ph]
26. D. Bečirevič, S. Fajfer, N. Košnik, O. Sumensari, Leptoquark model to explain the b-physics anomalies, R_K and R_D. Phys. Rev. D **94**, 115021 (2016). https://doi.org/10.1103/PhysRevD.94.115021. arXiv:1608.08501 [hep-ph]
27. D. Buttazzo, A. Greljo, G. Isidori, D. Marzocca, B-physics anomalies: a guide to combined explanations. JHEP **11**, 044 (2017). https://doi.org/10.1007/JHEP11(2017)044. arXiv:1706.07808 [hep-ph]
28. D. Marzocca, Addressing the B-physics anomalies in a fundamental composite Higgs model. JHEP **07**, 121 (2018). https://doi.org/10.1007/JHEP07(2018)121. arXiv:1803.10972 [hep-ph]
29. A. Azatov, D. Bardhan, D. Ghosh, F. Sgarlata, E. Venturini, Anatomy of $B \to C\tau\nu$ anomalies. JHEP **11**, 187 (2018). https://doi.org/10.1007/JHEP11(2018)187. arXiv:1805.03209 [hep-ph]
30. J. Kumar, D. London, R. Watanabe, Combined explanations of the $B \to S\mu^+\mu^-$ and $B \to C\tau^-\bar{\nu}$ anomalies: a general model analysis. Phys. Rev. D **99**, 015007 (2019). https://doi.org/10.1103/PhysRevD.99.015007. arXiv:1806.07403 [hep-ph]
31. R. Barbieri, G. Isidori, A. Pattori, F. Senia, Anomalies in B-decays and $U(2)$ flavor symmetry. Eur. Phys. J. C **76**, 67 (2016). https://doi.org/10.1140/epjc/s10052-016-3905-3. arXiv:1512.01560 [hep-ph]
32. D. Buttazzo, A. Greljo, G. Isidori, D. Marzocca, Toward a coherent solution of diphoton and flavor anomalies. JHEP **08**, 035 (2016). https://doi.org/10.1007/JHEP08(2016)035. arXiv:1604.03940 [hep-ph]
33. R. Barbieri, C.W. Murphy, F. Senia, B-decay anomalies in a composite leptoquark model. Eur. Phys. J. C **77**, 8 (2017). https://doi.org/10.1140/epjc/s10052-016-4578-7. arXiv:1611.04930 [hep-ph]
34. L. Luzio, A. Greljo, M. Nardecchia, Gauge leptoquark as the origin of B-physics anomalies. Phys. Rev. D **96**, 115011 (2017). https://doi.org/10.1103/PhysRevD.96.115011. arXiv:1708.08450 [hep-ph]
35. ATLAS Collaboration, Search for pairs of scalar leptoquarks decaying into quarks and electrons or muons in $\sqrt{s} = 13$ TeV pp collisions with the ATLAS detector. JHEP **10**, 112 (2020). https://doi.org/10.1007/JHEP10(2020)112. arXiv:2006.05872 [hep-ex]
36. ATLAS Collaboration, Search for pair production of third-generation leptoquarks decaying into a bottom quark and a τ-lepton with the ATLAS detector. Eur. Phys. J. C **83**, 1075 (2023). https://doi.org/10.1140/epjc/s10052-023-12104-7. arXiv:2303.01294 [hep-ex]
37. ATLAS Collaboration, Search for a scalar partner of the top quark in the all-hadronic $t\bar{t}$ plus missing transverse momentum final state at $\sqrt{s} = 13$ TeV with the ATLAS detector. Eur. Phys. J. C **80**, 737 (2020). https://doi.org/10.1140/epjc/s10052-020-8102-8. arXiv:2004.14060 [hep-ex]
38. ATLAS Collaboration, Search for pair production of third-generation scalar leptoquarks decaying into a top quark and a τ-lepton in pp collisions at $\sqrt{s} = 13$ TeV with the ATLAS detector. JHEP **06**, 179 (2021). https://doi.org/10.1007/JHEP06(2021)179. arXiv:2101.11582 [hep-ex]
39. ATLAS Collaboration, Search for new phenomena in final states with b-jets and missing transverse momentum in $\sqrt{s} = 13$ TeV pp collisions with the ATLAS detector. JHEP **05**, 093 (2021). https://doi.org/10.1007/JHEP05(2021)093. arXiv:2101.12527 [hep-ex]
40. ATLAS Collaboration, Search for leptoquark pair production decaying into $te^-\bar{t}e^+$ or $t\mu^-\bar{t}\mu^+$ in multi-lepton final states in pp collisions at 13 TeV with the ATLAS detector. Eur. Phys. J. C **84**, 818 (2024). https://doi.org/10.1140/epjc/s10052-024-12975-4. arXiv:2306.17642 [hep-ex]
41. M. Bordone, C. Cornella, J. Fuentes-Martín, G. Isidori, A three-site gauge model for flavor hierarchies and flavor anomalies. Phys. Lett. B **779**, 317 (2018). https://doi.org/10.1016/j.physletb.2018.02.011. arXiv:1712.01368 [hep-ph]
42. C. Cornella, D.A. Faroughy, J. Fuentes-Martín, G. Isidori, M. Neubert, Reading the footprints of the B-meson flavor anomalies. JHEP **08**, 050 (2021). https://doi.org/10.1007/JHEP08(2021)050. arXiv:2103.16558 [hep-ph]
43. C.M.S. Collaboration, Search for pair-produced vector-like leptons in final states with third-generation leptons and at least three B quark jets in proton–proton collisions at $\sqrt{s} = 13$ TeV. Phys. Lett. B **846**, 137713 (2023). https://doi.org/10.1016/j.physletb.2023.137713. arXiv:2208.09700 [hep-ex]
44. Y. Golfand, E. Likhtman, Extension of the algebra of Poincare group generators and violation of P invariance. JETP Lett. **13**, 323 (1971). [Pisma Zh. Eksp. Teor. Fiz. 13 (1971) 452]
45. D. Volkov, V. Akulov, Is the neutrino a goldstone particle? Phys. Lett. B **46**, 109 (1973). https://doi.org/10.1016/0370-2693(73)90490-5
46. J. Wess, B. Zumino, Supergauge transformations in four dimensions. Nucl. Phys. B **70**, 39 (1974). https://doi.org/10.1016/0550-3213(74)90355-1
47. J. Wess, B. Zumino, Supergauge invariant extension of quantum electrodynamics. Nucl. Phys. B **78**, 1 (1974). https://doi.org/10.1016/0550-3213(74)90112-6
48. S. Ferrara, B. Zumino, Supergauge invariant Yang–Mills theories. Nucl. Phys. B **79**, 413 (1974). https://doi.org/10.1016/0550-3213(74)90559-8
49. A. Salam, J. Strathdee, Super-symmetry and non-abelian gauges. Phys. Lett. B **51**, 353 (1974). https://doi.org/10.1016/0370-2693(74)90226-3
50. A. Chakraborty, S. Chakraborty, Probing $(g-2)_\mu$ at the LHC in the paradigm of R-parity violating MSSM. Phys. Rev. D **93**, 075035 (2016). https://doi.org/10.1103/PhysRevD.93.075035. arXiv:1511.08874 [hep-ph]
51. P. Fayet, Supersymmetry and weak, electromagnetic and strong interactions. Phys. Lett. B **64**, 159 (1976). https://doi.org/10.1016/0370-2693(76)90319-1
52. P. Fayet, Spontaneously broken supersymmetric theories of weak, electromagnetic and strong interactions. Phys. Lett. B **69**, 489 (1977). https://doi.org/10.1016/0370-2693(77)90852-8

53. ATLAS Collaboration, Search for heavy Higgs bosons with flavour-violating couplings in multi-lepton plus b-jets final states in pp collisions at 13 TeV with the ATLAS detector. JHEP **12**, 081 (2023). https://doi.org/10.1007/JHEP12(2023)081. arXiv:2307.14759 [hep-ex]
54. ATLAS Collaboration, The ATLAS Experiment at the CERN large hadron collider. JINST **3**, S08003 (2008). https://doi.org/10.1088/1748-0221/3/08/S08003
55. ATLAS Collaboration, ATLAS insertable B-layer: technical design report. ATLAS-TDR-19; CERN-LHCC-2010-013, 2010. https://cds.cern.ch/record/1291633. Addendum: ATLAS-TDR-19-ADD-1; CERN-LHCC-2012-009, 2012, https://cds.cern.ch/record/1451888
56. B. Abbott et al., Production and integration of the atlas insertable B-layer. JINST **13**, T05008 (2018). https://doi.org/10.1088/1748-0221/13/05/T05008. arXiv:1803.00844 [physics.ins-det]
57. ATLAS Collaboration, Performance of the ATLAS trigger system in 2015. Eur. Phys. J. C **77**, 317 (2017). https://doi.org/10.1140/epjc/s10052-017-4852-3. arXiv:1611.09661 [hep-ex]
58. ATLAS Collaboration, Software and computing for Run 3 of the ATLAS experiment at the LHC. Eur. Phys. J. C **85**, 234 (2025). https://doi.org/10.1140/epjc/s10052-024-13701-w. arXiv:2404.06335 [hep-ex]
59. ATLAS Collaboration, ATLAS data quality operations and performance for 2015–2018 data-taking. JINST **15**, P04003 (2020). https://doi.org/10.1088/1748-0221/15/04/P04003. arXiv:1911.04632 [physics.ins-det]
60. J. Alwall et al., The automated computation of tree-level and next-to-leading order differential cross sections, and their matching to parton shower simulations. JHEP **07**, 079 (2014). https://doi.org/10.1007/JHEP07(2014)079. arXiv:1405.0301 [hep-ph]
61. T. Sjöstrand, S. Mrenna, P. Skands, A brief introduction to PYTHIA 8.1. Comput. Phys. Commun. **178**, 852 (2008). https://doi.org/10.1016/j.cpc.2008.01.036. arXiv:0710.3820 [hep-ph]
62. F. Cascioli, P. Maierhöfer, S. Pozzorini, Scattering amplitudes with open loops. Phys. Rev. Lett. **108**, 111601 (2012). https://doi.org/10.1103/PhysRevLett.108.111601. arXiv:1111.5206 [hep-ph]
63. T. Gleisberg, S. Höche, Comix, a new matrix element generator. JHEP **12**, 039 (2008). https://doi.org/10.1088/1126-6708/2008/12/039. arXiv:0808.3674 [hep-ph]
64. S. Schumann, F. Krauss, A parton shower algorithm based on Catani–Seymour dipole factorisation. JHEP **03**, 038 (2008). https://doi.org/10.1088/1126-6708/2008/03/038. arXiv:0709.1027 [hep-ph]
65. S. Höche, F. Krauss, M. Schönherr, F. Siegert, QCD matrix elements + parton showers. The NLO case. JHEP **04**, 027 (2013). https://doi.org/10.1007/JHEP04(2013)027. arXiv:1207.5030 [hep-ph]
66. D.J. Lange, The EvtGen particle decay simulation package. Nucl. Instrum. Methods A **462**, 152 (2001). https://doi.org/10.1016/S0168-9002(01)00089-4
67. P. Golonka, Z. Was, Photos Monte Carlo: a precision tool for QED corrections in Z and W decays. Eur. Phys. J. C **45**, 97 (2006). https://doi.org/10.1140/epjc/s2005-02396-4. arXiv:hep-ph/0506026
68. NNPDF Collaboration, R.D. Ball et al., Parton distributions for the LHC Run II. JHEP **04**, 040 (2015). https://doi.org/10.1007/JHEP04(2015)040. arXiv:abs/1410.8849 [hep-ph]
69. ATLAS Collaboration, ATLAS Pythia 8 tunes to 7 TeV data ATL-PHYS-PUB-2014-021. (2014). https://cds.cern.ch/record/1966419
70. P. Nason, A new method for combining NLO QCD with shower Monte Carlo algorithms. JHEP **11**, 040 (2004). https://doi.org/10.1088/1126-6708/2004/11/040. arXiv:hep-ph/0409146
71. J. Bellm et al., Herwig 7.1 release note. (2017). arXiv:1705.06919 [hep-ph]
72. T. Ježo, J.M. Lindert, N. Moretti, S. Pozzorini, New NLOPS predictions for $t\bar{t} + b$-jet production at the LHC. Eur. Phys. J. C **78**, 502 (2018). https://doi.org/10.1140/epjc/s10052-018-5956-0. arXiv:1802.00426 [hep-ph]
73. E. Bothmann et al., Event generation with Sherpa 2.2. SciPost Phys. **7**, 034 (2019). https://doi.org/10.21468/SciPostPhys.7.3.034. arXiv:1905.09127 [hep-ph]
74. J. Bellm et al., Herwig 7.0/Herwig++ 3.0 release note. Eur. Phys. J. C **76**, 196 (2016). https://doi.org/10.1140/epjc/s10052-016-4018-8. arXiv:1512.01178 [hep-ph]
75. E. Re, Single-top Wt-channel production matched with parton showers using the POWHEG method. Eur. Phys. J. C **71**, 1547 (2011). https://doi.org/10.1140/epjc/s10052-011-1547-z. arXiv:1009.2450 [hep-ph]
76. S. Alioli, P. Nason, C. Oleari, E. Re, NLO Single-top Wt-channel production matched with parton showers using the POWHEG method. JHEP **09**, 111 (2009). https://doi.org/10.1088/1126-6708/2009/09/111. arXiv:0907.4076 [hep-ph]. [Erratum: 10.1007/JHEP02(2010)011 JHEP 02 (2010) 011]
77. NNPDF Collaboration, R.D. Ball et al., Parton distributions with LHC data. Nucl. Phys. B **867**, 244 (2013). https://doi.org/10.1016/j.nuclphysb.2012.10.003. arXiv:1207.1303 [hep-ph]
78. ATLAS Collaboration, The Pythia 8 A3 tune description of ATLAS minimum bias and inelastic measurements incorporating the Donnachie–Landshoff diffractive model. ATL-PHYS-PUB-2016-017, 2016. https://cds.cern.ch/record/2206965
79. ATLAS Collaboration, The ATLAS simulation infrastructure. Eur. Phys. J. C **70**, 823 (2010). https://doi.org/10.1140/epjc/s10052-010-1429-9. arXiv:1005.4568 [physics.ins-det]
80. S. Agostinelli et al., Geant4 – a simulation toolkit. Nucl. Instrum. Methods A **506**, 250 (2003). https://doi.org/10.1016/S0168-9002(03)01368-8
81. M.J. Baker, J. Fuentes-Martín, G. Isidori, M. König, High-p_t signatures in vector-leptoquark models. Eur. Phys. J. C **79**, 334 (2019). https://doi.org/10.1140/epjc/s10052-019-6853-x. arXiv:1901.10480 [hep-ph]
82. R. Frederix, S. Frixione, Merging meets matching in MC@NLO. JHEP **12**, 061 (2012). https://doi.org/10.1007/JHEP12(2012)061. arXiv:1209.6215 [hep-ph]
83. L. Lönnblad, Correcting the colour-dipole cascade model with fixed order matrix elements. JHEP **05**, 046 (2002). https://doi.org/10.1088/1126-6708/2002/05/046. arXiv:hep-ph/0112284
84. L. Lönnblad, S. Prestel, Matching tree-level matrix elements with interleaved showers. JHEP **03**, 019 (2012). https://doi.org/10.1007/JHEP03(2012)019. arXiv:1109.4829 [hep-ph]
85. C. Bierlich et al., A comprehensive guide to the physics and usage of PYTHIA 83. SciPost Phys. Codeb. (2022). https://doi.org/10.21468/SciPostPhysCodeb.8. arXiv:2203.11601 [hep-ph]
86. B. Fuks, M. Klasen, D.R. Lamprea, M. Rothering, Precision predictions for electroweak superpartner production at hadron colliders with resummino. Eur. Phys. J. C **73**, 2480 (2013). https://doi.org/10.1140/epjc/s10052-013-2480-0. arXiv:1304.0790 [hep-ph]
87. J. Butterworth et al., PDF4LHC recommendations for LHC Run II. J. Phys. G **43**, 023001 (2016). https://doi.org/10.1088/0954-3899/43/2/023001. arXiv:1510.03865 [hep-ph]
88. S. Frixione, G. Ridolfi, P. Nason, A positive-weight next-to-leading-order Monte Carlo for heavy flavour hadroproduction. JHEP **09**, 126 (2007). https://doi.org/10.1088/1126-6708/2007/09/126. arXiv:0707.3088 [hep-ph]
89. S. Frixione, P. Nason, C. Oleari, Matching NLO QCD computations with parton shower simulations: the POWHEG method. JHEP **11**, 070 (2007). https://doi.org/10.1088/1126-6708/2007/11/070. arXiv:0709.2092 [hep-ph]

90. S. Alioli, P. Nason, C. Oleari, E. Re, A general framework for implementing NLO calculations in shower Monte Carlo programs: the POWHEG box. JHEP **06**, 043 (2010). https://doi.org/10.1007/JHEP06(2010)043. arXiv:1002.2581 [hep-ph]
91. C. Anastasiou, L. Dixon, K. Melnikov, F. Petriello, High-precision QCD at hadron colliders: electroweak gauge boson rapidity distributions at next-to-next-to leading order. Phys. Rev. D **69**, 094008 (2004). https://doi.org/10.1103/PhysRevD.69.094008. arXiv:hep-ph/0312266
92. A.D. Martin, W.J. Stirling, R.S. Thorne, G. Watt, Parton distributions for the LHC. Eur. Phys. J. C **63**, 189 (2009). https://doi.org/10.1140/epjc/s10052-009-1072-5. arXiv:0901.0002 [hep-ph]
93. ATLAS Collaboration, Vertex reconstruction performance of the ATLAS detector at $\sqrt{s}$ = 13 TeV. ATL-PHYS-PUB-2015-026, 2015. https://cds.cern.ch/record/2037717
94. ATLAS Collaboration, Electron and photon performance measurements with the ATLAS detector using the 2015–2017 LHC proton–proton collision data. JINST **14**, P12006 (2019). https://doi.org/10.1088/1748-0221/14/12/P12006. arXiv:1908.00005 [hep-ex]
95. ATLAS Collaboration, Electron and photon efficiencies in LHC Run 2 with the ATLAS experiment. JHEP **05**, 162 (2024). https://doi.org/10.1007/JHEP05(2024)162. arXiv:2308.13362 [hep-ex]
96. ATLAS Collaboration, Electron and photon energy calibration with the ATLAS detector using LHC Run 2 data. JINST **19**, P02009 (2024). https://doi.org/10.1088/1748-0221/19/02/P02009. arXiv:2309.05471 [hep-ex]
97. ATLAS Collaboration, Studies of the muon momentum calibration and performance of the ATLAS detector with pp collisions at$\sqrt{s}$ = 13, TeV. Eur. Phys. J. C **83**, 686 (2023). https://doi.org/10.1140/epjc/s10052-023-11584-x. arXiv:2212.07338 [hep-ex]
98. ATLAS Collaboration, Muon reconstruction and identification efficiency in ATLAS using the full Run 2 pp collision data set at $\sqrt{s}$ = 13, TeV. Eur. Phys. J. C **81**, 578 (2021). https://doi.org/10.1140/epjc/s10052-021-09233-2. arXiv:2012.00578 [hep-ex]
99. ATLAS Collaboration, Reconstruction, identification, and calibration of hadronically decaying tau leptons with the ATLAS detector for the LHC Run 3 and reprocessed Run 2 data. ATL-PHYS-PUB-2022-044 (2022). https://cds.cern.ch/record/2827111
100. ATLAS Collaboration, Identification of hadronic tau lepton decays using neural networks in the ATLAS experiment. ATL-PHYS-PUB-2019-033, 2019. https://cds.cern.ch/record/2688062
101. ATLAS Collaboration, Measurement of the tau lepton reconstruction and identification performance in the ATLAS experiment using pp collisions at $\sqrt{s}$ = 13 TeV. ATLAS-CONF-2017-029, 2017. https://cds.cern.ch/record/2261772
102. ATLAS Collaboration, Jet reconstruction and performance using particle flow with the ATLAS detector. Eur. Phys. J. C **77**, 466 (2017). https://doi.org/10.1140/epjc/s10052-017-5031-2. arXiv:1703.10485 [hep-ex]
103. ATLAS Collaboration, Jet energy scale and resolution measured in proton–proton collisions at $\sqrt{s}$ = 13, TeV with the ATLAS detector. Eur. Phys. J. C **81**, 689 (2021). https://doi.org/10.1140/epjc/s10052-021-09402-3. arXiv:2007.02645 [hep-ex]
104. M. Cacciari, G.P. Salam, G. Soyez, The anti-k_t jet clustering algorithm. JHEP **04**, 063 (2008). https://doi.org/10.1088/1126-6708/2008/04/063. arXiv:0802.1189 [hep-ph]
105. M. Cacciari, G.P. Salam, Dispelling the N^3 myth for the k_t jet-finder. Phys. Lett. B **641**, 57 (2006). https://doi.org/10.1016/j.physletb.2006.08.037. arXiv:hep-ph/0512210
106. ATLAS Collaboration, Tagging and suppression of pileup jets with the ATLAS detector. ATLAS-CONF-2014-018, 2014. https://cds.cern.ch/record/1700870
107. ATLAS Collaboration, ATLAS b-jet identification performance and efficiency measurement with $t\bar{t}$ events in pp collisions at $\sqrt{s}$ = 13 TeV. Eur. Phys. J. C **79**, 970 (2019). https://doi.org/10.1140/epjc/s10052-019-7450-8. arXiv:1907.05120 [hep-ex]
108. ATLAS Collaboration, ATLAS flavour-tagging algorithms for the LHC Run 2 pp collision dataset. Eur. Phys. J. C **83**, 681 (2023). https://doi.org/10.1140/epjc/s10052-023-11699-1. arXiv:2211.16345 [physics.data-an]
109. ATLAS Collaboration, The performance of missing transverse momentum reconstruction and its significance with the ATLAS detector using 140 fb^{-1} of $\sqrt{s}$ = 13 TeV pp collisions. Eur. Phys. J. C **85**, 606 (2025). https://doi.org/10.1140/epjc/s10052-025-14062-8. arXiv:2402.05858 [hep-ex]
110. ATLAS Collaboration, Performance of the missing transverse momentum triggers for the ATLAS detector during Run-2 data taking. JHEP **08**, 080 (2020). https://doi.org/10.1007/JHEP08(2020)080 arXiv:2005.09554 [hep-ex]
111. ATLAS Collaboration, The ATLAS tau trigger in Run 2. ATLAS-CONF-2017-061, 2017. https://cds.cern.ch/record/2274201
112. ATLAS Collaboration, Search for resonant and non-resonant Higgs boson pair production in the $b\bar{b}\tau^+\tau^-$ decay channel using 13 TeV pp collision data from the ATLAS detector. JHEP **07**, 040 (2023). https://doi.org/10.1007/JHEP07(2023)040. arXiv:2209.10910 [hep-ex]
113. ATLAS Collaboration, Configuration and performance of the ATLAS b-jet triggers in Run 2. Eur. Phys. J. C **81**, 1087 (2021). https://doi.org/10.1140/epjc/s10052-021-09775-5. arXiv:2106.03584 [hep-ex]
114. ATLAS Collaboration, Performance of the ATLAS muon triggers in Run 2. JINST **15**, P09015 (2020). https://doi.org/10.1088/1748-0221/15/09/p09015. arXiv:2004.13447 [physics.ins-det]
115. ATLAS Collaboration, Performance of electron and photon triggers in ATLAS during LHC Run 2. Eur. Phys. J. C **80**, 47 (2020). https://doi.org/10.1140/epjc/s10052-019-7500-2. arXiv:1909.00761 [hep-ex]
116. ATLAS Collaboration, Search for pair production of Higgsinos in events with two Higgs bosons and missing transverse momentum in $\sqrt{s}$ = 13 TeV pp collisions at the ATLAS experiment. Phys. Rev. D **109**, 112011 (2024). https://doi.org/10.1103/PhysRevD.109.112011. arXiv:2401.14922 [hep-ex]
117. C.M.S. Collaboration, Inclusive and differential cross section measurements of $t\bar{t}b\bar{b}$ production in the lepton+jets channel at $\sqrt{s}$ = 13 TeV. JHEP **05**, 042 (2024). https://doi.org/10.1007/JHEP05(2024)042. arXiv:2309.14442 [hep-ex]
118. ATLAS Collaboration, Measurements of differential cross sections of top quark pair production in association with jets in pp collisions at $\sqrt{s}$ = 13 TeV using the ATLAS detector. JHEP **10**, 159 (2018). https://doi.org/10.1007/JHEP10(2018)159. arXiv:1802.06572 [hep-ex]
119. P. Baldi, K. Cranmer, T. Faucett, P. Sadowski, D. Whiteson, Parameterized neural networks for high-energy physics. Eur. Phys. J. C **76**, 235 (2016). https://doi.org/10.1140/epjc/s10052-016-4099-4. arXiv:1601.07913 [hep-ex]
120. F. Chollet et al., Keras. (2015). https://keras.io
121. M. Abadi et al., TensorFlow: large-scale machine learning on heterogeneous systems. Software available from tensorflow.org. 2015. https://www.tensorflow.org/
122. M. Czakon et al., Top-pair production at the LHC through NNLO QCD and NLO EW. JHEP **2017**, 186 (2017). https://doi.org/10.1103/PhysRevD.99.052009. arXiv:1705.04105 [hep-ph]
123. ATLAS Collaboration, Search for four-top-quark production in the single-lepton and opposite-sign dilepton final states in pp collisions at $\sqrt{s}$ = 13 TeV with the ATLAS detector. Phys. Rev. D **99**, 052009 (2019). https://doi.org/10.1103/PhysRevD.99.052009 [hep-ex]. arXiv:1811.02305
124. ATLAS Collaboration, Measurement of Higgs boson decay into b-quarks in associated production with a top-quark pair in pp collisions at $\sqrt{s}$ = 13 TeV with the ATLAS detector.

JHEP **06**, 097 (2022). https://doi.org/10.1007/JHEP06(2022)097. arXiv:2111.06712 [hep-ex]
125. R. Ellis, I. Hinchliffe, M. Soldate, J. Bij, Higgs decay to $\tau^+\tau^-$ a possible signature of intermediate mass Higgs bosons at high energy hadron colliders. Nucl. Phys. B **297**, 221 (1988). https://doi.org/10.1016/0550-3213(88)90019-3
126. ATLAS Collaboration, Tools for estimating fake/non-prompt lepton backgrounds with the ATLAS detector at the LHC. JINST **18**, T11004 (2023). https://doi.org/10.1088/1748-0221/18/11/T11004. arXiv:2211.16178 [hep-ex]
127. ATLAS Collaboration, Luminosity determination in pp collisions at $\sqrt{s} = 13$ TeV using the ATLAS detector at the LHC. Eur. Phys. J. C **83**, 982 (2023). https://doi.org/10.1140/epjc/s10052-023-11747-w. arXiv:2212.09379 [hep-ex]
128. ATLAS Collaboration, Identification and energy calibration of hadronically decaying tau leptons with the ATLAS experiment in pp collisions at $\sqrt{s} = 8$ TeV. Eur. Phys. J. C **75**, 303 (2015). https://doi.org/10.1140/epjc/s10052-015-3500-z. arXiv:1412.7086 [hep-ex]
129. ATLAS Collaboration, Performance of pile-up mitigation techniques for jets in ppcollisions at $\sqrt{s} = 8$ TeV using the ATLAS detector. Eur. Phys. J. C **76**, 581 (2016). https://doi.org/10.1140/epjc/s10052-018-5771-7. arXiv:1510.03823 [hep-ex]
130. ATLAS Collaboration, Constituent-level pile-up mitigation techniques in ATLAS. ATLAS-CONF-2017-065, 2017. https://cds.cern.ch/record/2281055
131. ATLAS Collaboration, Performance of the ATLAS inner detector track and vertex reconstruction in the high pile-up LHC Environment. ATLAS-CONF-2012-042, 2012. https://cds.cern.ch/record/1435196
132. M. Grazzini, S. Kallweit, M. Wiesemann, Fully differential NNLO computations with matrix. Eur. Phys. J. C **2018**, 537 (2018). https://doi.org/10.1140/epjc/s10052-018-5771-7. arXiv:1711.06631 [hep-ph]
133. ATLAS Collaboration, Search for vector-like leptons coupling to first- and second-generation Standard Model leptons in pp collisions at$\sqrt{s} = 13$ TeV with the ATLAS detector. JHEP **05**, 075 (2025). https://doi.org/10.1007/JHEP05(2025)075. arXiv:2411.07143 [hep-ex]
134. ATLAS Collaboration, Measurements of the inclusive and differential production cross sections of a top-quark-antiquark pair in association with a Z boson at $\sqrt{s} = 13$ TeV with the ATLAS detector. Eur. Phys. J. C **81**, 737 (2021). https://doi.org/10.1140/epjc/s10052-021-09439-4. arXiv:2103.12603 [hep-ex]
135. ATLAS Collaboration, Inclusive and differential cross-section measurements of $t\bar{t}Z$ production in pp collisions at $\sqrt{s} = 13$ TeV with the ATLAS detector, including EFT and spin-correlation interpretations. JHEP **07**, 163 (2024). https://doi.org/10.1007/JHEP07(2024)163. arXiv:2312.04450 [hep-ex]
136. D. de Florian et al., Handbook of LHC Higgs cross sections: 4. Deciphering the nature of the Higgs sector. (2017). https://doi.org/10.23731/CYRM-2017-002. arXiv:1610.07922 [hep-ph]
137. ATLAS Collaboration, Observation of four-top-quark production in the multilepton final state with the ATLAS detector. Eur. Phys. J. C **83**, 496 (2023). https://doi.org/10.1140/epjc/s10052-023-11573-0. arXiv:2303.15061 [hep-ex]. [Erratum: 10.1140/epjc/s10052-024-12458-6. Eur. Phys. J. C 84 (2024) 156]
138. K. Cranmer, G. Lewis, L. Moneta, A. Shibata, W. Verkerke, HistFactory: a tool for creating statistical models for use with RooFit and RooStats. CERN-OPEN-2012-016 (2012). https://cds.cern.ch/record/1456844
139. R. Barlow, C. Beeston, Fitting using finite Monte Carlo samples. Comput. Phys. Commun. **77**, 219 (1993). https://doi.org/10.1016/0010-4655(93)90005-W
140. W. Verkerke, D. Kirkby, The RooFit toolkit for data modeling. (2003). arXiv:physics/0306116 [physics.data-an]
141. G. Cowan, K. Cranmer, E. Gross, O. Vitells, Asymptotic formulae for likelihood-based tests of new physics. Eur. Phys. J. C **71**, 1554 (2011). https://doi.org/10.1140/epjc/s10052-011-1554-0. arXiv:1007.1727 [physics.data-an]. [Erratum: 10.1140/epjc/s10052-013-2501-z. Eur. Phys. J. C 73 (2013) 2501]
142. T. Junk, Confidence level computation for combining searches with small statistics. Nucl. Instrum. Methods A **434**, 435 (1999). https://doi.org/10.1016/S0168-9002(99)00498-2. arXiv:hep-ex/9902006
143. A.L. Read, Presentation of search results: the cl_s technique. J. Phys. G **28**, 2693 (2002). https://doi.org/10.1088/0954-3899/28/10/313
144. ATLAS Collaboration, ATLAS computing acknowledgements. ATL-SOFT-PUB-2025-001 (2025). https://cds.cern.ch/record/2922210
145. CERN. CERN Open Data Policy for the LHC Experiments. CERN-OPEN-2020-013. https://cds.cern.ch/record/2745133

ATLAS Collaboration[★]

G. Aad[104], E. Aakvaag[17], B. Abbott[123], S. Abdelhameed[119a], K. Abeling[55], N. J. Abicht[49], S. H. Abidi[30], M. Aboelela[45], A. Aboulhorma[36e], H. Abramowicz[157], Y. Abulaiti[120], B. S. Acharya[69a,69b,n], A. Ackermann[63a], C. Adam Bourdarios[4], L. Adamczyk[87a], S. V. Addepalli[149], M. J. Addison[103], J. Adelman[118], A. Adiguzel[22c], T. Adye[137], A. A. Affolder[139], Y. Afik[40], M. N. Agaras[13], A. Aggarwal[102], C. Agheorghiesei[28c], F. Ahmadov[39,ae], S. Ahuja[97], X. Ai[143b], G. Aielli[76a,76b], A. Aikot[169], M. Ait Tamlihat[36e], B. Aitbenchikh[36a], M. Akbiyik[102], T. P. A. Åkesson[100], A. V. Akimov[151], D. Akiyama[174], N. N. Akolkar[25], S. Aktas[22a], G. L. Alberghi[24b], J. Albert[171], P. Albicocco[53], G. L. Albouy[60], S. Alderweireldt[52], Z. L. Alegria[124], M. Aleksa[37], I. N. Aleksandrov[39], C. Alexa[28b], T. Alexopoulos[10], F. Alfonsi[24b], M. Algren[56], M. Alhroob[173], B. Ali[135], H. M. J. Ali[93,x], S. Ali[32], S. W. Alibocus[94], M. Aliev[34c], G. Alimonti[71a], W. Alkakhi[55], C. Allaire[66], B. M. M. Allbrooke[152], J. S. Allen[103], J. F. Allen[52], P. P. Allport[21], A. Aloisio[72a,72b], F. Alonso[92], C. Alpigiani[142], Z. M. K. Alsolami[93], A. Alvarez Fernandez[102], M. Alves Cardoso[56], M. G. Alviggi[72a,72b], M. Aly[103], Y. Amaral Coutinho[83b], A. Ambler[106], C. Amelung[37], M. Amerl[103], C. G. Ames[111], T. Amezza[130], D. Amidei[108], B. Amini[54], K. Amirie[161], A. Amirkhanov[39], S. P. Amor Dos Santos[133a], K. R. Amos[169], D. Amperiadou[158], S. An[84], C. Anastopoulos[145], T. Andeen[11], J. K. Anders[94], A. C. Anderson[59], A. Andreazza[71a,71b], S. Angelidakis[9], A. Angerami[42], A. V. Anisenkov[39], A. Annovi[74a], C. Antel[56], E. Antipov[151], M. Antonelli[53], F. Anulli[75a], M. Aoki[84], T. Aoki[159], M. A. Aparo[152], L. Aperio Bella[48], M. Apicella[31], C. Appelt[157], A. Apyan[27], S. J. Arbiol Val[88], C. Arcangeletti[53], A. T. H. Arce[51], J-F. Arguin[110], S. Argyropoulos[158], J.-H. Arling[48], O. Arnaez[4], H. Arnold[151], G. Artoni[75a,75b], H. Asada[113], K. Asai[121], S. Asai[159], S. Asatryan[179], N. A. Asbah[37], R. A. Ashby Pickering[173], A. M. Aslam[97], K. Assamagan[30], R. Astalos[29a], K. S. V. Astrand[100], S. Atashi[165], R. J. Atkin[34a], H. Atmani[36f], P. A. Atmasiddha[131], K. Augsten[135], A. D. Auriol[41], V. A. Austrup[103], G. Avolio[37], K. Axiotis[56], G. Azuelos[110,ai], D. Babal[29b], H. Bachacou[138], K. Bachas[158,r], A. Bachiu[35], E. Bachmann[50], M. J. Backes[63a], A. Badea[40], T. M. Baer[108], P. Bagnaia[75a,75b], M. Bahmani[19], D. Bahner[54], K. Bai[126], J. T. Baines[137], L. Baines[96], O. K. Baker[178], E. Bakos[16], D. Bakshi Gupta[8], L. E. Balabram Filho[83b], V. Balakrishnan[123], R. Balasubramanian[4], E. M. Baldin[38], P. Balek[87a], E. Ballabene[24a,24b], F. Balli[138], L. M. Baltes[63a], W. K. Balunas[33], J. Balz[102], I. Bamwidhi[119b], E. Banas[88], M. Bandieramonte[132], A. Bandyopadhyay[25], S. Bansal[25], L. Barak[157], M. Barakat[48], E. L. Barberio[107], D. Barberis[18b], M. Barbero[104], M. Z. Barel[117], T. Barillari[112], M-S. Barisits[37], T. Barklow[149], P. Baron[136], D. A. Baron Moreno[103], A. Baroncelli[62], A. J. Barr[129], J. D. Barr[98], F. Barreiro[101], J. Barreiro Guimarães da Costa[14], M. G. Barros Teixeira[133a], S. Barsov[38], F. Bartels[63a], R. Bartoldus[149], A. E. Barton[93], P. Bartos[29a], A. Basan[102], M. Baselga[49], S. Bashiri[88], A. Bassalat[66,b], M. J. Basso[162a], S. Bataju[45], R. Bate[170], R. L. Bates[59], S. Batlamous[101], M. Battaglia[139], D. Battulga[19], M. Bauce[75a,75b], M. Bauer[79], P. Bauer[25], L. T. Bayer[48], L. T. Bazzano Hurrell[31], J. B. Beacham[112], T. Beau[130], J. Y. Beaucamp[92], P. H. Beauchemin[164], P. Bechtle[25], H. P. Beck[20,q], K. Becker[173], A. J. Beddall[82], V. A. Bednyakov[39], C. P. Bee[151], L. J. Beemster[16], M. Begalli[83d], M. Begel[30], J. K. Behr[48], J. F. Beirer[37], F. Beisiegel[25], M. Belfkir[119b], G. Bella[157], L. Bellagamba[24b], A. Bellerive[35], C. D. Bellgraph[68], P. Bellos[21], K. Beloborodov[38], D. Benchekroun[36a], F. Bendebba[36a], Y. Benhammou[157], K. C. Benkendorfer[61], L. Beresford[48], M. Beretta[53], E. Bergeaas Kuutmann[167], N. Berger[4], B. Bergmann[135], J. Beringer[18a], G. Bernardi[5], C. Bernius[149], F. U. Bernlochner[25], F. Bernon[37], A. Berrocal Guardia[13], T. Berry[97], P. Berta[136], A. Berthold[50], A. Berti[133a], R. Bertrand[104], S. Bethke[112], A. Betti[75a,75b], A. J. Bevan[96], L. Bezio[56], N. K. Bhalla[54], S. Bharthuar[112], S. Bhatta[151], P. Bhattarai[149], Z. M. Bhatti[120], K. D. Bhide[54], V. S. Bhopatkar[124], R. M. Bianchi[132], G. Bianco[24a,24b], O. Biebel[111], M. Biglietti[77a], C. S. Billingsley[45], Y. Bimgdi[36f], M. Bindi[55], A. Bingham[177], A. Bingul[22b], C. Bini[75a,75b], G. A. Bird[33], M. Birman[175], M. Biros[136], S. Biryukov[152], T. Bisanz[49], E. Bisceglie[24a,24b], J. P. Biswal[137], D. Biswas[147], I. Bloch[48], A. Blue[59], U. Blumenschein[96], J. Blumenthal[102], V. S. Bobrovnikov[39], M. Boehler[54], B. Boehm[172], D. Bogavac[13], A. G. Bogdanchikov[38], L. S. Boggia[130], V. Boisvert[97], P. Bokan[37], T. Bold[87a], M. Bomben[5], M. Bona[96], M. Boonekamp[138], A. G. Borbély[59], I. S. Bordulev[38], G. Borissov[93], D. Bortoletto[129], D. Boscherini[24b], M. Bosman[13], K. Bouaouda[36a], N. Bouchhar[169], L. Boudet[4], J. Boudreau[132], E. V. Bouhova-Thacker[93], D. Boumediene[41], R. Bouquet[57a,57b], A. Boveia[122], J. Boyd[37], D. Boye[30], I. R. Boyko[39], L. Bozianu[56], J. Bracinik[21], N. Brahimi[4], G. Brandt[177], O. Brandt[33], B. Brau[105], J. E. Brau[126], R. Brener[175], L. Brenner[117], R. Brenner[167], S. Bressler[175], G. Brianti[78a,78b],

D. Britton[59], D. Britzger[112], I. Brock[25], R. Brock[109], G. Brooijmans[42], A. J. Brooks[68], E. M. Brooks[162b], E. Brost[30], L. M. Brown[162a,171], L. E. Bruce[61], T. L. Bruckler[129], P. A. Bruckman de Renstrom[88], B. Brüers[48], A. Bruni[24b], G. Bruni[24b], D. Brunner[47a,47b], M. Bruschi[24b], N. Bruscino[75a,75b], T. Buanes[17], Q. Buat[142], D. Buchin[112], A. G. Buckley[59], O. Bulekov[82], B. A. Bullard[149], S. Burdin[94], C. D. Burgard[49], A. M. Burger[91], B. Burghgrave[8], O. Burlayenko[54], J. Burleson[168], J. C. Burzynski[148], E. L. Busch[42], V. Büscher[102], P. J. Bussey[59], J. M. Butler[26], C. M. Buttar[59], J. M. Butterworth[98], W. Buttinger[137], C. J. Buxo Vazquez[109], A. R. Buzykaev[39], S. Cabrera Urbán[169], L. Cadamuro[66], D. Caforio[58], H. Cai[132], Y. Cai[24a,24b,114c], Y. Cai[114a], V. M. M. Cairo[37], O. Cakir[3a], N. Calace[37], P. Calafiura[18a], G. Calderini[130], P. Calfayan[35], G. Callea[59], L. P. Caloba[83b], D. Calvet[41], S. Calvet[41], R. Camacho Toro[130], S. Camarda[37], D. Camarero Munoz[27], P. Camarri[76a,76b], C. Camincher[171], M. Campanelli[98], A. Camplani[43], V. Canale[72a,72b], A. C. Canbay[3a], E. Canonero[97], J. Cantero[169], Y. Cao[168], F. Capocasa[27], M. Capua[44a,44b], A. Carbone[71a,71b], R. Cardarelli[76a], J. C. J. Cardenas[8], M. P. Cardiff[27], G. Carducci[44a,44b], T. Carli[37], G. Carlino[72a], J. I. Carlotto[13], B. T. Carlson[132,s], E. M. Carlson[171], J. Carmignani[94], L. Carminati[71a,71b], A. Carnelli[4], M. Carnesale[37], S. Caron[116], E. Carquin[140f], I. B. Carr[107], S. Carrá[73a,73b], G. Carratta[24a,24b], A. M. Carroll[126], M. P. Casado[13,i], M. Caspar[48], F. L. Castillo[4], L. Castillo Garcia[13], V. Castillo Gimenez[169], N. F. Castro[133a,133e], A. Catinaccio[37], J. R. Catmore[128], T. Cavaliere[4], V. Cavaliere[30], L. J. Caviedes Betancourt[23b], E. Celebi[82], S. Cella[37], V. Cepaitis[56], K. Cerny[125], A. S. Cerqueira[83a], A. Cerri[74a,74b,al], L. Cerrito[76a,76b], F. Cerutti[18a], B. Cervato[71a,71b], A. Cervelli[24b], G. Cesarini[53], S. A. Cetin[82], P. M. Chabrillat[130], S. Chakraborty[173], J. Chan[18a], W. Y. Chan[159], J. D. Chapman[33], E. Chapon[138], B. Chargeishvili[155b], D. G. Charlton[21], C. Chauhan[136], Y. Che[114a], S. Chekanov[6], S. V. Chekulaev[162a], G. A. Chelkov[39,a], B. Chen[157], B. Chen[171], H. Chen[114a], H. Chen[30], J. Chen[144a], J. Chen[148], M. Chen[129], S. Chen[89], S. J. Chen[114a], X. Chen[144a], X. Chen[15,ah], Z. Chen[62], C. L. Cheng[176], H. C. Cheng[64a], S. Cheong[149], A. Cheplakov[39], E. Cherepanova[117], R. Cherkaoui El Moursli[36e], E. Cheu[7], K. Cheung[65], L. Chevalier[138], V. Chiarella[53], G. Chiarelli[74a], G. Chiodini[70a], A. S. Chisholm[21], A. Chitan[28b], M. Chitishvili[169], M. V. Chizhov[39,t], K. Choi[11], Y. Chou[142], E. Y. S. Chow[116], K. L. Chu[175], M. C. Chu[64a], X. Chu[14,114c], Z. Chubinidze[53], J. Chudoba[134], J. J. Chwastowski[88], D. Cieri[112], K. M. Ciesla[87a], V. Cindro[95], A. Ciocio[18a], F. Cirotto[72a,72b], Z. H. Citron[175], M. Citterio[71a], D. A. Ciubotaru[28b], A. Clark[56], P. J. Clark[52], N. Clarke Hall[98], C. Clarry[161], S. E. Clawson[48], C. Clement[47a,47b], Y. Coadou[104], M. Cobal[69a,69c], A. Coccaro[57b], R. F. Coelho Barrue[133a], R. Coelho Lopes De Sa[105], S. Coelli[71a], L. S. Colangeli[161], B. Cole[42], P. Collado Soto[101], J. Collot[60], R. Coluccia[70a,70b], P. Conde Muiño[133a,133g], M. P. Connell[34c], S. H. Connell[34c], E. I. Conroy[129], M. Contreras Cossio[11], F. Conventi[72a,aj], H. G. Cooke[21], A. M. Cooper-Sarkar[129], L. Corazzina[75a,75b], F. A. Corchia[24a,24b], A. Cordeiro Oudot Choi[142], L. D. Corpe[41], M. Corradi[75a,75b], F. Corriveau[106,ac], A. Cortes-Gonzalez[159], M. J. Costa[169], F. Costanza[4], D. Costanzo[145], B. M. Cote[122], J. Couthures[4], G. Cowan[97], K. Cranmer[176], L. Cremer[49], D. Cremonini[24a,24b], S. Crépé-Renaudin[60], F. Crescioli[130], T. Cresta[73a,73b], M. Cristinziani[147], M. Cristoforetti[78a,78b], V. Croft[117], J. E. Crosby[124], G. Crosetti[44a,44b], A. Cueto[101], H. Cui[98], Z. Cui[7], W. R. Cunningham[59], F. Curcio[169], J. R. Curran[52], M. J. Da Cunha Sargedas De Sousa[57a,57b], J.V. Da Fonseca Pinto[83b], C. Da Via[103], W. Dabrowski[87a], T. Dado[37], S. Dahbi[154], T. Dai[108], D. Dal Santo[20], C. Dallapiccola[105], M. Dam[43], G. D'amen[30], V. D'Amico[111], J. Damp[102], J. R. Dandoy[35], D. Dannheim[37], G. D'anniballe[74a,74b], M. Danninger[148], V. Dao[151], G. Darbo[57b], S. J. Das[30], F. Dattola[48], S. D'Auria[71a,71b], A. D'Avanzo[72a,72b], T. Davidek[136], J. Davidson[173], I. Dawson[96], K. De[8], C. De Almeida Rossi[161], R. De Asmundis[72a], N. De Biase[48], S. De Castro[24a,24b], N. De Groot[116], P. de Jong[117], H. De la Torre[118], A. De Maria[114a], A. De Salvo[75a], U. De Sanctis[76a,76b], F. De Santis[70a,70b], A. De Santo[152], J. B. De Vivie De Regie[60], J. Debevc[95], D. V. Dedovich[39], J. Degens[94], A. M. Deiana[45], J. Del Peso[101], L. Delagrange[130], F. Deliot[138], C. M. Delitzsch[49], M. Della Pietra[72a,72b], D. Della Volpe[56], A. Dell'Acqua[37], L. Dell'Asta[71a,71b], M. Delmastro[4], C. C. Delogu[102], P. A. Delsart[60], S. Demers[178], M. Demichev[39], S. P. Denisov[38], H. Denizli[22a,m], L. D'Eramo[41], D. Derendarz[88], F. Derue[130], P. Dervan[94], K. Desch[25], F. A. Di Bello[57a,57b], A. Di Ciaccio[76a,76b], L. Di Ciaccio[4], A. Di Domenico[75a,75b], C. Di Donato[72a,72b], A. Di Girolamo[37], G. Di Gregorio[37], A. Di Luca[78a,78b], B. Di Micco[77a,77b], R. Di Nardo[77a,77b], K. F. Di Petrillo[40], M. Diamantopoulou[35], F. A. Dias[117], M. A. Diaz[140a,140b], A. R. Didenko[39], M. Didenko[169], S. D. Diefenbacher[18a], E. B. Diehl[108], S. Díez Cornell[48], C. Diez Pardos[147], C. Dimitriadi[150], A. Dimitrievska[21], A. Dimri[151], J. Dingfelder[25], T. Dingley[129], I-M. Dinu[28b], S.J. Dittmeier[63b], F. Dittus[37], M. Divisek[136], B. Dixit[94], F. Djama[104], T. Djobava[155b], C. Doglioni[100,103],

A. Dohnalova[29a], Z. Dolezal[136], K. Domijan[87a], K. M. Dona[40], M. Donadelli[83d], B. Dong[109], J. Donini[41], A. D'Onofrio[72a,72b], M. D'Onofrio[94], J. Dopke[137], A. Doria[72a], N. Dos Santos Fernandes[133a], P. Dougan[103], M. T. Dova[92], A. T. Doyle[59], M. A. Draguet[129], M. P. Drescher[55], E. Dreyer[175], I. Drivas-koulouris[10], M. Drnevich[120], M. Drozdova[56], D. Du[62], T. A. du Pree[117], Z. Duan[114a], F. Dubinin[39], M. Dubovsky[29a], E. Duchovni[175], G. Duckeck[111], P. K. Duckett[98], O. A. Ducu[28b], D. Duda[52], A. Dudarev[37], E. R. Duden[27], M. D'uffizi[103], L. Duflot[66], M. Dührssen[37], I. Duminica[28g], A. E. Dumitriu[28b], M. Dunford[63a], S. Dungs[49], K. Dunne[47a,47b], A. Duperrin[104], H. Duran Yildiz[3a], M. Düren[58], A. Durglishvili[155b], D. Duvnjak[35], B. L. Dwyer[118], G. I. Dyckes[18a], M. Dyndal[87a], B. S. Dziedzic[37], Z. O. Earnshaw[152], G. H. Eberwein[129], B. Eckerova[29a], S. Eggebrecht[55], E. Egidio Purcino De Souza[83e], G. Eigen[17], K. Einsweiler[18a], T. Ekelof[167], P. A. Ekman[100], S. El Farkh[36b], Y. El Ghazali[62], H. El Jarrari[37], A. El Moussaouy[36a], V. Ellajosyula[167], M. Ellert[167], F. Ellinghaus[177], N. Ellis[37], J. Elmsheuser[30], M. Elsawy[119a], M. Elsing[37], D. Emeliyanov[137], Y. Enari[84], I. Ene[18a], S. Epari[110], D. Ernani Martins Neto[88], F. Ernst[37], M. Errenst[177], M. Escalier[66], C. Escobar[169], E. Etzion[157], G. Evans[133a,133b], H. Evans[68], L. S. Evans[97], A. Ezhilov[38], S. Ezzarqtouni[36a], F. Fabbri[24a,24b], L. Fabbri[24a,24b], G. Facini[98], V. Fadeyev[139], R. M. Fakhrutdinov[38], D. Fakoudis[102], S. Falciano[75a], L. F. Falda Ulhoa Coelho[133a], F. Fallavollita[112], G. Falsetti[44a,44b], J. Faltova[136], C. Fan[168], K. Y. Fan[64b], Y. Fan[14], Y. Fang[14,114c], M. Fanti[71a,71b], M. Faraj[69a,69b], Z. Farazpay[99], A. Farbin[8], A. Farilla[77a], T. Farooque[109], J. N. Farr[178], S. M. Farrington[52,137], F. Fassi[36e], D. Fassouliotis[9], L. Fayard[66], P. Federic[136], P. Federicova[134], O. L. Fedin[38,a], M. Feickert[176], L. Feligioni[104], D. E. Fellers[18a], C. Feng[143a], Z. Feng[117], M. J. Fenton[165], L. Ferencz[48], B. Fernandez Barbadillo[93], P. Fernandez Martinez[67], M. J. V. Fernoux[104], J. Ferrando[93], A. Ferrari[167], P. Ferrari[116,117], R. Ferrari[73a], D. Ferrere[56], C. Ferretti[108], M. P. Fewell[1], D. Fiacco[75a,75b], F. Fiedler[102], P. Fiedler[135], S. Filimonov[39], M. S. Filip[28b,u], A. Filipčič[95], E. K. Filmer[162a], F. Filthaut[116], M. C. N. Fiolhais[133a,133c,c], L. Fiorini[169], W. C. Fisher[109], T. Fitschen[103], P. M. Fitzhugh[138], I. Fleck[147], P. Fleischmann[108], T. Flick[177], M. Flores[34d,ag], L. R. Flores Castillo[64a], L. Flores Sanz De Acedo[37], F. M. Follega[78a,78b], N. Fomin[33], J. H. Foo[161], A. Formica[138], A. C. Forti[103], E. Fortin[37], A. W. Fortman[18a], L. Foster[18a], L. Fountas[9,j], D. Fournier[66], H. Fox[93], P. Francavilla[74a,74b], S. Francescato[61], S. Franchellucci[56], M. Franchini[24a,24b], S. Franchino[63a], D. Francis[37], L. Franco[116], V. Franco Lima[37], L. Franconi[48], M. Franklin[61], G. Frattari[27], Y. Y. Frid[157], J. Friend[59], N. Fritzsche[37], A. Froch[56], D. Froidevaux[37], J. A. Frost[129], Y. Fu[109], S. Fuenzalida Garrido[140f], M. Fujimoto[104], K. Y. Fung[64a], E. Furtado De Simas Filho[83e], M. Furukawa[159], J. Fuster[169], A. Gaa[55], A. Gabrielli[24a,24b], A. Gabrielli[161], P. Gadow[37], G. Gagliardi[57a,57b], L. G. Gagnon[18a], S. Gaid[85b], S. Galantzan[157], J. Gallagher[1], E. J. Gallas[129], A. L. Gallen[167], B. J. Gallop[137], K. K. Gan[122], S. Ganguly[159], Y. Gao[52], A. Garabaglu[142], F. M. Garay Walls[140a,140b], C. García[169], A. Garcia Alonso[117], A. G. Garcia Caffaro[178], J. E. García Navarro[169], M. Garcia-Sciveres[18a], G. L. Gardner[131], R. W. Gardner[40], N. Garelli[164], R. B. Garg[149], J. M. Gargan[52], C. A. Garner[161], C. M. Garvey[34a], V. K. Gassmann[164], G. Gaudio[73a], V. Gautam[13], P. Gauzzi[75a,75b], J. Gavranovic[95], I. L. Gavrilenko[133a], A. Gavrilyuk[38], C. Gay[170], G. Gaycken[126], E. N. Gazis[10], A. Gekow[122], C. Gemme[57b], M. H. Genest[60], A. D. Gentry[115], S. George[97], T. Geralis[46], A. A. Gerwin[123], P. Gessinger-Befurt[37], M. E. Geyik[177], M. Ghani[173], K. Ghorbanian[96], A. Ghosal[147], A. Ghosh[165], A. Ghosh[7], B. Giacobbe[24b], S. Giagu[75a,75b], T. Giani[117], A. Giannini[62], S. M. Gibson[97], M. Gignac[139], D. T. Gil[87b], A. K. Gilbert[87a], B. J. Gilbert[42], D. Gillberg[35], G. Gilles[117], D. M. Gingrich[2,ai], M. P. Giordani[69a,69c], P. F. Giraud[138], G. Giugliarelli[69a,69c], D. Giugni[71a], F. Giuli[76a,76b], I. Gkialas[9,j], L. K. Gladilin[38], C. Glasman[101], M. Glazewska[20], R. M. Gleason[165], G. Glemža[48], M. Glisic[126], I. Gnesi[44b], Y. Go[30], M. Goblirsch-Kolb[37], B. Gocke[49], D. Godin[110], B. Gokturk[22a], S. Goldfarb[107], T. Golling[56], M. G. D. Gololo[34c], D. Golubkov[38], J. P. Gombas[109], A. Gomes[133a,133b], G. Gomes Da Silva[147], A. J. Gomez Delegido[169], R. Gonçalo[133a], L. Gonella[21], A. Gongadze[155c], F. Gonnella[21], J. L. Gonski[149], R. Y. González Andana[52], S. González de la Hoz[169], M. V. Gonzalez Rodrigues[48], R. Gonzalez Suarez[167], S. Gonzalez-Sevilla[56], L. Goossens[37], B. Gorini[37], E. Gorini[70a,70b], A. Gorišek[95], T. C. Gosart[131], A. T. Goshaw[51], M. I. Gostkin[39], S. Goswami[124], C. A. Gottardo[37], S. A. Gotz[111], M. Gouighri[36b], A. G. Goussiou[142], N. Govender[34c], R. P. Grabarczyk[129], I. Grabowska-Bold[87a], K. Graham[35], E. Gramstad[128], S. Grancagnolo[70a,70b], C. M. Grant[1], P. M. Gravila[28f], F. G. Gravili[70a,70b], H. M. Gray[18a], M. Greco[112], M.J. Green[1], C. Grefe[25], A. S. Grefsrud[17], I. M. Gregor[48], K. T. Greif[165], P. Grenier[149], S. G. Grewe[112], A. A. Grillo[139], K. Grimm[32], S. Grinstein[13,y], J.-F. Grivaz[66], E. Gross[175], J. Grosse-Knetter[55], L. Guan[108], G. Guerrieri[37], R. Guevara[128], R. Gugel[102], J. A. M. Guhit[108], A. Guida[19], E. Guilloton[173], S. Guindon[37], F. Guo[14,114c], J. Guo[144a], L. Guo[48], L. Guo[114b,w],

Y. Guo[108], A. Gupta[49], R. Gupta[132], S. Gupta[27], S. Gurbuz[25], S. S. Gurdasani[48], G. Gustavino[75a,75b], P. Gutierrez[123], L. F. Gutierrez Zagazeta[131], M. Gutsche[50], C. Gutschow[98], C. Gwenlan[129], C. B. Gwilliam[94], E. S. Haaland[128], A. Haas[120], M. Habedank[59], C. Haber[18a], H. K. Hadavand[8], A. Haddad[41], A. Hadef[50], A. I. Hagan[93], J. J. Hahn[147], E. H. Haines[98], M. Haleem[172], J. Haley[124], G. D. Hallewell[104], L. Halser[20], K. Hamano[171], M. Hamer[25], S. E. D. Hammoud[66], E. J. Hampshire[97], J. Han[143a], L. Han[114a], L. Han[62], S. Han[18a], K. Hanagaki[84], M. Hance[139], D. A. Hangal[42], H. Hanif[148], M. D. Hank[131], J. B. Hansen[43], P. H. Hansen[43], D. Harada[56], T. Harenberg[177], S. Harkusha[179], M. L. Harris[105], Y. T. Harris[25], J. Harrison[13], N. M. Harrison[122], P. F. Harrison[173], M. L. E. Hart[98], N. M. Hartman[112], N. M. Hartmann[111], R. Z. Hasan[97,137], Y. Hasegawa[146], F. Haslbeck[129], S. Hassan[17], R. Hauser[109], M. Haviernik[136], C. M. Hawkes[21], R. J. Hawkings[37], Y. Hayashi[159], D. Hayden[109], C. Hayes[108], R. L. Hayes[117], C. P. Hays[129], J. M. Hays[96], H. S. Hayward[94], M. He[14,114c], Y. He[48], Y. He[98], N. B. Heatley[96], V. Hedberg[100], C. Heidegger[54], K. K. Heidegger[54], J. Heilman[35], S. Heim[48], T. Heim[18a], J. G. Heinlein[131], J. J. Heinrich[126], L. Heinrich[112], J. Hejbal[134], M. Helbig[50], A. Held[176], S. Hellesund[17], C. M. Helling[170], S. Hellman[47a,47b], A. M. Henriques Correia[37], H. Herde[100], Y. Hernández Jiménez[151], L. M. Herrmann[25], T. Herrmann[50], G. Herten[54], R. Hertenberger[111], L. Hervas[37], M. E. Hesping[102], N. P. Hessey[162a], J. Hessler[112], M. Hidaoui[36b], N. Hidic[136], E. Hill[161], T. S. Hillersoy[17], S. J. Hillier[21], J. R. Hinds[109], F. Hinterkeuser[25], M. Hirose[127], S. Hirose[163], D. Hirschbuehl[177], T. G. Hitchings[103], B. Hiti[95], J. Hobbs[151], R. Hobincu[28e], N. Hod[175], A. M. Hodges[168], M. C. Hodgkinson[145], B. H. Hodkinson[129], A. Hoecker[37], D. D. Hofer[108], J. Hofer[169], M. Holzbock[37], L. B. A. H. Hommels[33], V. Homsak[129], B. P. Honan[103], J. J. Hong[68], T. M. Hong[132], B. H. Hooberman[168], W. H. Hopkins[6], M. C. Hoppesch[168], Y. Horii[113], M. E. Horstmann[112], S. Hou[154], M. R. Housenga[168], A. S. Howard[95], J. Howarth[59], J. Hoya[6], M. Hrabovsky[125], T. Hryn'ova[4], P. J. Hsu[65], S.-C. Hsu[142], T. Hsu[66], M. Hu[18a], Q. Hu[62], S. Huang[33], X. Huang[14,114c], Y. Huang[136], Y. Huang[114b], Y. Huang[102], Y. Huang[14], Z. Huang[66], Z. Hubacek[135], M. Huebner[25], F. Huegging[25], T. B. Huffman[129], M. Hufnagel Maranha De Faria[83a], C. A. Hugli[48], M. Huhtinen[37], S. K. Huiberts[17], R. Hulsken[106], C. E. Hultquist[18a], N. Huseynov[12,g], J. Huston[109], J. Huth[61], R. Hyneman[7], G. Iacobucci[56], G. Iakovidis[30], L. Iconomidou-Fayard[66], J. P. Iddon[37], P. Iengo[72a,72b], R. Iguchi[159], Y. Iiyama[159], T. Iizawa[159], Y. Ikegami[84], D. Iliadis[158], N. Ilic[161], H. Imam[36a], G. Inacio Goncalves[83d], S. A. Infante Cabanas[140c], T. Ingebretsen Carlson[47a,47b], J. M. Inglis[96], G. Introzzi[73a,73b], M. Iodice[77a], V. Ippolito[75a,75b], R. K. Irwin[94], M. Ishino[159], W. Islam[176], C. Issever[19], S. Istin[22a,an], K. Itabashi[84], H. Ito[174], R. Iuppa[78a,78b], A. Ivina[175], V. Izzo[72a], P. Jacka[134], P. Jackson[1], P. Jain[48], K. Jakobs[54], T. Jakoubek[175], J. Jamieson[59], W. Jang[159], S. Jankovych[136], M. Javurkova[105], P. Jawahar[103], L. Jeanty[126], J. Jejelava[155a,af], P. Jenni[54,f], C. E. Jessiman[35], C. Jia[143a], H. Jia[170], J. Jia[151], X. Jia[14,114c], Z. Jia[114a], C. Jiang[52], Q. Jiang[64b], S. Jiggins[48], M. Jimenez Ortega[169], J. Jimenez Pena[13], S. Jin[114a], A. Jinaru[28b], O. Jinnouchi[141], P. Johansson[145], K. A. Johns[7], J. W. Johnson[139], F. A. Jolly[48], D. M. Jones[152], E. Jones[48], K. S. Jones[8], P. Jones[33], R. W. L. Jones[93], T. J. Jones[94], H. L. Joos[37,55], R. Joshi[122], J. Jovicevic[16], X. Ju[18a], J. J. Junggeburth[37], T. Junkermann[63a], A. Juste Rozas[13,y], M. K. Juzek[88], S. Kabana[140e], A. Kaczmarska[88], M. Kado[112], H. Kagan[122], M. Kagan[149], A. Kahn[131], C. Kahra[102], T. Kaji[159], E. Kajomovitz[156], N. Kakati[175], N. Kakoty[13], I. Kalaitzidou[54], S. Kandel[8], N. J. Kang[139], D. Kar[34g], K. Karava[129], E. Karentzos[25], O. Karkout[117], S. N. Karpov[39], Z. M. Karpova[39], V. Kartvelishvili[93], A. N. Karyukhin[38], E. Kasimi[158], J. Katzy[48], S. Kaur[35], K. Kawade[146], M. P. Kawale[123], C. Kawamoto[89], T. Kawamoto[62], E. F. Kay[37], F. I. Kaya[164], S. Kazakos[109], V. F. Kazanin[38], J. M. Keaveney[34a], R. Keeler[171], G. V. Kehris[61], J. S. Keller[35], J. J. Kempster[152], O. Kepka[134], J. Kerr[162b], B. P. Kerridge[137], B. P. Kerševan[95], L. Keszeghova[29a], R. A. Khan[132], A. Khanov[124], A. G. Kharlamov[38], T. Kharlamova[38], E. E. Khoda[142], M. Kholodenko[133a], T. J. Khoo[19], G. Khoriauli[172], Y. Khoulaki[36a], J. Khubua[155b,*], Y. A. R. Khwaira[130], B. Kibirige[34g], D. Kim[6], D. W. Kim[47a,47b], Y. K. Kim[40], N. Kimura[98], M. K. Kingston[55], A. Kirchhoff[55], C. Kirfel[25], F. Kirfel[25], J. Kirk[137], A. E. Kiryunin[112], S. Kita[163], O. Kivernyk[25], M. Klassen[164], C. Klein[35], L. Klein[172], M. H. Klein[45], S. B. Klein[56], U. Klein[94], A. Klimentov[30], T. Klioutchnikova[37], P. Kluit[117], S. Kluth[112], E. Kneringer[79], T. M. Knight[161], A. Knue[49], M. Kobel[50], D. Kobylianskii[175], S. F. Koch[129], M. Kocian[149], P. Kodyš[136], D. M. Koeck[126], T. Koffas[35], O. Kolay[50], I. Koletsou[4], T. Komarek[88], K. Köneke[55], A. X. Y. Kong[1], T. Kono[121], N. Konstantinidis[98], P. Kontaxakis[56], B. Konya[100], R. Kopeliansky[42], S. Koperny[87a], K. Korcyl[88], K. Kordas[158,d], A. Korn[98], S. Korn[55], I. Korolkov[13], N. Korotkova[38], B. Kortman[117], O. Kortner[112], S. Kortner[112], W. H. Kostecka[118], M. Kostov[29a], V. V. Kostyukhin[147],

A. Kotsokechagia[37], A. Kotwal[51], A. Koulouris[37], A. Kourkoumeli-Charalampidi[73a,73b], C. Kourkoumelis[9], E. Kourlitis[112], O. Kovanda[126], R. Kowalewski[171], W. Kozanecki[126], A. S. Kozhin[38], V. A. Kramarenko[38], G. Kramberger[95], P. Kramer[25], M. W. Krasny[130], A. Krasznahorkay[105], A. C. Kraus[118], J. W. Kraus[177], J. A. Kremer[48], N. B. Krengel[147], T. Kresse[50], L. Kretschmann[177], J. Kretzschmar[94], K. Kreul[19], P. Krieger[161], K. Krizka[21], K. Kroeninger[49], H. Kroha[112], J. Kroll[134], J. Kroll[131], K. S. Krowpman[109], U. Kruchonak[39], H. Krüger[25], N. Krumnack[81], M. C. Kruse[51], O. Kuchinskaia[39], S. Kuday[3a], S. Kuehn[37], R. Kuesters[54], T. Kuhl[48], V. Kukhtin[39], Y. Kulchitsky[39], S. Kuleshov[140b,140d], J. Kull[1], M. Kumar[34g], N. Kumari[48], P. Kumari[162b], A. Kupco[134], T. Kupfer[49], A. Kupich[38], O. Kuprash[54], H. Kurashige[86], L. L. Kurchaninov[162a], O. Kurdysh[4], Y. A. Kurochkin[38], A. Kurova[38], M. Kuze[141], A. K. Kvam[105], J. Kvita[125], N. G. Kyriacou[108], C. Lacasta[169], F. Lacava[75a,75b], H. Lacker[19], D. Lacour[130], N. N. Lad[98], E. Ladygin[39], A. Lafarge[41], B. Laforge[130], T. Lagouri[178], F. Z. Lahbabi[36a], S. Lai[55], J. E. Lambert[171], S. Lammers[68], W. Lampl[7], C. Lampoudis[158,d], G. Lamprinoudis[102], A.N. Lancaster[118], E. Lançon[30], U. Landgraf[54], M. P. J. Landon[96], V. S. Lang[54], O. K. B. Langrekken[128], A. J. Lankford[165], F. Lanni[37], K. Lantzsch[25], A. Lanza[73a], M. Lanzac Berrocal[169], J. F. Laporte[138], T. Lari[71a], D. Larsen[17], L. Larson[11], F. Lasagni Manghi[24b], M. Lassnig[37], S. D. Lawlor[145], R. Lazaridou[173], M. Lazzaroni[71a,71b], H. D. M. Le[109], E. M. Le Boulicaut[178], L. T. Le Pottier[18a], B. Leban[24a,24b], F. Ledroit-Guillon[60], T. F. Lee[162b], L. L. Leeuw[34c], M. Lefebvre[171], C. Leggett[18a], G. Lehmann Miotto[37], M. Leigh[56], W. A. Leight[105], W. Leinonen[116], A. Leisos[158,v], M. A. L. Leite[83c], C. E. Leitgeb[19], R. Leitner[136], K. J. C. Leney[45], T. Lenz[25], S. Leone[74a], C. Leonidopoulos[52], A. Leopold[150], J. H. Lepage Bourbonnais[35], R. Les[109], C. G. Lester[33], M. Levchenko[38], J. Levêque[4], L. J. Levinson[175], G. Levrini[24a,24b], M. P. Lewicki[88], C. Lewis[142], D. J. Lewis[4], L. Lewitt[145], A. Li[30], B. Li[143a], C. Li[108], C-Q. Li[112], H. Li[143a], H. Li[103], H. Li[15], H. Li[62], H. Li[143a], J. Li[144a], K. Li[14], L. Li[144a], R. Li[178], S. Li[14,114c], S. Li[144a,144b], T. Li[5], X. Li[106], Z. Li[159], Z. Li[14,114c], Z. Li[62], S. Liang[14,114c], Z. Liang[14], M. Liberatore[138], B. Liberti[76a], K. Lie[64c], J. Lieber Marin[83e], H. Lien[68], H. Lin[108], S. F. Lin[151], L. Linden[111], R. E. Lindley[7], J. H. Lindon[37], J. Ling[61], E. Lipeles[131], A. Lipniacka[17], A. Lister[170], J. D. Little[68], B. Liu[14], B. X. Liu[114b], D. Liu[144a,144b], D. Liu[139], E. H. L. Liu[21], J. K. K. Liu[120], K. Liu[144b], K. Liu[144a,144b], M. Liu[62], M. Y. Liu[62], P. Liu[14], Q. Liu[142,144a,144b], X. Liu[62], X. Liu[143a], Y. Liu[114b,114c], Y. L. Liu[143a], Y. W. Liu[62], Z. Liu[66,l], S. L. Lloyd[96], E. M. Lobodzinska[48], P. Loch[7], E. Lodhi[161], T. Lohse[19], K. Lohwasser[145], E. Loiacono[48], J. D. Lomas[21], J. D. Long[42], I. Longarini[165], R. Longo[168], A. Lopez Solis[13], N. A. Lopez-canelas[7], N. Lorenzo Martinez[4], A. M. Lory[111], M. Losada[119a], G. Löschcke Centeno[152], X. Lou[47a,47b], X. Lou[14,114c], A. Lounis[66], P. A. Love[93], M. Lu[66], S. Lu[131], Y. J. Lu[154], H. J. Lubatti[142], C. Luci[75a,75b], F. L. Lucio Alves[114a], F. Luehring[68], B. S. Lunday[131], O. Lundberg[150], J. Lunde[37], N. A. Luongo[6], M. S. Lutz[37], A. B. Lux[26], D. Lynn[30], R. Lysak[134], V. Lysenko[135], E. Lytken[100], V. Lyubushkin[39], T. Lyubushkina[39], M. M. Lyukova[151], M. Firdaus M. Soberi[52], H. Ma[30], K. Ma[62], L. L. Ma[143a], W. Ma[62], Y. Ma[124], J. C. MacDonald[102], P. C. Machado De Abreu Farias[83e], R. Madar[41], T. Madula[98], J. Maeda[86], T. Maeno[30], P. T. Mafa[34c,k], H. Maguire[145], V. Maiboroda[66], A. Maio[133a,133b,133d], K. Maj[87a], O. Majersky[48], S. Majewski[126], R. Makhmanazarov[38], N. Makovec[66], V. Maksimovic[16], B. Malaescu[130], J. Malamant[128], Pa. Malecki[88], V. P. Maleev[38], F. Malek[60,p], M. Mali[95], D. Malito[97], U. Mallik[80,*], A. Maloizel[5], S. Maltezos[10], A. Malvezzi Lopes[83d], S. Malyukov[39], J. Mamuzic[13], G. Mancini[53], M. N. Mancini[27], G. Manco[73a,73b], J. P. Mandalia[96], S. S. Mandarry[152], I. Mandić[95], L. Manhaes de Andrade Filho[83a], I. M. Maniatis[175], J. Manjarres Ramos[91], D.C. Mankad[175], A. Mann[111], T. Manoussos[37], M. N. Mantinan[40], S. Manzoni[37], L. Mao[144a], X. Mapekula[34c], A. Marantis[158], R. R. Marcelo Gregorio[96], G. Marchiori[5], M. Marcisovsky[134], C. Marcon[71a], E. Maricic[16], M. Marinescu[48], S. Marium[48], M. Marjanovic[123], A. Markhoos[54], M. Markovitch[66], M. K. Maroun[105], G. T. Marsden[103], E. J. Marshall[93], Z. Marshall[18a], S. Marti-Garcia[169], J. Martin[98], T. A. Martin[137], V. J. Martin[52], B. Martin dit Latour[17], L. Martinelli[75a,75b], M. Martinez[13,y], P. Martinez Agullo[169], V.I. Martinez Outschoorn[105], P. Martinez Suarez[13], S. Martin-Haugh[137], G. Martinovicova[136], V. S. Martoiu[28b], A. C. Martyniuk[98], A. Marzin[37], D. Mascione[78a,78b], L. Masetti[102], J. Masik[103], A. L. Maslennikov[39], S. L. Mason[42], P. Massarotti[72a,72b], P. Mastrandrea[74a,74b], A. Mastroberardino[44a,44b], T. Masubuchi[127], T. T. Mathew[126], J. Matousek[136], D. M. Mattern[49], J. Maurer[28b], T. Maurin[59], A. J. Maury[66], B. Maček[95], C. Mavungu Tsava[104], D. A. Maximov[38], A. E. May[103], E. Mayer[41], R. Mazini[34g], I. Maznas[118], S. M. Mazza[139], E. Mazzeo[37], J. P. Mc Gowan[171], S. P. Mc Kee[108], C. A. Mc Lean[6], C. C. McCracken[170], E. F. McDonald[107], A. E. McDougall[117], L. F. Mcelhinney[93], J. A. Mcfayden[152], R. P. McGovern[131],

R. P. Mckenzie[34g], T. C. Mclachlan[48], D. J. Mclaughlin[98], S. J. McMahon[137], C. M. Mcpartland[94], R. A. McPherson[171,ac], S. Mehlhase[111], A. Mehta[94], D. Melini[169], B. R. Mellado Garcia[34g], A. H. Melo[55], F. Meloni[48], A. M. Mendes Jacques Da Costa[103], L. Meng[93], S. Menke[112], M. Mentink[37], E. Meoni[44a,44b], G. Mercado[118], S. Merianos[158], C. Merlassino[69a,69c], C. Meroni[71a,71b], J. Metcalfe[6], A. S. Mete[6], E. Meuser[102], C. Meyer[68], J-P. Meyer[138], Y. Miao[114a], R. P. Middleton[137], M. Mihovilovic[66], L. Mijović[52], G. Mikenberg[175], M. Mikestikova[134], M. Mikuž[95], H. Mildner[102], A. Milic[37], D. W. Miller[40], E. H. Miller[149], L. S. Miller[35], A. Milov[175], D. A. Milstead[47a,47b], T. Min[114a], A. A. Minaenko[38], I. A. Minashvili[155b], A. I. Mincer[120], B. Mindur[87a], M. Mineev[39], Y. Mino[89], L. M. Mir[13], M. Miralles Lopez[59], M. Mironova[18a], M. Missio[116], A. Mitra[173], V. A. Mitsou[169], Y. Mitsumori[113], O. Miu[161], P. S. Miyagawa[96], T. Mkrtchyan[63a], M. Mlinarevic[98], T. Mlinarevic[98], M. Mlynarikova[37], S. Mobius[20], M. H. Mohamed Farook[115], S. Mohapatra[42], S. Mohiuddin[124], G. Mokgatitswane[34g], L. Moleri[175], U. Molinatti[129], L. G. Mollier[20], B. Mondal[134], S. Mondal[135], K. Mönig[48], E. Monnier[104], L. Monsonis Romero[169], J. Montejo Berlingen[13], A. Montella[47a,47b], M. Montella[122], F. Montereali[77a,77b], F. Monticelli[92], S. Monzani[69a,69c], A. Morancho Tarda[43], N. Morange[66], A. L. Moreira De Carvalho[48], M. Moreno Llácer[169], C. Moreno Martinez[56], J. M. Moreno Perez[23b], P. Morettini[57b], S. Morgenstern[37], M. Morii[61], M. Morinaga[159], M. Moritsu[90], F. Morodei[75a,75b], P. Moschovakos[37], B. Moser[54], M. Mosidze[155b], T. Moskalets[45], P. Moskvitina[116], J. Moss[32], P. Moszkowicz[87a], A. Moussa[36d], Y. Moyal[175], H. Moyano Gomez[13], E. J. W. Moyse[105], O. Mtintsilana[34g], S. Muanza[104], M. Mucha[25], J. Mueller[132], R. Müller[37], G. A. Mullier[167], A. J. Mullin[33], J. J. Mullin[51], A. C. Mullins[45], A. E. Mulski[61], D. P. Mungo[161], D. Munoz Perez[169], F. J. Munoz Sanchez[103], W. J. Murray[137,173], M. Muškinja[95], C. Mwewa[48], A. G. Myagkov[38,a], A. J. Myers[8], G. Myers[108], M. Myska[135], B. P. Nachman[18a], K. Nagai[129], K. Nagano[84], R. Nagasaka[159], J. L. Nagle[30,ak], E. Nagy[104], A. M. Nairz[37], Y. Nakahama[84], K. Nakamura[84], K. Nakkalil[5], A. Nandi[63b], H. Nanjo[127], E. A. Narayanan[45], Y. Narukawa[159], I. Naryshkin[38], L. Nasella[71a,71b], S. Nasri[119b], C. Nass[25], G. Navarro[23a], J. Navarro-Gonzalez[169], A. Nayaz[19], P. Y. Nechaeva[38], S. Nechaeva[24a,24b], F. Nechansky[134], L. Nedic[129], T. J. Neep[21], A. Negri[73a,73b], M. Negrini[24b], C. Nellist[117], C. Nelson[106], K. Nelson[108], S. Nemecek[134], M. Nessi[37,h], M. S. Neubauer[168], J. Newell[94], P. R. Newman[21], Y. W. Y. Ng[168], B. Ngair[119a], H. D. N. Nguyen[110], J. D. Nichols[123], R. B. Nickerson[129], R. Nicolaidou[138], J. Nielsen[139], M. Niemeyer[55], J. Niermann[37], N. Nikiforou[37], V. Nikolaenko[38,a], I. Nikolic-Audit[130], P. Nilsson[30], I. Ninca[48], G. Ninio[157], A. Nisati[75a], N. Nishu[2], R. Nisius[112], N. Nitika[69a,69c], J-E. Nitschke[50], E. K. Nkadimeng[34b], T. Nobe[159], T. Nommensen[153], M. B. Norfolk[145], B. J. Norman[35], M. Noury[36a], J. Novak[95], T. Novak[95], R. Novotny[135], L. Nozka[125], K. Ntekas[165], N. M. J. Nunes De Moura Junior[83b], J. Ocariz[130], A. Ochi[86], I. Ochoa[133a], S. Oerdek[48,z], J. T. Offermann[40], A. Ogrodnik[136], A. Oh[103], C. C. Ohm[150], H. Oide[84], M. L. Ojeda[37], Y. Okumura[159], L. F. Oleiro Seabra[133a], I. Oleksiyuk[56], G. Oliveira Correa[13], D. Oliveira Damazio[30], J. L. Oliver[165], Ö. O. Öncel[54], A. P. O'Neill[20], A. Onofre[133a,133e,e], P. U. E. Onyisi[11], M. J. Oreglia[40], D. Orestano[77a,77b], R. Orlandini[77a,77b], R. S. Orr[161], L. M. Osojnak[131], Y. Osumi[113], G. Otero y Garzon[31], H. Otono[90], G. J. Ottino[18a], M. Ouchrif[36d], F. Ould-Saada[128], T. Ovsiannikova[142], M. Owen[59], R. E. Owen[137], V. E. Ozcan[22a], F. Ozturk[88], N. Ozturk[8], S. Ozturk[82], H. A. Pacey[129], K. Pachal[162a], A. Pacheco Pages[13], C. Padilla Aranda[13], G. Padovano[75a,75b], S. Pagan Griso[18a], G. Palacino[68], A. Palazzo[70a,70b], J. Pampel[25], J. Pan[178], T. Pan[64a], D. K. Panchal[11], C. E. Pandini[60], J. G. Panduro Vazquez[137], H. D. Pandya[1], H. Pang[138], P. Pani[48], G. Panizzo[69a,69c], L. Panwar[130], L. Paolozzi[56], S. Parajuli[168], A. Paramonov[6], C. Paraskevopoulos[53], D. Paredes Hernandez[64b], A. Pareti[73a,73b], K. R. Park[42], T. H. Park[112], F. Parodi[57a,57b], J. A. Parsons[42], U. Parzefall[54], B. Pascual Dias[41], L. Pascual Dominguez[101], E. Pasqualucci[75a], S. Passaggio[57b], F. Pastore[97], P. Patel[88], U. M. Patel[51], J. R. Pater[103], T. Pauly[37], F. Pauwels[136], C. I. Pazos[164], M. Pedersen[128], R. Pedro[133a], S. V. Peleganchuk[38], O. Penc[37], E. A. Pender[52], S. Peng[15], G. D. Penn[178], K. E. Penski[111], M. Penzin[38], B. S. Peralva[83d], A. P. Pereira Peixoto[142], L. Pereira Sanchez[149], D. V. Perepelitsa[30,ak], G. Perera[105], E. Perez Codina[37], M. Perganti[10], H. Pernegger[37], S. Perrella[75a,75b], O. Perrin[41], K. Peters[48], R. F. Y. Peters[103], B. A. Petersen[37], T. C. Petersen[43], E. Petit[104], V. Petousis[135], A. R. Petri[71a,71b], C. Petridou[158,d], T. Petru[136], A. Petrukhin[147], M. Pettee[18a], A. Petukhov[82], K. Petukhova[37], R. Pezoa[140f], L. Pezzotti[24a,24b], G. Pezzullo[178], L. Pfaffenbichler[37], A. J. Pfleger[37], T. M. Pham[176], T. Pham[107], P. W. Phillips[137], G. Piacquadio[151], E. Pianori[18a], F. Piazza[126], R. Piegaia[31], D. Pietreanu[28b], A. D. Pilkington[103], M. Pinamonti[69a,69c], J. L. Pinfold[2], B. C. Pinheiro Pereira[133a], J. Pinol Bel[13], A. E. Pinto Pinoargote[130], L. Pintucci[69a,69c], K. M. Piper[152],

A. Pirttikoski[56], D. A. Pizzi[35], L. Pizzimento[64b], A. Plebani[33], M. -A. Pleier[30], V. Pleskot[136], E. Plotnikova[39], G. Poddar[96], R. Poettgen[100], L. Poggioli[130], S. Polacek[136], G. Polesello[73a], A. Poley[148], A. Polini[24b], C. S. Pollard[173], Z. B. Pollock[122], E. Pompa Pacchi[123], N. I. Pond[98], D. Ponomarenko[68], L. Pontecorvo[37], S. Popa[28a], G. A. Popeneciu[28d], A. Poreba[37], D. M. Portillo Quintero[162a], S. Pospisil[135], M. A. Postill[145], P. Postolache[28c], K. Potamianos[173], P. A. Potepa[87a], I. N. Potrap[39], C. J. Potter[33], H. Potti[153], J. Poveda[169], M. E. Pozo Astigarraga[37], R. Pozzi[37], A. Prades Ibanez[76a,76b], J. Pretel[171], D. Price[103], M. Primavera[70a], L. Primomo[69a,69c], M. A. Principe Martin[101], R. Privara[125], T. Procter[87b], M. L. Proffitt[142], N. Proklova[131], K. Prokofiev[64c], G. Proto[112], J. Proudfoot[6], M. Przybycien[87a], W. W. Przygoda[87b], A. Psallidas[46], J. E. Puddefoot[145], D. Pudzha[53], D. Pyatiizbyantseva[116], J. Qian[108], R. Qian[109], D. Qichen[103], Y. Qin[13], T. Qiu[52], A. Quadt[55], M. Queitsch-Maitland[103], G. Quetant[56], R. P. Quinn[170], G. Rabanal Bolanos[61], D. Rafanoharana[112], F. Raffaeli[76a,76b], F. Ragusa[71a,71b], J. L. Rainbolt[40], J. A. Raine[56], S. Rajagopalan[30], E. Ramakoti[39], L. Rambelli[57a,57b], I. A. Ramirez-Berend[35], K. Ran[48,114c], D. S. Rankin[131], N. P. Rapheeha[34g], H. Rasheed[28b], D. F. Rassloff[63a], A. Rastogi[18a], S. Rave[102], S. Ravera[57a,57b], B. Ravina[37], I. Ravinovich[175], M. Raymond[37], A. L. Read[128], N. P. Readioff[145], D. M. Rebuzzi[73a,73b], A. S. Reed[112], K. Reeves[27], J. A. Reidelsturz[177], D. Reikher[126], A. Rej[49], C. Rembser[37], H. Ren[62], M. Renda[28b], F. Renner[48], A. G. Rennie[59], A. L. Rescia[48], S. Resconi[71a], M. Ressegotti[57a,57b], S. Rettie[37], W. F. Rettie[35], E. Reynolds[18a], O. L. Rezanova[39], P. Reznicek[136], H. Riani[36d], N. Ribaric[51], E. Ricci[78a,78b], R. Richter[112], S. Richter[47a,47b], E. Richter-Was[87b], M. Ridel[130], S. Ridouani[36d], P. Rieck[120], P. Riedler[37], E. M. Riefel[47a,47b], J. O. Rieger[117], M. Rijssenbeek[151], M. Rimoldi[37], L. Rinaldi[24a,24b], P. Rincke[55,167], G. Ripellino[167], I. Riu[13], J. C. Rivera Vergara[171], F. Rizatdinova[124], E. Rizvi[96], B. R. Roberts[18a], S. S. Roberts[139], D. Robinson[33], M. Robles Manzano[102], A. Robson[59], A. Rocchi[76a,76b], C. Roda[74a,74b], S. Rodriguez Bosca[37], Y. Rodriguez Garcia[23a], A. M. Rodríguez Vera[118], S. Roe[37], J. T. Roemer[37], O. Røhne[128], R. A. Rojas[37], C. P. A. Roland[130], A. Romaniouk[79], E. Romano[73a,73b], M. Romano[24b], A. C. Romero Hernandez[168], N. Rompotis[94], L. Roos[130], S. Rosati[75a], B. J. Rosser[40], E. Rossi[129], E. Rossi[72a,72b], L. P. Rossi[61], L. Rossini[54], R. Rosten[122], M. Rotaru[28b], B. Rottler[54], D. Rousseau[66], D. Rousso[48], S. Roy-Garand[161], A. Rozanov[104], Z. M. A. Rozario[59], Y. Rozen[156], A. Rubio Jimenez[169], V. H. Ruelas Rivera[19], T. A. Ruggeri[1], A. Ruggiero[129], A. Ruiz-Martinez[169], A. Rummler[37], Z. Rurikova[54], N. A. Rusakovich[39], H. L. Russell[171], G. Russo[75a,75b], J. P. Rutherfoord[7], S. Rutherford Colmenares[33], M. Rybar[136], P. Rybczynski[87a], A. Ryzhov[45], J. A. Sabater Iglesias[56], H.F-W. Sadrozinski[139], F. Safai Tehrani[75a], S. Saha[1], M. Sahinsoy[82], B. Sahoo[175], A. Saibel[169], B. T. Saifuddin[123], M. Saimpert[138], G. T. Saito[83c], M. Saito[159], T. Saito[159], A. Sala[71a,71b], A. Salnikov[149], J. Salt[169], A. Salvador Salas[157], F. Salvatore[152], A. Salzburger[37], D. Sammel[54], E. Sampson[93], D. Sampsonidis[158,d], D. Sampsonidou[126], J. Sánchez[169], V. Sanchez Sebastian[169], H. Sandaker[128], C. O. Sander[48], J. A. Sandesara[176], M. Sandhoff[177], C. Sandoval[23b], L. Sanfilippo[63a], D. P. C. Sankey[137], T. Sano[89], A. Sansoni[53], L. Santi[37], C. Santoni[41], H. Santos[133a,133b], A. Santra[175], E. Sanzani[24a,24b], K. A. Saoucha[85b], J. G. Saraiva[133a,133d], J. Sardain[7], O. Sasaki[84], K. Sato[163], C. Sauer[37], E. Sauvan[4], P. Savard[161,ai], R. Sawada[159], C. Sawyer[137], L. Sawyer[99], C. Sbarra[24b], A. Sbrizzi[24a,24b], T. Scanlon[98], J. Schaarschmidt[142], U. Schäfer[102], A. C. Schaffer[45,66], D. Schaile[111], R. D. Schamberger[151], C. Scharf[19], M. M. Schefer[20], V. A. Schegelsky[38], D. Scheirich[136], M. Schernau[140e], C. Scheulen[56], C. Schiavi[57a,57b], M. Schioppa[44a,44b], B. Schlag[149], S. Schlenker[37], J. Schmeing[177], E. Schmidt[112], M. A. Schmidt[177], K. Schmieden[102], C. Schmitt[102], N. Schmitt[102], S. Schmitt[48], L. Schoeffel[138], A. Schoening[63b], P. G. Scholer[35], E. Schopf[147], M. Schott[25], S. Schramm[56], T. Schroer[56], H-C. Schultz-Coulon[63a], M. Schumacher[54], B. A. Schumm[139], Ph. Schune[138], H. R. Schwartz[139], A. Schwartzman[149], T. A. Schwarz[108], Ph. Schwemling[138], R. Schwienhorst[109], F. G. Sciacca[20], A. Sciandra[30], G. Sciolla[27], F. Scuri[74a], C. D. Sebastiani[37], K. Sedlaczek[118], S. C. Seidel[115], A. Seiden[139], B. D. Seidlitz[42], C. Seitz[48], J. M. Seixas[83b], G. Sekhniaidze[72a], L. Selem[60], N. Semprini-Cesari[24a,24b], A. Semushin[179], D. Sengupta[56], V. Senthilkumar[169], L. Serin[66], M. Sessa[72a,72b], H. Severini[123], F. Sforza[57a,57b], A. Sfyrla[56], Q. Sha[14], E. Shabalina[55], H. Shaddix[118], A. H. Shah[33], R. Shaheen[150], J. D. Shahinian[131], M. Shamim[37], L. Y. Shan[14], M. Shapiro[18a], A. Sharma[37], A. S. Sharma[170], P. Sharma[30], P. B. Shatalov[38], K. Shaw[152], S. M. Shaw[103], Q. Shen[14], D. J. Sheppard[148], P. Sherwood[98], L. Shi[98], X. Shi[14], S. Shimizu[84], C. O. Shimmin[178], I. P. J. Shipsey[129,*], S. Shirabe[90], M. Shiyakova[39,aa], M. J. Shochet[40], D. R. Shope[128], B. Shrestha[123], S. Shrestha[122,am], I. Shreyber[39], M.J. Shroff[171], P. Sicho[134], A. M. Sickles[168], E. Sideras Haddad[34g,166], A. C. Sidley[117], A. Sidoti[24b], F. Siegert[50], Dj. Sijacki[16], F. Sili[92], J. M. Silva[52], I. Silva Ferreira[83b],

M. V. Silva Oliveira[30], S. B. Silverstein[47a], S. Simion[66], R. Simoniello[37], E. L. Simpson[103], H. Simpson[152], L. R. Simpson[6], S. Simsek[82], S. Sindhu[55], P. Sinervo[161], S. N. Singh[27], S. Singh[30], S. Sinha[48], S. Sinha[103], M. Sioli[24a,24b], K. Sioulas[9], I. Siral[37], E. Sitnikova[48], J. Sjölin[47a,47b], A. Skaf[55], E. Skorda[21], P. Skubic[123], M. Slawinska[88], I. Slazyk[17], I. Sliusar[128], V. Smakhtin[175], B. H. Smart[137], S. Yu. Smirnov[140b], Y. Smirnov[82], L. N. Smirnova[38,a], O. Smirnova[100], A. C. Smith[42], D. R. Smith[165], J. L. Smith[103], M. B. Smith[35], R. Smith[149], H. Smitmanns[102], M. Smizanska[93], K. Smolek[135], P. Smolyanskiy[135], A. A. Snesarev[39], H. L. Snoek[117], S. Snyder[30], R. Sobie[171,ac], A. Soffer[157], C. A. Solans Sanchez[37], E. Yu. Soldatov[39], U. Soldevila[169], A. A. Solodkov[34g], S. Solomon[27], A. Soloshenko[39], K. Solovieva[54], O. V. Solovyanov[41], P. Sommer[50], A. Sonay[13], A. Sopczak[135], A. L. Sopio[52], F. Sopkova[29b], J. D. Sorenson[115], I. R. Sotarriva Alvarez[141], V. Sothilingam[63a], O. J. Soto Sandoval[140b,140c], S. Sottocornola[68], R. Soualah[85a], Z. Soumaimi[36e], D. South[48], N. Soybelman[175], S. Spagnolo[70a,70b], M. Spalla[112], D. Sperlich[54], B. Spisso[72a,72b], D. P. Spiteri[59], L. Splendori[104], M. Spousta[136], E. J. Staats[35], R. Stamen[63a], E. Stanecka[88], W. Stanek-Maslouska[48], M. V. Stange[50], B. Stanislaus[18a], M. M. Stanitzki[48], B. Stapf[48], E. A. Starchenko[38], G. H. Stark[139], J. Stark[91], P. Staroba[134], P. Starovoitov[85b], R. Staszewski[88], G. Stavropoulos[46], A. Stefl[37], P. Steinberg[30], B. Stelzer[148,162a], H. J. Stelzer[132], O. Stelzer[162a], H. Stenzel[58], T. J. Stevenson[152], G. A. Stewart[37], J. R. Stewart[124], M. C. Stockton[37], G. Stoicea[28b], M. Stolarski[133a], S. Stonjek[112], A. Straessner[50], J. Strandberg[150], S. Strandberg[47a,47b], M. Stratmann[177], M. Strauss[123], T. Strebler[104], P. Strizenec[29b], R. Ströhmer[172], D. M. Strom[126], R. Stroynowski[45], A. Strubig[47a,47b], S. A. Stucci[30], B. Stugu[17], J. Stupak[123], N. A. Styles[48], D. Su[149], S. Su[62], X. Su[62], D. Suchy[29a], K. Sugizaki[131], V. V. Sulin[38], M. J. Sullivan[94], D. M. S. Sultan[129], L. Sultanaliyeva[38], S. Sultansoy[3b], S. Sun[176], W. Sun[14], O. Sunneborn Gudnadottir[167], N. Sur[100], M. R. Sutton[152], H. Suzuki[163], M. Svatos[134], P. N. Swallow[33], M. Swiatlowski[162a], T. Swirski[172], I. Sykora[29a], M. Sykora[136], T. Sykora[136], D. Ta[102], K. Tackmann[48,z], A. Taffard[165], R. Tafirout[162a], Y. Takubo[84], M. Talby[104], A. A. Talyshev[38], K. C. Tam[64b], N. M. Tamir[157], A. Tanaka[159], J. Tanaka[159], R. Tanaka[66], M. Tanasini[151], Z. Tao[170], S. Tapia Araya[140f], S. Tapprogge[102], A. Tarek Abouelfadl Mohamed[109], S. Tarem[156], K. Tariq[14], G. Tarna[28b], G. F. Tartarelli[71a], M. J. Tartarin[91], P. Tas[136], M. Tasevsky[134], E. Tassi[44a,44b], A. C. Tate[168], G. Tateno[159], Y. Tayalati[36e,ab], G. N. Taylor[107], W. Taylor[162b], A. S. Tegetmeier[91], P. Teixeira-Dias[97], J. J. Teoh[161], K. Terashi[159], J. Terron[101], S. Terzo[13], M. Testa[53], R. J. Teuscher[161,ac], A. Thaler[79], O. Theiner[56], T. Theveneaux-Pelzer[104], D. W. Thomas[97], J. P. Thomas[21], E. A. Thompson[18a], P. D. Thompson[21], E. Thomson[131], R. E. Thornberry[45], C. Tian[62], Y. Tian[56], V. Tikhomirov[82], Yu. A. Tikhonov[39], S. Timoshenko[38], D. Timoshyn[136], E. X. L. Ting[1], P. Tipton[178], A. Tishelman-Charny[30], K. Todome[141], S. Todorova-Nova[136], S. Todt[50], L. Toffolin[69a,69c], M. Togawa[84], J. Tojo[90], S. Tokár[29a], O. Toldaiev[68], G. Tolkachev[104], M. Tomoto[84,113], L. Tompkins[149,o], E. Torrence[126], H. Torres[91], E. Torró Pastor[169], M. Toscani[31], C. Tosciri[40], M. Tost[11], D. R. Tovey[145], T. Trefzger[172], P. M. Tricarico[13], A. Tricoli[30], I. M. Trigger[162a], S. Trincaz-Duvoid[130], D. A. Trischuk[27], A. Tropina[39], L. Truong[34c], M. Trzebinski[88], A. Trzupek[88], F. Tsai[151], M. Tsai[108], A. Tsiamis[158], P. V. Tsiareshka[39], S. Tsigaridas[162a], A. Tsirigotis[158,v], V. Tsiskaridze[161], E. G. Tskhadadze[155a], M. Tsopoulou[158], Y. Tsujikawa[89], I.I. Tsukerman[38], V. Tsulaia[18a], S. Tsuno[84], K. Tsuri[121], D. Tsybychev[151], Y. Tu[64b], A. Tudorache[28b], V. Tudorache[28b], S. B. Tuncay[129], S. Turchikhin[57a,57b], I. Turk Cakir[3a], R. Turra[71a], T. Turtuvshin[39,ad], P. M. Tuts[42], S. Tzamarias[158,d], E. Tzovara[102], Y. Uematsu[84], F. Ukegawa[163], P. A. Ulloa Poblete[140b,140c], E. N. Umaka[30], G. Unal[37], A. Undrus[30], G. Unel[165], J. Urban[29b], P. Urrejola[140a], G. Usai[8], R. Ushioda[160], M. Usman[110], F. Ustuner[52], Z. Uysal[82], V. Vacek[135], B. Vachon[106], T. Vafeiadis[37], A. Vaitkus[98], C. Valderanis[111], E. Valdes Santurio[47a,47b], M. Valente[37], S. Valentinetti[24a,24b], A. Valero[169], E. Valiente Moreno[169], A. Vallier[91], J. A. Valls Ferrer[169], D. R. Van Arneman[117], T. R. Van Daalen[142], A. Van Der Graaf[49], H. Z. Van Der Schyf[34g], P. Van Gemmeren[6], M. Van Rijnbach[37], S. Van Stroud[98], I. Van Vulpen[117], P. Vana[136], M. Vanadia[76a,76b], U. M. Vande Voorde[150], W. Vandelli[37], E. R. Vandewall[124], D. Vannicola[157], L. Vannoli[53], R. Vari[75a], M. Varma[178], E. W. Varnes[7], C. Varni[18b], D. Varouchas[66], L. Varriale[169], K. E. Varvell[153], M. E. Vasile[28b], L. Vaslin[84], M. D. Vassilev[149], A. Vasyukov[39], L. M. Vaughan[124], R. Vavricka[136], T. Vazquez Schroeder[13], J. Veatch[32], V. Vecchio[103], M. J. Veen[105], I. Veliscek[30], I. Velkovska[95], L. M. Veloce[161], F. Veloso[133a,133c], S. Veneziano[75a], A. Ventura[70a,70b], S. Ventura Gonzalez[138], A. Verbytskyi[112], M. Verducci[74a,74b], C. Vergis[96], M. Verissimo De Araujo[83b], W. Verkerke[117], J. C. Vermeulen[117], C. Vernieri[149], M. Vessella[165], M. C. Vetterli[148,ai], A. Vgenopoulos[102], N. Viaux Maira[140f], T. Vickey[145], O. E. Vickey Boeriu[145], G. H. A. Viehhauser[129], L. Vigani[63b],

M. Vigl[112], M. Villa[24a,24b], M. Villaplana Perez[169], E. M. Villhauer[40], E. Vilucchi[53], M. Vincent[169], M. G. Vincter[35], A. Visibile[117], C. Vittori[37], I. Vivarelli[24a,24b], E. Voevodina[112], F. Vogel[111], J. C. Voigt[50], P. Vokac[135], Yu. Volkotrub[87b], E. Von Toerne[25], B. Vormwald[37], K. Vorobev[51], M. Vos[169], K. Voss[147], M. Vozak[37], L. Vozdecky[123], N. Vranjes[16], M. Vranjes Milosavljevic[16], M. Vreeswijk[117], N. K. Vu[144a,144b], R. Vuillermet[37], O. Vujinovic[102], I. Vukotic[40], I. K. Vyas[35], J. F. Wack[33], S. Wada[163], C. Wagner[149], J. M. Wagner[18a], W. Wagner[177], S. Wahdan[177], H. Wahlberg[92], C. H. Waits[123], J. Walder[137], R. Walker[111], K. Walkingshaw Pass[59], W. Walkowiak[147], A. Wall[131], E. J. Wallin[100], T. Wamorkar[18a], A. Wang[62], A. Z. Wang[139], C. Wang[102], C. Wang[11], H. Wang[18a], J. Wang[64c], P. Wang[103], P. Wang[98], R. Wang[61], R. Wang[6], S. M. Wang[154], S. Wang[14], T. Wang[62], T. Wang[62], W. T. Wang[80], W. Wang[14], X. Wang[168], X. Wang[144a], X. Wang[48], Y. Wang[114a], Y. Wang[62], Z. Wang[108], Z. Wang[144b], Z. Wang[108], C. Wanotayaroj[84], A. Warburton[106], A. L. Warnerbring[147], N. Warrack[59], S. Waterhouse[97], A. T. Watson[21], H. Watson[52], M. F. Watson[21], E. Watton[59], G. Watts[142], B. M. Waugh[98], J. M. Webb[54], C. Weber[30], H. A. Weber[19], M. S. Weber[20], S. M. Weber[63a], C. Wei[62], Y. Wei[54], A. R. Weidberg[129], E. J. Weik[120], J. Weingarten[49], C. Weiser[54], C. J. Wells[48], T. Wenaus[30], B. Wendland[49], T. Wengler[37], N. S. Wenke[112], N. Wermes[25], M. Wessels[63a], A. M. Wharton[93], A. S. White[61], A. White[8], M. J. White[1], D. Whiteson[165], L. Wickremasinghe[127], W. Wiedenmann[176], M. Wielers[137], R. Wierda[150], C. Wiglesworth[43], H. G. Wilkens[37], J. J. H. Wilkinson[33], D. M. Williams[42], H. H. Williams[131], S. Williams[33], S. Willocq[105], B. J. Wilson[103], D. J. Wilson[103], P. J. Windischhofer[40], F. I. Winkel[31], F. Winklmeier[126], B. T. Winter[54], M. Wittgen[149], M. Wobisch[99], T. Wojtkowski[60], Z. Wolffs[117], J. Wollrath[37], M. W. Wolter[88], H. Wolters[133a,133c], M. C. Wong[139], E. L. Woodward[42], S. D. Worm[48], B. K. Wosiek[88], K. W. Woźniak[88], S. Wozniewski[55], K. Wraight[59], C. Wu[161], C. Wu[21], J. Wu[159], M. Wu[114b], M. Wu[116], S. L. Wu[176], S. Wu[14], X. Wu[62], Y. Wu[62], Z. Wu[4], J. Wuerzinger[112], T. R. Wyatt[103], B. M. Wynne[52], S. Xella[43], L. Xia[114a], M. Xia[15], M. Xie[62], A. Xiong[126], J. Xiong[18a], D. Xu[14], H. Xu[62], L. Xu[62], R. Xu[131], T. Xu[108], Y. Xu[142], Z. Xu[52], Z. Xu[114a], B. Yabsley[153], S. Yacoob[34a], Y. Yamaguchi[84], E. Yamashita[159], H. Yamauchi[163], T. Yamazaki[18a], Y. Yamazaki[86], S. Yan[59], Z. Yan[105], H. J. Yang[144a,144b], H. T. Yang[62], S. Yang[62], T. Yang[64c], X. Yang[37], X. Yang[14], Y. Yang[159], Y. Yang[62], W-M. Yao[18a], C. L. Yardley[152], J. Ye[14], S. Ye[30], X. Ye[62], Y. Yeh[98], I. Yeletskikh[39], B. Yeo[18b], M. R. Yexley[98], T. P. Yildirim[129], P. Yin[42], K. Yorita[174], C. J. S. Young[37], C. Young[149], N. D. Young[126], Y. Yu[62], J. Yuan[14,114c], M. Yuan[108], R. Yuan[144a,144b], L. Yue[98], M. Zaazoua[62], B. Zabinski[88], I. Zahir[36a], A. Zaio[57a,57b], Z. K. Zak[88], T. Zakareishvili[169], S. Zambito[56], J. A. Zamora Saa[140d], J. Zang[159], R. Zanzottera[71a,71b], O. Zaplatilek[135], C. Zeitnitz[177], H. Zeng[14], J. C. Zeng[168], D. T. Zenger Jr[27], O. Zenin[38], T. Ženiš[29a], S. Zenz[96], D. Zerwas[66], M. Zhai[14,114c], D. F. Zhang[145], G. Zhang[14], J. Zhang[143a], J. Zhang[6], K. Zhang[14,114c], L. Zhang[62], L. Zhang[114a], P. Zhang[14,114c], R. Zhang[114a], S. Zhang[91], T. Zhang[159], Y. Zhang[142], Y. Zhang[98], Y. Zhang[62], Y. Zhang[114a], Z. Zhang[143a], Z. Zhang[66], H. Zhao[142], T. Zhao[143a], Y. Zhao[35], Z. Zhao[62], Z. Zhao[62], A. Zhemchugov[39], J. Zheng[114a], K. Zheng[168], X. Zheng[62], Z. Zheng[149], D. Zhong[168], B. Zhou[108], H. Zhou[7], N. Zhou[144a], Y. Zhou[15], Y. Zhou[114a], Y. Zhou[7], C. G. Zhu[143a], J. Zhu[108], X. Zhu[144b], Y. Zhu[144a], Y. Zhu[62], X. Zhuang[14], K. Zhukov[68], N. I. Zimine[39], J. Zinsser[63b], M. Ziolkowski[147], L. Živković[16], A. Zoccoli[24a,24b], K. Zoch[61], A. Zografos[37], T. G. Zorbas[145], O. Zormpa[46], L. Zwalinski[37]

[1] Department of Physics, University of Adelaide, Adelaide, Australia
[2] Department of Physics, University of Alberta, Edmonton, AB, Canada
[3] [(a)]Department of Physics, Ankara University, Ankara, Türkiye; [(b)]Division of Physics, TOBB University of Economics and Technology, Ankara, Türkiye
[4] LAPP, Université Savoie Mont Blanc, CNRS/IN2P3, Annecy, France
[5] APC, Université Paris Cité, CNRS/IN2P3, Paris, France
[6] High Energy Physics Division, Argonne National Laboratory, Argonne, IL, USA
[7] Department of Physics, University of Arizona, Tucson, AZ, USA
[8] Department of Physics, University of Texas at Arlington, Arlington, TX, USA
[9] Physics Department, National and Kapodistrian University of Athens, Athens, Greece
[10] Physics Department, National Technical University of Athens, Zografou, Greece
[11] Department of Physics, University of Texas at Austin, Austin, TX, USA
[12] Institute of Physics, Azerbaijan Academy of Sciences, Baku, Azerbaijan
[13] Institut de Física d'Altes Energies (IFAE), Barcelona Institute of Science and Technology, Barcelona, Spain

[14] Institute of High Energy Physics, Chinese Academy of Sciences, Beijing, China
[15] Physics Department, Tsinghua University, Beijing, China
[16] Institute of Physics, University of Belgrade, Belgrade, Serbia
[17] Department for Physics and Technology, University of Bergen, Bergen, Norway
[18] [(a)]Physics Division, Lawrence Berkeley National Laboratory, Berkeley, CA, USA; [(b)]University of California, Berkeley, CA, USA
[19] Institut für Physik, Humboldt Universität zu Berlin, Berlin, Germany
[20] Albert Einstein Center for Fundamental Physics and Laboratory for High Energy Physics, University of Bern, Bern, Switzerland
[21] School of Physics and Astronomy, University of Birmingham, Birmingham, UK
[22] [(a)]Department of Physics, Bogazici University, Istanbul, Türkiye; [(b)]Department of Physics Engineering, Gaziantep University, Gaziantep, Türkiye; [(c)]Department of Physics, Istanbul University, Istanbul, Türkiye
[23] [(a)]Facultad de Ciencias y Centro de Investigaciónes, Universidad Antonio Nariño, Bogotá, Colombia; [(b)]Departamento de Física, Universidad Nacional de Colombia, Bogotá, Colombia
[24] [(a)]Dipartimento di Fisica e Astronomia A. Righi, Università di Bologna, Bologna, Italy; [(b)]INFN Sezione di Bologna, Bologna, Italy
[25] Physikalisches Institut, Universität Bonn, Bonn, Germany
[26] Department of Physics, Boston University, Boston, MA, USA
[27] Department of Physics, Brandeis University, Waltham, MA, USA
[28] [(a)]Transilvania University of Brasov, Brasov, Romania; [(b)]Horia Hulubei National Institute of Physics and Nuclear Engineering, Bucharest, Romania; [(c)]Department of Physics, Alexandru Ioan Cuza University of Iasi, Iasi, Romania; [(d)]Physics Department, National Institute for Research and Development of Isotopic and Molecular Technologies, Cluj-Napoca, Romania; [(e)]National University of Science and Technology Politechnica, Bucharest, Romania; [(f)]West University in Timisoara, Timisoara, Romania; [(g)]Faculty of Physics, University of Bucharest, Bucharest, Romania
[29] [(a)]Faculty of Mathematics, Physics and Informatics, Comenius University, Bratislava, Slovakia; [(b)]Department of Subnuclear Physics, Institute of Experimental Physics of the Slovak Academy of Sciences, Kosice, Slovak Republic
[30] Physics Department, Brookhaven National Laboratory, Upton, NY, USA
[31] Universidad de Buenos Aires, Facultad de Ciencias Exactas y Naturales, Departamento de Física, y CONICET, Instituto de Física de Buenos Aires (IFIBA), Buenos Aires, Argentina
[32] California State University, Long Beach, CA, USA
[33] Cavendish Laboratory, University of Cambridge, Cambridge, UK
[34] [(a)]Department of Physics, University of Cape Town, Cape Town, South Africa; [(b)]iThemba Labs, Cape Town, Western Cape, South Africa; [(c)]Department of Mechanical Engineering Science, University of Johannesburg, Johannesburg, South Africa; [(d)]National Institute of Physics, University of the Philippines Diliman (Philippines), Quezon City, Philippines; [(e)]Department of Physics, University of South Africa, Pretoria, South Africa; [(f)]University of Zululand, KwaDlangezwa, Ongoye, South Africa; [(g)]School of Physics, University of the Witwatersrand, Johannesburg, South Africa
[35] Department of Physics, Carleton University, Ottawa, ON, Canada
[36] [(a)]Faculté des Sciences Ain Chock, Université Hassan II de Casablanca, Casablanca, Morocco; [(b)]Faculté des Sciences, Université Ibn-Tofail, Kénitra, Morocco; [(c)]Faculté des Sciences Semlalia, Université Cadi Ayyad, LPHEA-Marrakech, Marrakesh, Morocco; [(d)]LPMR, Faculté des Sciences, Université Mohamed Premier, Oujda, Morocco; [(e)]Faculté des sciences, Université Mohammed V, Rabat, Morocco; [(f)]Institute of Applied Physics, Mohammed VI Polytechnic University, Ben Guerir, Morocco
[37] CERN, Geneva, Switzerland
[38] Affiliated with an Institute Formerly Covered by a Cooperation Agreement with CERN, Geneva, Switzerland
[39] Affiliated with an International Laboratory Covered by a Cooperation Agreement with CERN, Geneva, Switzerland
[40] Enrico Fermi Institute, University of Chicago, Chicago, IL, USA
[41] LPC, Université Clermont Auvergne, CNRS/IN2P3, Clermont-Ferrand, France
[42] Nevis Laboratory, Columbia University, Irvington, NY, USA
[43] Niels Bohr Institute, University of Copenhagen, Copenhagen, Denmark
[44] [(a)]Dipartimento di Fisica, Università della Calabria, Rende, Italy; [(b)]INFN Gruppo Collegato di Cosenza, Laboratori Nazionali di Frascati, Frascati, Italy

[45] Physics Department, Southern Methodist University, Dallas, TX, USA
[46] National Centre for Scientific Research "Demokritos", Agia Paraskevi, Greece
[47] [(a)]Department of Physics, Stockholm University, Stockholm, Sweden; [(b)]Oskar Klein Centre, Stockholm, Sweden
[48] Deutsches Elektronen-Synchrotron DESY, Hamburg and Zeuthen, Germany
[49] Fakultät Physik , Technische Universität Dortmund, Dortmund, Germany
[50] Institut für Kern- und Teilchenphysik, Technische Universität Dresden, Dresden, Germany
[51] Department of Physics, Duke University, Durham, NC, USA
[52] SUPA-School of Physics and Astronomy, University of Edinburgh, Edinburgh, UK
[53] INFN e Laboratori Nazionali di Frascati, Frascati, Italy
[54] Physikalisches Institut, Albert-Ludwigs-Universität Freiburg, Freiburg, Germany
[55] II. Physikalisches Institut, Georg-August-Universität Göttingen, Göttingen, Germany
[56] Département de Physique Nucléaire et Corpusculaire, Université de Genève, Geneva, Switzerland
[57] [(a)]Dipartimento di Fisica, Università di Genova, Genoa, Italy; [(b)]INFN Sezione di Genova, Genoa, Italy
[58] II. Physikalisches Institut, Justus-Liebig-Universität Giessen, Giessen, Germany
[59] SUPA-School of Physics and Astronomy, University of Glasgow, Glasgow, UK
[60] LPSC, Université Grenoble Alpes, CNRS/IN2P3, Grenoble INP, Grenoble, France
[61] Laboratory for Particle Physics and Cosmology, Harvard University, Cambridge, MA, USA
[62] Department of Modern Physics and State Key Laboratory of Particle Detection and Electronics, University of Science and Technology of China, Hefei, China
[63] [(a)]Kirchhoff-Institut für Physik, Ruprecht-Karls-Universität Heidelberg, Heidelberg, Germany; [(b)]Physikalisches Institut, Ruprecht-Karls-Universität Heidelberg, Heidelberg, Germany
[64] [(a)]Department of Physics, Chinese University of Hong Kong, Shatin, N.T., Hong Kong; [(b)]Department of Physics, University of Hong Kong, Pokfulam, Hong Kong; [(c)]Department of Physics and Institute for Advanced Study, Hong Kong University of Science and Technology, Clear Water Bay, Kowloon, Hong Kong, China
[65] Department of Physics, National Tsing Hua University, Hsinchu, Taiwan
[66] IJCLab, Université Paris-Saclay, CNRS/IN2P3, 91405, Orsay, France
[67] Centro Nacional de Microelectrónica (IMB-CNM-CSIC), Barcelona, Spain
[68] Department of Physics, Indiana University, Bloomington, IN, USA
[69] [(a)]INFN Gruppo Collegato di Udine, Sezione di Trieste, Udine, Italy; [(b)]ICTP, Trieste, Italy; [(c)]Dipartimento Politecnico di Ingegneria e Architettura, Università di Udine, Udine, Italy
[70] [(a)]INFN Sezione di Lecce, Lecce, Italy; [(b)]Dipartimento di Matematica e Fisica, Università del Salento, Lecce, Italy
[71] [(a)]INFN Sezione di Milano, Milan, Italy; [(b)]Dipartimento di Fisica, Università di Milano, Milan, Italy
[72] [(a)]INFN Sezione di Napoli, Naples, Italy; [(b)]Dipartimento di Fisica, Università di Napoli, Naples, Italy
[73] [(a)]INFN Sezione di Pavia, Pavia, Italy; [(b)]Dipartimento di Fisica, Università di Pavia, Pavia, Italy
[74] [(a)]INFN Sezione di Pisa, Pisa, Italy; [(b)]Dipartimento di Fisica E. Fermi, Università di Pisa, Pisa, Italy
[75] [(a)]INFN Sezione di Roma, Rome, Italy; [(b)]Dipartimento di Fisica, Sapienza Università di Roma, Rome, Italy
[76] [(a)]INFN Sezione di Roma Tor Vergata, Rome, Italy; [(b)]Dipartimento di Fisica, Università di Roma Tor Vergata, Rome, Italy
[77] [(a)]INFN Sezione di Roma Tre, Rome, Italy; [(b)]Dipartimento di Matematica e Fisica, Università Roma Tre, Rome, Italy
[78] [(a)]INFN-TIFPA, Povo, Italy; [(b)]Università degli Studi di Trento, Trento, Italy
[79] Universität Innsbruck, Department of Astro and Particle Physics, Innsbruck, Austria
[80] University of Iowa, Iowa City, IA, USA
[81] Department of Physics and Astronomy, Iowa State University, Ames, IA, USA
[82] Istinye University, Sariyer, Istanbul, Türkiye
[83] [(a)]Departamento de Engenharia Elétrica, Universidade Federal de Juiz de Fora (UFJF), Juiz de Fora, Brazil; [(b)]Universidade Federal do Rio De Janeiro COPPE/EE/IF, Rio de Janeiro, Brazil; [(c)]Instituto de Física, Universidade de São Paulo, São Paulo, Brazil; [(d)]Rio de Janeiro State University, Rio de Janeiro, Brazil; [(e)]Federal University of Bahia, Bahia, Brazil
[84] KEK, High Energy Accelerator Research Organization, Tsukuba, Japan
[85] [(a)]Khalifa University of Science and Technology, Abu Dhabi, United Arab Emirates; [(b)]University of Sharjah, Sharjah, United Arab Emirates
[86] Graduate School of Science, Kobe University, Kobe, Japan

[87] [(a)] AGH University of Krakow, Faculty of Physics and Applied Computer Science, Krakow, Poland; [(b)] Marian Smoluchowski Institute of Physics, Jagiellonian University, Krakow, Poland
[88] Institute of Nuclear Physics Polish Academy of Sciences, Krakow, Poland
[89] Faculty of Science, Kyoto University, Kyoto, Japan
[90] Research Center for Advanced Particle Physics and Department of Physics, Kyushu University, Fukuoka , Japan
[91] L2IT, Université de Toulouse, CNRS/IN2P3, UPS, Toulouse, France
[92] Instituto de Física La Plata, Universidad Nacional de La Plata and CONICET, La Plata, Argentina
[93] Physics Department, Lancaster University, Lancaster, UK
[94] Oliver Lodge Laboratory, University of Liverpool, Liverpool, UK
[95] Department of Experimental Particle Physics, Jožef Stefan Institute and Department of Physics, University of Ljubljana, Ljubljana, Slovenia
[96] Department of Physics and Astronomy, Queen Mary University of London, London, UK
[97] Department of Physics, Royal Holloway University of London, Egham, UK
[98] Department of Physics and Astronomy, University College London, London, UK
[99] Louisiana Tech University, Ruston, LA, USA
[100] Fysiska institutionen, Lunds universitet, Lund, Sweden
[101] Departamento de Física Teorica C-15 and CIAFF, Universidad Autónoma de Madrid, Madrid, Spain
[102] Institut für Physik, Universität Mainz, Mainz, Germany
[103] School of Physics and Astronomy, University of Manchester, Manchester, UK
[104] CPPM, Aix-Marseille Université, CNRS/IN2P3, Marseille, France
[105] Department of Physics, University of Massachusetts, Amherst, MA, USA
[106] Department of Physics, McGill University, Montreal, QC, Canada
[107] School of Physics, University of Melbourne, Melbourne, VIC, Australia
[108] Department of Physics, University of Michigan, Ann Arbor, MI, USA
[109] Department of Physics and Astronomy, Michigan State University, East Lansing, MI, USA
[110] Group of Particle Physics, University of Montreal, Montreal, QC, Canada
[111] Fakultät für Physik, Ludwig-Maximilians-Universität München, Munich, Germany
[112] Max-Planck-Institut für Physik (Werner-Heisenberg-Institut), Munich, Germany
[113] Graduate School of Science and Kobayashi-Maskawa Institute, Nagoya University, Nagoya, Japan
[114] [(a)] Department of Physics, Nanjing University, Nanjing, China; [(b)] School of Science, Shenzhen Campus of Sun Yat-sen University, Shenzhen, China; [(c)] University of Chinese Academy of Science (UCAS), Beijing, China
[115] Department of Physics and Astronomy, University of New Mexico, Albuquerque, NM, USA
[116] Institute for Mathematics, Astrophysics and Particle Physics, Radboud University/Nikhef, Nijmegen, The Netherlands
[117] Nikhef National Institute for Subatomic Physics and University of Amsterdam, Amsterdam, The Netherlands
[118] Department of Physics, Northern Illinois University, DeKalb, IL, USA
[119] [(a)] New York University Abu Dhabi, Abu Dhabi, United Arab Emirates; [(b)] United Arab Emirates University, Al Ain, United Arab Emirates
[120] Department of Physics, New York University, New York, NY, USA
[121] Ochanomizu University, Otsuka, Bunkyo-ku, Tokyo, Japan
[122] Ohio State University, Columbus, OH, USA
[123] Homer L. Dodge Department of Physics and Astronomy, University of Oklahoma, Norman, OK, USA
[124] Department of Physics, Oklahoma State University, Stillwater, OK, USA
[125] Palacký University, Joint Laboratory of Optics, Olomouc, Czech Republic
[126] Institute for Fundamental Science, University of Oregon, Eugene,, OR, USA
[127] Graduate School of Science, University of Osaka, Osaka, Japan
[128] Department of Physics, University of Oslo, Oslo, Norway
[129] Department of Physics, Oxford University, Oxford, UK
[130] LPNHE, Sorbonne Université, Université Paris Cité, CNRS/IN2P3, Paris, France
[131] Department of Physics, University of Pennsylvania, Philadelphia, PA, USA
[132] Department of Physics and Astronomy, University of Pittsburgh, Pittsburgh, PA, USA
[133] [(a)] Laboratório de Instrumentação e Física Experimental de Partículas-LIP, Lisbon, Portugal; [(b)] Departamento de Física, Faculdade de Ciências, Universidade de Lisboa, Lisbon, Portugal; [(c)] Departamento de Física, Universidade de Coimbra, Coimbra, Portugal; [(d)] Centro de Física Nuclear da Universidade de Lisboa, Lisbon, Portugal; [(e)] Departamento de Física,

Escola de Ciências, Universidade do Minho, Braga, Portugal; [f]Departamento de Física Teórica y del Cosmos, Universidad de Granada, Granada, Spain; [g]Departamento de Física, Instituto Superior Técnico, Universidade de Lisboa, Lisbon, Portugal
[134] Institute of Physics of the Czech Academy of Sciences, Prague, Czech Republic
[135] Czech Technical University in Prague, Prague, Czech Republic
[136] Charles University, Faculty of Mathematics and Physics, Prague, Czech Republic
[137] Particle Physics Department, Rutherford Appleton Laboratory, Didcot, UK
[138] IRFU, CEA, Université Paris-Saclay, Gif-sur-Yvette, France
[139] Santa Cruz Institute for Particle Physics, University of California Santa Cruz, Santa Cruz, CA, USA
[140] [a]Departamento de Física, Pontificia Universidad Católica de Chile, Santiago, Chile; [b]Millennium Institute for Subatomic physics at high energy frontier (SAPHIR), Santiago, Chile; [c]Instituto de Investigación Multidisciplinario en Ciencia y Tecnología, y Departamento de Física, Universidad de La Serena, La Serena, Chile; [d]Department of Physics, Universidad Andres Bello, Santiago, Chile; [e]Instituto de Alta Investigación, Universidad de Tarapacá, Arica, Chile; [f]Departamento de Física, Universidad Técnica Federico Santa María, Valparaíso, Chile
[141] Department of Physics, Institute of Science, Tokyo, Japan
[142] Department of Physics, University of Washington, Seattle, WA, USA
[143] [a]Institute of Frontier and Interdisciplinary Science and Key Laboratory of Particle Physics and Particle Irradiation (MOE), Shandong University, Qingdao, China; [b]School of Physics, Zhengzhou University, Zhengzhou, China
[144] [a]State Key Laboratory of Dark Matter Physics, School of Physics and Astronomy, Shanghai Jiao Tong University, Key Laboratory for Particle Astrophysics and Cosmology (MOE), SKLPPC, Shanghai, China; [b]State Key Laboratory of Dark Matter Physics, Tsung-Dao Lee Institute, Shanghai Jiao Tong University, Shanghai, China
[145] Department of Physics and Astronomy, University of Sheffield, Sheffield, UK
[146] Department of Physics, Shinshu University, Nagano, Japan
[147] Department Physik, Universität Siegen, Siegen, Germany
[148] Department of Physics, Simon Fraser University, Burnaby, BC, Canada
[149] SLAC National Accelerator Laboratory, Stanford, CA, USA
[150] Department of Physics, Royal Institute of Technology, Stockholm, Sweden
[151] Departments of Physics and Astronomy, Stony Brook University, Stony Brook, NY, USA
[152] Department of Physics and Astronomy, University of Sussex, Brighton, UK
[153] School of Physics, University of Sydney, Sydney, Australia
[154] Institute of Physics, Academia Sinica, Taipei, Taiwan
[155] [a]E. Andronikashvili Institute of Physics, Iv. Javakhishvili Tbilisi State University, Tbilisi, Georgia; [b]High Energy Physics Institute, Tbilisi State University, Tbilisi, Georgia; [c]University of Georgia, Tbilisi, Georgia
[156] Department of Physics, Technion, Israel Institute of Technology, Haifa, Israel
[157] Raymond and Beverly Sackler School of Physics and Astronomy, Tel Aviv University, Tel Aviv, Israel
[158] Department of Physics, Aristotle University of Thessaloniki, Thessaloniki, Greece
[159] International Center for Elementary Particle Physics and Department of Physics, University of Tokyo, Tokyo, Japan
[160] Graduate School of Science and Technology, Tokyo Metropolitan University, Tokyo, Japan
[161] Department of Physics, University of Toronto, Toronto, ON, Canada
[162] [a]TRIUMF, Vancouver, BC, Canada; [b]Department of Physics and Astronomy, York University, Toronto, ON, Canada
[163] Division of Physics and Tomonaga Center for the History of the Universe, Faculty of Pure and Applied Sciences, University of Tsukuba, Tsukuba, Japan
[164] Department of Physics and Astronomy, Tufts University, Medford, MA, USA
[165] Department of Physics and Astronomy, University of California Irvine, Irvine, CA, USA
[166] University of West Attica, Athens, Greece
[167] Department of Physics and Astronomy, University of Uppsala, Uppsala, Sweden
[168] Department of Physics, University of Illinois, Urbana, IL, USA
[169] Instituto de Física Corpuscular (IFIC), Centro Mixto Universidad de Valencia-CSIC, Valencia, Spain
[170] Department of Physics, University of British Columbia, Vancouver, BC, Canada
[171] Department of Physics and Astronomy, University of Victoria, Victoria, BC, Canada
[172] Fakultät für Physik und Astronomie, Julius-Maximilians-Universität Würzburg, Würzburg, Germany
[173] Department of Physics, University of Warwick, Coventry, UK
[174] Waseda University, Tokyo, Japan

[175] Department of Particle Physics and Astrophysics, Weizmann Institute of Science, Rehovot, Israel
[176] Department of Physics, University of Wisconsin, Madison, WI, USA
[177] Fakultät für Mathematik und Naturwissenschaften, Fachgruppe Physik, Bergische Universität Wuppertal, Wuppertal, Germany
[178] Department of Physics, Yale University, New Haven, CT, USA
[179] Yerevan Physics Institute, Yerevan, Armenia

[a] Also at Affiliated with an Institute Formerly Covered by a Cooperation Agreement with CERN, Geneva, Switzerland
[b] Also at An-Najah National University, Nablus, Palestine
[c] Also at Borough of Manhattan Community College, City University of New York, New York, NY, USA
[d] Also at Center for Interdisciplinary Research and Innovation (CIRI-AUTH), Thessaloniki, Greece
[e] Also at Centre of Physics of the Universities of Minho and Porto (CF-UM-UP), Braga, Portugal
[f] Also at CERN, Geneva, Switzerland
[g] Also at CMD-AC UNEC Research Center, Azerbaijan State University of Economics (UNEC), Baku, Azerbaijan
[h] Also at Département de Physique Nucléaire et Corpusculaire, Université de Genève, Geneva, Switzerland
[i] Also at Departament de Fisica de la Universitat Autonoma de Barcelona, Barcelona, Spain
[j] Also at Department of Financial and Management Engineering, University of the Aegean, Chios, Greece
[k] Also at Department of Mathematical Sciences, University of South Africa, Johannesburg, South Africa
[l] Also at Department of Modern Physics and State Key Laboratory of Particle Detection and Electronics, University of Science and Technology of China, Hefei, China
[m] Also at Department of Physics, Bolu Abant Izzet Baysal University, Bolu, Türkiye
[n] Also at Department of Physics, King's College London, London, UK
[o] Also at Department of Physics, Stanford University, Stanford, CA, USA
[p] Also at Department of Physics, Stellenbosch University, South Africa
[q] Also at Department of Physics, University of Fribourg, Fribourg, Switzerland
[r] Also at Department of Physics, University of Thessaly, Greece
[s] Also at Department of Physics, Westmont College, Santa Barbara, USA
[t] Also at Faculty of Physics, Sofia University, 'St. Kliment Ohridski', Sofia, Bulgaria
[u] Also at Faculty of Physics, University of Bucharest, Bucharest, Romania
[v] Also at Hellenic Open University, Patras, Greece
[w] Also at Henan University, Kaifeng, China
[x] Also at Imam Mohammad Ibn Saud Islamic University, Riyadh, Saudi Arabia
[y] Also at Institucio Catalana de Recerca i Estudis Avancats, ICREA, Barcelona, Spain
[z] Also at Institut für Experimentalphysik, Universität Hamburg, Hamburg, Germany
[aa] Also at Institute for Nuclear Research and Nuclear Energy (INRNE) of the Bulgarian Academy of Sciences, Sofia, Bulgaria
[ab] Also at Institute of Applied Physics, Mohammed VI Polytechnic University, Ben Guerir, Morocco
[ac] Also at Institute of Particle Physics (IPP), Toronto, Canada
[ad] Also at Institute of Physics and Technology, Mongolian Academy of Sciences, Ulaanbaatar, Mongolia
[ae] Also at Institute of Physics, Azerbaijan Academy of Sciences, Baku, Azerbaijan
[af] Also at Institute of Theoretical Physics, Ilia State University, Tbilisi, Georgia
[ag] Also at National Institute of Physics, University of the Philippines Diliman (Philippines), Quezon City, Philippines
[ah] Also at The Collaborative Innovation Center of Quantum Matter (CICQM), Beijing, China
[ai] Also at TRIUMF, Vancouver, BC, Canada
[aj] Also at Università di Napoli Parthenope, Naples, Italy
[ak] Also at Department of Physics, University of Colorado Boulder, Boulder, CO, USA
[al] Also at University of Sienna, Siena, Italy
[am] Also at Washington College, Chestertown, MD, USA
[an] Also at Yeditepe University, Physics Department, Istanbul, Türkiye
* Deceased